Role of Nogo-A in regulating synaptic transmission in the hippocampus – The involvement of inhibition

Von der Fakultät für Lebenswissenschaften

der Technischen Universität Carolo-Wilhelmina zu Braunschweig

zur Erlangung des Grades eines

Doktors der Naturwissenschaften

(Dr. rer. nat.)

genehmigte

D i s s e r t a t i o n

von Steffen Sven Fricke
aus Braunschweig

1. Referent:	Professor Dr. Martin Korte
2. Referent	Professor Dr. Jochen Meier
eingereicht am:	18.09.2019
mündliche Prüfung (Disputation) am:	17.10.2019

Druckjahr 2020

Vorveröffentlichungen der Dissertation

Teilergebnisse aus dieser Arbeit wurden mit Genehmigung der Fakultät für Lebenswissenschaften, vertreten durch den Mentor der Arbeit, in den folgenden Beiträgen vorab veröffentlicht:

Publikationen

Zagrebelsky, M., Lonnemann, N., **Fricke, S**., Kellner, Y., Preuß, E., Michaelsen-Preusse, K., & Korte, M. (2017). Nogo-A regulates spatial learning as well as memory formation and modulates structural plasticity in the adult mouse hippocampus. *Neurobiology of learning and memory, 138, 154-163.*

Kellner, Y., **Fricke, S.**, Kramer, S., Iobbi, C., Wierenga, C. J., Schwab, M. E., Korte, M. & Zagrebelsky, M. (2016). Nogo- A controls structural plasticity at dendritic spines by rapidly modulating actin dynamics. *Hippocampus, 26(6), 816-831.*

Fricke, S., Metzdorf, K., Ohm, M., Haak, S., Heine, M., Korte, M., Zagrebelsky, M. Fast regulation of $GABA_AR$ diffusion dynamics by Nogo-A signaling. *Cell Reports* (*in press*).

Tagungsbeiträge

Fricke, S., Lonnemann, N., Kellner, Y., Metzdorf, K., Korte, M. & Zagrebelsky, M. Role of Nogo-A signaling in regulating spatial learning and memory formation by modulating hippocampal parvalbumin (PV)-interneuron networks. *12^{th} Meeting of the German Neuroscience Society, Göttingen (2017).*

Fricke, S., Metzdorf, K., Korte, M., Zagrebelsky, M. Fast effects of Nogo-A neutralization on the excitation/inhibition (E/I) balance in the hippocampus. *11^{th} FENS Forum of Neuroscience, Berlin (2018).*

Metzdorf, K., **Fricke, S.**, Haak, S., Ohm, M., Korte, M. & Zagrebelsky, M. Nogo-A signaling modulates synaptic transmission on a fast time scale. *13th Meeting of the German Neuroscience Society, Göttingen (2019).*

Table of Contents

Abstract

Learning and memory processes shape the function and structure in the brain. The precise temporal modulation of the synaptic connections in the neuronal network is important to regulate their function. While it is necessary that synapses are plastic in order to enable the acquisition and implementation of new information, the stabilization of synapses is crucial to allow long-term storage and recall of these data. A set of molecules has been described to modify this delicate balance between plastic changes and stabilization. In this study, the role of one of these molecules, namely Nogo-A, in regulating the interplay between plasticity and stability was investigated. Nogo-A has been shown to limit functional and structural recovery after an injury in the adult central nervous system (CNS) and has recently been implicated as a suppressor of activity-dependent synaptic plasticity as well as learning and memory processes. However, the underlying mechanisms of how Nogo-A modulates synaptic function and especially its acute actions on synaptic transmission remained unknown. This work shows via patch clamp electrophysiology that Nogo-A bidirectionally regulates neuronal transmission on a fast time scale. While Nogo-A loss-of-function resulted in an increase in excitatory synaptic transmission within few minutes, inhibitory synaptic transmission was decreased simultaneously. Western blotting analysis and live labeling of synaptic neurotransmitter receptors demonstrated that Nogo-A regulates synaptic transmission by restricting the localization of AMPA receptors at excitatory synapses and promoting the number of $GABA_A$ receptors at inhibitory synapses. Moreover, quantum dot-based single particle tracking paired with calcium imaging revealed that the lateral diffusion of $GABA_A$ receptors at synaptic and extrasynaptic sites as well as the concentration of intracellular calcium in dendrites was simultaneously increased within few minutes of Nogo-A loss-of-function. Furthermore, Nogo-A was found to limit the number and length of dendritic spines of CA3 hippocampal neurons in an activity-dependent manner as demonstrated via live cell imaging. Finally, spatial learning of mice in the Morris water maze and paired immunohistochemistry showed that Nogo-A seems not to control the activity of parvalbumin-positive inhibitory neuron networks to control spatial learning.

Taken together, this study reveals a new mechanism by which Nogo-A modulates neuronal transmission on a fast time scale and contributes to the understanding of how Nogo-A stabilizes neuronal circuits, which has its price, it limits plasticity in the mature brain.

Zusammenfassung

Lernen und Gedächtnisvorgänge beruhen auf der Funktion und Struktur neuronaler Verschaltungen im Gehirn. Die präzise zeitliche Modulation von synaptischen Verbindungen im neuronalen Netzwerk ist essentiell, um ihre Funktion zu regulieren. Während es notwendig ist, dass Synapsen plastisch sind, um die Aufnahme neuer Informationen zu ermöglichen, ist die Stabilisierung vonnöten, um ihre Langzeitspeicherung und Wiederabrufbarkeit zu gewährleisten. Es wurden verschiedene Moleküle identifiziert, die das Gleichgewicht zwischen plastischen Veränderungen und Stabilisierung regulieren. In dieser Dissertation wurde die Rolle eines dieser Moleküle namens Nogo-A in der Regulierung dieser Balance zwischen Veränderbarkeit und Stabilisierung untersucht. Es wurde bereits in vorherigen Arbeiten gezeigt, dass Nogo-A funktionelle und strukturelle Genesung nach einer Verletzung im zentralen Nervensystem (ZNS) einschränkt und konnte als Inhibitor von aktivitätsabhängiger synaptischer Plastizität und der Gedächtnisbildung identifiziert werden. Die zugrundeliegenden Mechanismen der Regulierung von synaptischer Funktion und speziell die akute Wirkung auf neuronale Transmission von Nogo-A sind jedoch nur wenig bekannt. Diese Arbeit zeigt anhand von Patch clamp Elektrophysiologie, dass Nogo-A die neuronale Transmission auf schnelle und bidirektionale Weise moduliert. Während die Inhibierung von Nogo-A dazu führt, dass exzitatorische synaptische Transmission verstärkt wird, führt sie ebenso zu einer simultanen Erniedrigung der inhibitorischen synaptischen Transmission von hippocampalen Neuronen. Mittels Western Blot Analyse und Immunfärbungen konnte gezeigt werden, dass Nogo-A synaptische Transmission reguliert, indem es die Lokalisierung von AMPA Rezeptoren an exzitatorischen Synapsen einschränkt und die Anzahl von $GABA_A$ Rezeptoren an der inhibitorischen Synapse erhöht. Anhand von Quantum Dot basiertem Single particle tracking und simultanem Calcium Imaging konnte festgestellt werden, dass die synaptische und extrasynaptische laterale Diffusion von $GABA_A$ Rezeptoren sowie die intrazelluläre Calciumkonzentration in Dendriten durch Inhibierung von Nogo-A erhöht wurden. Des Weiteren wurde mittels Live-Imaging festgestellt, dass Nogo-A die Anzahl und Länge von dendritischen Spines an CA3 Neuronen aktivitätsanhängig begrenzt. Zudem konnte anhand von Morris water maze Tests und Immunohistochemie gezeigt werden, dass Nogo-A räumliches Lernen nicht reguliert, indem es die Aktivität von Parvalbumin-positiven inhibitorischen Netzwerken kontrolliert. Zusammengefasst konnte in dieser Arbeit ein neuer Mechanismus aufgedeckt werden, mit dem Nogo-A neuronale Transmission moduliert, was somit zum weiteren Verständnis der Regulierung neuronaler Netzwerke durch Nogo-A im adulten Gehirn beiträgt.

Introduction

To gather and recall information based on experience are the basis for humans and animals alike to profitable decision making within their environment. Thus, learning and memory are amongst the most important biological processes for existence and survival. However, during life memories are established that might be rapidly forgotten while others last for a lifetime. This implies the ability of the neuronal network to undergo permanent change, for newly gathered information to be stored until needed while erasing allegedly redundant data. Indeed, the underlying synaptic connections in the brain are plastic structures that can be formed, strengthened, weakened and lost in response to activity. These observations imply the existence of a tightly regulated balance between the ability of the neuronal network to change on the one hand and the ability to persist on the other hand. This thesis addresses the molecular mechanisms regulating the balance between plasticity and stability in the brain focusing on the role of Nogo-A, a protein well-known for its inhibitory function on synaptic plasticity.

1.1. Hippocampus, pyramidal neurons and memory

Today, the hippocampus represents one of the most intensely studied regions in the brain, especially related to its role in learning and memory processes. The link between hippocampus and memory became particularly obvious with the report on the patient H. M. who lost the ability to store newly formed, declarative memories due to surgical removal of the hippocampus and nearby temporal lobe structures in an attempt to cure his epilepsy (Scoville and Milner, 1957). Over the years, it has been found to transfer short- into long-term memory (Alvarez and Squire, 1994) and to be involved in the consolidation of spatial, contextual and episodic memory (Vargha Khadem et al., 1997; Burgess et al., 2002; Eichenbaum, 2004; Squire, 2004). In detail, spatial information in the hippocampus is encoded via place cells whose firing patterns create a representation of the environment (O'Keefe and Dostrovsky, 1971). Interestingly, the hippocampus located in the right hemisphere appears to exert different functions compared to the hippocampus located in the left hemisphere: while the right hippocampus has been reported to play a role in spatial memory (Smith et al., 1981), the left hippocampus is involved in episodic memory (Frisk and Milner, 1990; Burgess

et al., 2002). The function of the hippocampus in this context relies on the tri-synaptic circuit (Andersen et al., 1971). Structurally, the hippocampus is divided into dentate gyrus (DG) and *cornu ammonis* (CA), subcategorized as the CA1, CA2, CA3 and CA4 areas (Figure 1), and it receives input from and projects back to the entorhinal cortex (EC). In detail, the EC projects via the perforant path axons to granule cells located in the DG which in turn projects to the proximal part of the neurons in CA3 via the mossy fibers. Over the schaffer collateral axons the CA3 area is connected to the apical and in part also basal regions of CA1 neurons from where axons project

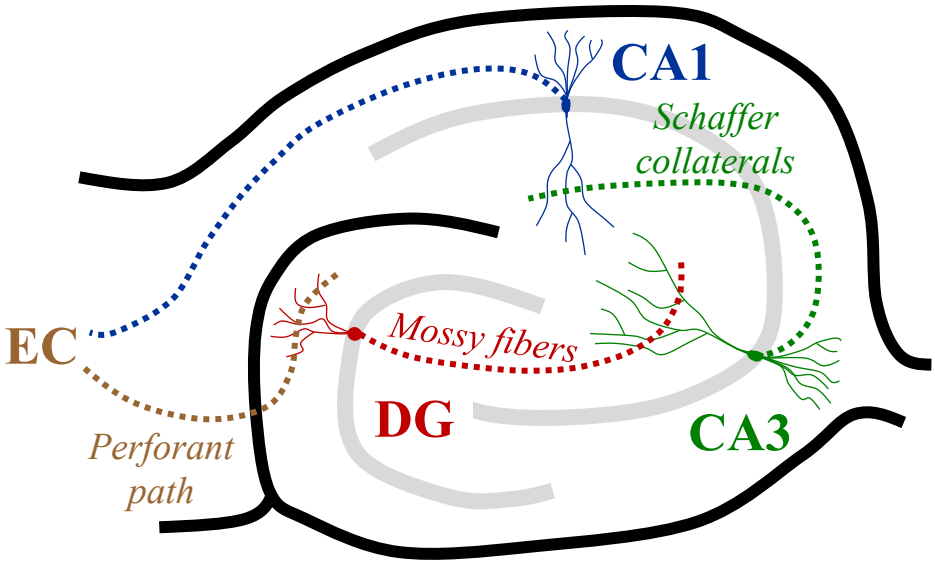

Figure 1: The trisynaptic pathway in the hippocampus

The entorhinal cortex (EC) projects to the dentage gyrus (DG) via the perforant path. In turn the mossy fibers connect the DG to the CA3 region that projects to the CA1 area via the schaffer collaterals. From the CA1 area axons project back to the EC. Adapted from Deng et al., 2010.

back to the EC (Ishizuka et al., 1990; Li et al., 1994; Figure 1). However, many more complex projections from and to the hippocampal subregions are present in the brain. The CA regions are themselves vertically subdivided into different strata as follows: *stratum lacunosum-moleculare* (sl-m), *stratum radiatum* (sr), *stratum lucidum* (sl, only in CA3), *stratum pyramidale* (sp) and *stratum oriens* (so; Figure 2A and 2B). Pyramidal neurons, the major neuronal cell type in the CA regions display a characteristic architecture with short basal dendrites and long apical dendrites both originally emerging from the pyramidal shaped soma (Figure 2B). This thesis focuses primarily on the CA3 pyramidal neurons categorized by a strong heterogeneity in their morphology, axonal projection, gene expression patterns, intrinsic electrophysiological properties

and synaptic connectivity depending on their localization along the proximodistal axis of the hippocampus (Ishizuka et al., 1990; Li et al., 1994; Ishizuka et al., 1995; Turner et al., 1995; Thompson et al., 2008; Sun et al., 2017). In the proximal apical part of the soma, CA3 pyramidal neurons carry large dendritic protrusions, the thorny excrescences that receive strong excitatory input by mossy fiber terminals from the DG (Gonzales et al., 2001).

The dendritic arbors of all pyramidal neurons are characterized by the presence of smaller protoplasmic membrane protrusions that are called dendritic spines. Dendritic spines vary profoundly in their number, size and architecture (Figure 2C; Sorra and Harris, 2000) and their

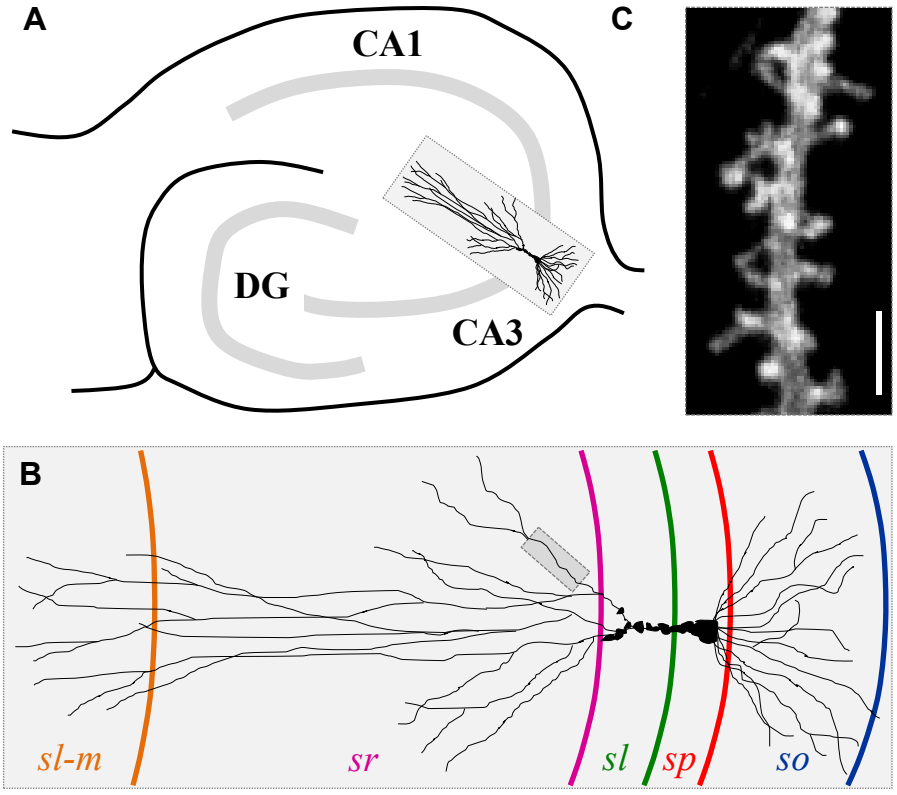

Figure 2: Pyramidal neurons in the hippocampus carry dendritic spines

(A) Example of a CA3 pyramidal neuron in the hippocampus. (B) Higher magnification scheme of the CA3 pyramidal neuron from (A). Colored lines indicate borders between hippocampal strata (from left to right): *stratum lacunosum-moleculare* (sl-m), *stratum radiatum* (sr), *stratum lucidum* (sl), *stratum pyramidale* (sp) and *stratum oriens* (so). (C) Maximum intensity projection of a CA3 apical dendrite confocal image carrying dendritic spines as indicated by the dark grey square in (B). Scale bar is 2 µm.

form is commonly subdivided into the 3 parts spine head, spine neck and base. The head is a round structure that is connected to the base on the dendrite via the neck (Figure 2C). While long and thin

spines are suggested to be available for learning processes, larger spines might be involved in the long-term storage of memories (Kasai et al., 2003; Bourne and Harris, 2007). Interestingly, spines have been found to form the postsynaptic compartment of synapses that are functionally active. The postsynapse is generally present within the spine head while the neck acts as a filter of the synaptic potential onto the dendrite (Tønnesen et al., 2014). A common synapse consists of 3 main parts: 1) a presynaptic active zone filled with synaptic vesicles, 2) a synaptic cleft in which the vesicles release neurotransmitters and 3) a postsynaptic density (PSD) that covers ~10 % of the surface of the dendritic spine (Harris et al., 1992). The protein-dense PSD contains postsynaptic receptors, ion channels, signal transduction proteins as well as scaffolding and cytoskeletal components, altogether forming a mesh-like network (Sheng and Hoogenraad, 2007; Bosch and Hayashi, 2012). Coupling morphology and function, the size of the PSD has been found to be positively correlated to the area of the presynaptic active zone, spine size and the abundance of the neurotransmitter receptor AMPAR (α-amino-3-hydroxy-5-methyl-4-isoxazolepropionic acid-type receptor). Upon binding its agonist glutamate, AMPARs enable the influx of sodium (Na^+) into the neuron resulting in the depolarization and therefore excitation of the neuron (Figure 3). The amount of AMPARs at the PSD is thus positively correlated to synaptic strength (Spacek and Harris, 1997; Bosch and Hayashi, 2012). Indeed, dendritic spines have been shown to be dynamic structures that undergo activity-dependent changes in their architecture and functionality, a process called synaptic plasticity (Matus et al., 2000; Bonhoeffer and Yuste, 2002; Matzusaki et al., 2004).

1.2. Activity-dependent synaptic plasticity – structure and function

While the overall structure of the CNS is genetically hard-wired, the synaptic connections in the brain can be altered and rearranged in response to neuronal activity. These processes, that are considered crucial for learning and memory, are called “synaptic plasticity”, first introduced by the Polish psychologist Jerzy Konorski (Konorski, 1948). Almost half a century ago, the most famous form of synaptic plasticity, the long-term potentiation (LTP), has been described experimentally by applying high frequency stimulation to the perforant path resulting in a long-lasting increase in the postsynaptic potential of the DG (Bliss and Lomo, 1973). This activity-dependent increase in the postsynaptic field potential is used nowadays in distinct regions of the hippocampus including the DG-CA3 mossy fiber pathway (for review see Evstratova and Tóth, 2014) and the CA3-CA1 Schaffer collateral pathway (for review see Kumar, 2011) as a read out for activity-dependent

functional synaptic plasticity. During the 1970s, morphological changes of the postsynapse were observed upon induction of functional plasticity. Stimulation of the EC axons led to an increase in the size of dendritic spines in granule cells of the DG (Fifková and Van Herreveld, 1975). Moreover, LTP induction was also found to be associated to an increase in the number of dendritic spines (Engert and Bonhoeffer, 1999; Maletic-Savatic et al., 1999). On the contrary, low-frequency stimulation was found to induce a decrease in synaptic potential, namely long-term depression (LTD), which is associated with the shrinkage and, ultimately, the loss of dendritic spines (Nägerl et al., 2004; Zhou et al., 2004). Finally, with the help of new techniques, the link between functional and structural plasticity could be described experimentally at a single cell level: LTP induction at single spines resulted in an increase in the spine head volume (Matzusaki et al., 2004).

Taken together, synaptic plasticity is characterized by pre- and postsynaptic changes and goes along with long-lasting alterations in synaptic strength and structure (Engert and Bonhoeffer, 1999; Bourne et al., 2013), both described to be correlated to learning and memory (Bliss and Collingridge, 1993; Kandel, 2001; Holtmaat and Svoboda, 2009; Xu et al., 2009).

1.3. The importance of inhibition

While most of the neurons located in the hippocampus are excitatory and use glutamate as neurotransmitter (glutamatergic), about 10-15 % of all hippocampal neurons are of inhibitory nature. These cells are called interneurons and predominantly use GABA (gamma-aminobutyric acid) as neurotransmitter (GABAergic) leading, upon binding with specific receptors to chloride (Cl^-) influx and to the hyperpolarization of the postsynaptic neuron thereby decreasing the likelihood for an action potential to be generated (Figure 3). Interneurons are present throughout all hippocampal regions and proximodistal layers and their morphology and dendritic arborization is highly diverse (for review see Pelkey et al., 2017). In general, inhibitory synaptic transmission is a key regulator of the neuronal network in the hippocampus and its plasticity represents a key mechanism underlying learning and memory processes (Isaacson and Scanziani, 2011; Maffei, 2011; Barron et al., 2017).

1.3.1. GABAergic synaptic transmission and its regulation by Ca^{2+}

Analogous to AMPA receptors at glutamatergic synapses, the number of surface GABA type A receptors ($GABA_AR$) defines the strength of inhibitory synapses (Moss and Smart, 2001; Kilman et al., 2002). In detail, the number of $GABA_ARs$ at hippocampal synapses depends on the localization at the membrane surface (insertion into and removal from the membrane) and their lateral diffusion dynamics (Choquet and Triller, 2013), the latter being regulated by Ca^{2+} in an NMDAR- (N-methyl-D-aspartate receptor) dependent manner. Briefly, upon Ca^{2+} influx, the phosphatase Calcineurin (CaN) is activated and dephosphorylates $GABA_ARs$ at serine 327 of the

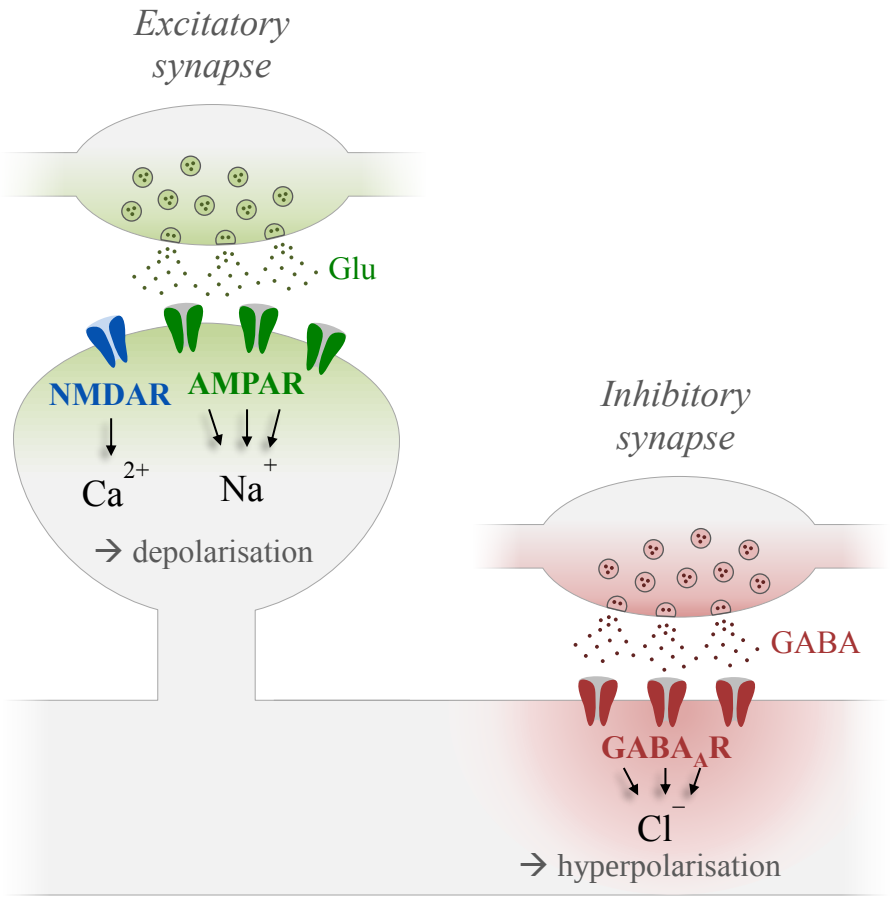

Figure 3: Excitatory and inhibitory synaptic transmission

(Left) At the excitatory presynapse glutamate (Glu) is released from vesicles into the synaptic cleft. Glutamate binds to AMPARs and NMDARs which open and enable Na^+ and Ca^{2+} influx, depolarizing the spine. (Right) At the inhibitory synapse GABA is released into the synaptic cleft, binds to $GABA_ARs$ and enables influx of Cl^- into the neuron leading to hyperpolarization of the dendritic segment.

γ2 subunit resulting in an increase in the lateral diffusion and decreased clustering of $GABA_ARs$ at

synapses (Bannai et al., 2009; Muir et al., 2010). However, how the mechanisms are regulated and which mediators control the diffusion dynamics and the synaptic presence of $GABA_ARs$ remained obscure until today.

1.4. PV^+ interneurons

One of the main types of hippocampal interneurons is characterized by its expression of the Ca^{2+} binding protein parvalbumin (PV). PV-positive (PV^+) inhibitory neurons have long, aspiny dendrites that often cross multiple layers enabling the input from a large population of principal neurons as well as distinct afferent projections like feedforward and feedback pathways (Gulyás et al., 1999; Nörenberg et al., 2010; Kubota et al., 2011; Tukker et al., 2013; for review see Hu et al., 2014). Moreover, PV^+ interneurons are suggested to generate a particularly strong inhibition as their axons form terminals either at the perisomatic domain or close to the axon initial segment (AIS) thus innervating target cells near the sites of action potential generation (Klausberger and Somogyi, 2008). The activity of PV^+ neurons, especially its mutability, has been found to play a major role in various processes such as the critical period for plasticity during development (Kuhlman et al., 2013; Yazaki-Sugiyama et al., 2009) or associative fear learning (Letzkus et al., 2011; Wolff et al., 2014). Interestingly, it was recently reported that changes in the inhibitory activity of PV^+ interneurons in the hippocampus are crucial to regulate spatial learning and memory formation in mice. These changes are directly correlated to the expression of PV in these interneurons and can therefore be detected by immunofluorescence (Donato et al., 2013). In this particular study Donato and colleagues found that inhibition by PV^+ interneurons onto CA3 pyramidal neurons decreased during the initial phase (days 2-5) of the Morris water maze task (MWM), a hippocampus-dependent spatial learning paradigm, accompanied by a drop in PV expression in these cells. Moreover, at the late phase in the MWM (day 10) where the spatial learning is complete, inhibition through PV^+ neurons was strengthened mirrored by an increase in PV immunofluorescence. Hence, while disinhibition of pyramidal neurons by suppression of PV^+ interneurons might be necessary for spatial learning, activation of PV^+ cells might promote consolidation (for review see Caroni, 2015). In summary, this suggests that plasticity of PV^+ interneurons controls the network activity in the hippocampus and thereby dynamically regulates learning and memory processes.

1.5. Nogo-A signaling in synaptic transmission and plasticity

1.5.1. Nogo-A and its receptors

In the mature brain, synaptic changes are promoted by plasticity enhancing molecules such as BDNF (brain-derived neurotrophic factor; for review see Kowiański et al., 2018). However, a set of molecules has been identified to limit synaptic plasticity in the adult CNS; amongst them: Nogo-A. Initially discovered as a myelin-associated neurite outgrowth suppressor, Nogo-A has been identified as an inhibitor of axonal sprouting and regeneration after injury in the adult nervous system (Schwab, 2010). At the end of development Nogo-A is expressed in oligodendrocytes and excitatory as well as inhibitory neurons of highly plastic brain areas such as the hippocampus and the cortex (Huber et al., 2002; Meier et al., 2003; Mingorance et al., 2004; Cheatwood et al., 2008; Zagrebelsky et al., 2016). It is encoded by the *reticulon 4* gene (RTN4), alike its splice or alternate promoter variants Nogo-B and Nogo-C (GrandPré et al., 2000; Dodd et al., 2005). In neurons, Nogo-A is predominantly located (~90 %) in the membrane of the endoplasmic reticulum (ER) with smaller fractions at the plasma membrane explaining the name "reticulon" (Oertle et al., 2003; Dodd et al., 2005). While the carboxyl terminus (C-terminus) and the reticulon homology domain (RTN) that includes the inhibitory active Nogo-66 domain flanked by two hydrophobic transmembrane domains (TMD) are shared by all 3 Nogo isoforms (Figure 4A), the amino-terminus (N-terminus) varies (Kempf and Schwab, 2013). Inside the 800 amino acid (aa) long N-terminus of Nogo-A lies another inhibitory domain, namely Nogo-A-Δ20 (Oertle et al., 2003; Figure 4). Both regions Nogo-66 and Nogo-A-Δ20 exhibit inhibitory activity through different receptor systems (Kempf and Schwab, 2013; Kempf et al., 2014). On the one hand, Nogo-66 can either bind to the paired immunoglobulin-like receptor B (PirB) or to Nogo Receptor 1 (NgR1). The latter lacks an intracellular signaling domain and therefore interacts with the leucine-rich repeat and immunoglobulin domain-containing nogo receptor-interacting protein 1 (Lingo1) and either p75 neurotrophin receptor ($p75^{NTR}$) or tumor necrosis dactor superfamily member 19 (TROY) to form a downstream signaling complex (Wang et al., 2002; Mi et al., 2004; Park et al., 2005; Figure 4). On the other hand, Nogo-A-Δ20 binds to the sphingosine 1-phosphate receptor 2 (S1PR2) as recently discovered (Kempf et al., 2014; Figure 4). Both Nogo-66 and Nogo-A-Δ20 have been found to signal via the small GTPase Ras homolog gene family member A (RhoA) and

rho-associated coiled-coil-containing protein kinase (ROCK, Niederöst et al., 2002; Nash et al., 2009; Kellner et al., 2016; Iobbi et al., 2017).

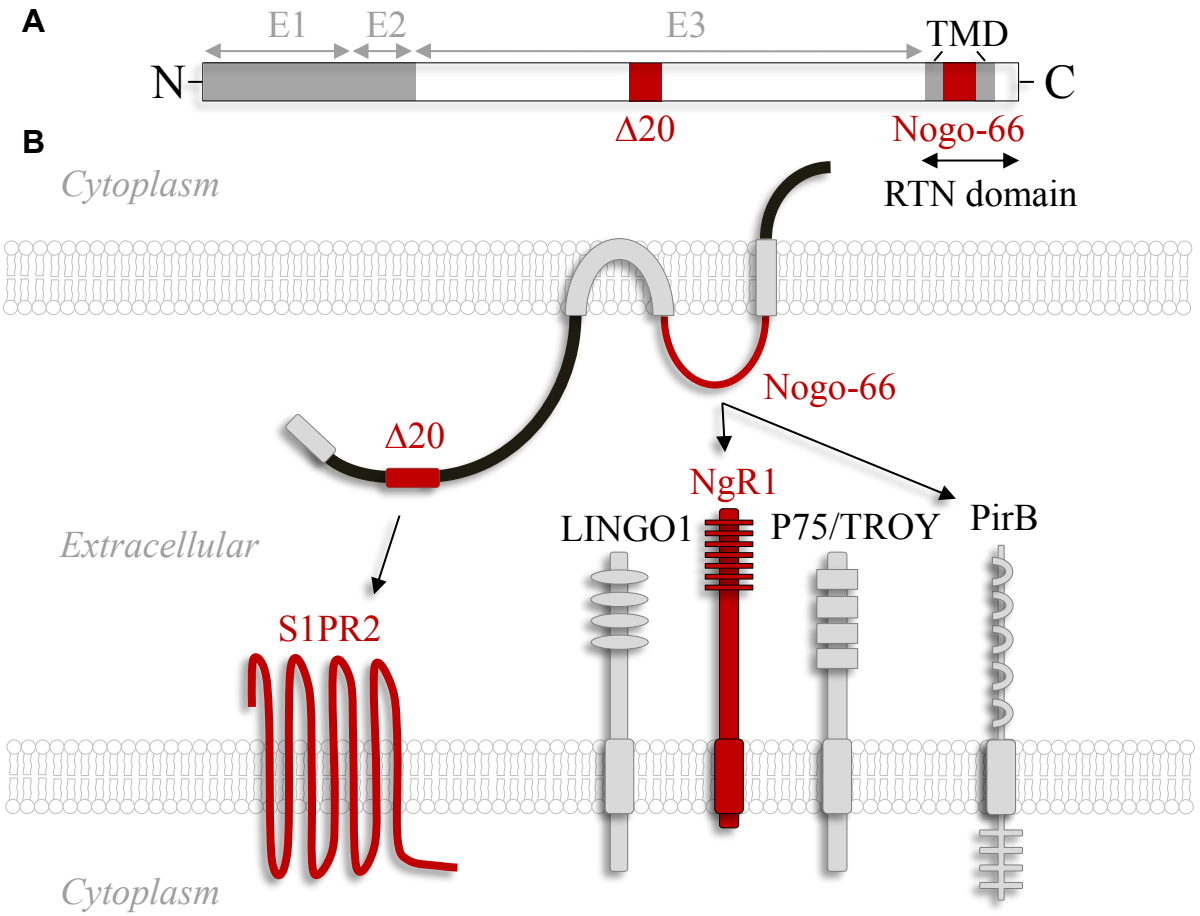

Figure 4: Nogo-A gene and signaling mechanism

(A) reticulon-4 gene carrying the two major inhibitory domains Δ20 and Nogo-66 (both red). The Nogo-66 region is flanked by transmembrane domains (TMD) and together with the C-terminus forms the reticulon (RTN) domain. E1-3 = exon 1-3. (B) Nogo-A signaling mechanism: The Δ20 region binds to S1PR2 while Nogo-66 binds NgR1 or PirB. Downstream signaling via NgR1 is mediated by interaction with LINGO1 or P75/TROY (adapted from Schwab, 2010; Y. Kellner, 2014; S. Fricke, 2015).

1.5.2. Nogo-A regulates neuronal architecture and synaptic plasticity

Over the course of the last years, Nogo-A has been found to be involved in shaping the neuronal morphology: In the spinal cord Nogo-A regulates the regeneration of axons after injury (Liebscher et al., 2005) with a similar function in the brain (Mdzomba et al., 2018; Schwab, 2004; Schwab

and Strittmatter, 2014). However, Nogo-A was also described to control the architecture of uninjured neurons in the intact CNS: In the cortex, Nogo-A restricts neurite outgrowth of cortical neurons during development (Mingorance-Le Meur et al., 2006) while it restricts axonal sprouting of uninjured Purkinje cell axons (Buffo et al., 2000). Moreover, Nogo-A negatively influences axonal and dendritic complexity of pyramidal neurons in the hippocampus (Zagrebelsky et al., 2010). Additionally, Nogo-A and its receptors also regulate structural plasticity at dendritic spines in the hippocampus and the cortex. Acute neutralization of Nogo-A induced a shift in dendritic spine distribution towards a less mature and possibly more plastic type in the hippocampus (Zagrebelsky et al., 2010). Further, Nogo-A loss-of-function led to a rapid increase in spine density and length (Kellner et al., 2016). Nogo signaling via NgR1 was revealed to regulate the experience-dependent turnover of dendritic spines and axonal varicosities in the somatosensory cortex (Akbik et al., 2013). In addition to regulating anatomical plasticity, Nogo-A has also been involved in the regulation of functional changes at synapses. Interestingly, both Nogo-A and its receptor NgR1 are present at pre- and postsynaptic compartments in the CNS, indicating an involvement of Nogo signaling in synaptic activity (Wang et al., 2002; Liu et al., 2003; Aloy et al., 2006; Lee et al., 2008). Indeed, Nogo-A restricts LTP at the CA3-CA1 Schaffer collateral pathway in the hippocampus via both receptors NgR1 and S1PR2 without affecting LTD (Lee et al., 2008; Raiker et al., 2010; Delekate et al., 2011; Mironova and Giger, 2013; Kempf et al., 2014; Zemmar et al., 2014; Iobbi et al., 2016). Interestingly, both excitatory synaptic transmission and the abundance of AMPA receptors at postsynapses reflecting the excitatory synaptic strength have been found to be restricted by Nogo-A (Jitsuki et al., 2015; Kellner et al., 2016). The role of Nogo-A signaling in synaptic plasticity hence suggests a possible involvement in learning and memory. Indeed, Nogo-A signaling via NgR1 has been found to restrict motor learning, LTP and structural plasticity of dendritic spines in the motor cortex of rodents (Zemmar et al., 2014). In addition, both Nogo-A and NgR1 have been found to regulate spatial learning and memory formation in the Morris water maze (MWM; Karlén et al., 2009; Karlsson et al., 2016; Zagrebelsky et al., 2016).

1.5.3. Nogo-A and inhibitory transmission

As Nogo-A has been found to be abundantly expressed in PV^+ inhibitory interneurons (Zagrebelsky et al., 2016) the question arose whether it is involved in the regulation of PV networks and therefore also in synaptic plasticity, learning and memory processes (see section 1.4.). Interestingly, specific

deletion of NgR1 in PV^+ interneurons decreased inhibitory synaptic transmission onto cortical pyramidal neurons and prevented the closure of the critical period, a developmental stage of enhanced plasticity in the visual cortex (Stephany et al., 2014). Moreover, the PV^+ cell-specific NgR1 KO also resulted in experience-dependent changes in the PV immunofluorescence indicating a change in the activity of PV^+ interneurons (Stephany et al., 2016). In addition, Nogo-A and NgR1 have been shown to strengthen the persistence of fear memories as selective deletion of NgR1 in PV^+ neurons was sufficient to reduce the fear expression in mice after fear conditioning. This study further reports that KO of NgR1 enhanced anatomical changes of inhibitory synapse markers after extinction training (Bhagat et al., 2016). Taken together, the involvement of Nogo signaling in PV^+ interneuron activity along with the high abundance of Nogo-A in PV^+ cells suggest a possible regulation of inhibition through Nogo proteins.

1.6. Aim of the thesis

This thesis is divided into 3 different aims:

Processes of learning and memory formation depend on the interplay between the ability of synaptic connections to change and their ability to persist which requires a tight balance between plasticity and stability. As a negative regulator of synaptic plasticity Nogo-A shifts this balance in favor of the stability possibly by suppressing functional and structural changes at synapses. Indeed, recent studies showed that Nogo-A signaling regulates structural dynamics of dendritic spines in the hippocampus. However, the question remained whether and how these plastic changes are driven by neuronal activity.

(1) Therefore, the first aim of this study is to examine the role of Nogo-A in spine dynamics in CA3 hippocampal neurons over time and elucidate which role neuronal activity plays in this context.

Lately, Nogo-A was found to be involved in the regulation of excitatory synaptic transmission in the hippocampus by restricting the number of surface AMPA receptors at postsynapses. However, it remains open whether Nogo signaling is also involved in the regulation of inhibitory synaptic transmission.

(2) In the second aim of this thesis, to elucidate a possible role of Nogo-A in inhibition, inhibitory synaptic transmission, $GABA_A$ receptor clustering at synapses as well as the diffusion dynamics of $GABA_A$ receptors were examined upon Nogo-A loss-of-function.

Spatial learning and memory formation have been found to be dependent on the plasticity of PV^+ inhibitory neurons in the hippocampus. Recent reports show a high expression level of Nogo-A in these interneurons and suggest a possible regulation of the function of PV^+ neurons by Nogo signaling.

(3) In the third aim of this work, to elucidate whether Nogo-A regulates PV plasticity upon hippocampus-dependent learning, the effect of a deletion of Nogo-A on PV expression upon spatial learning in the Morris water maze was analyzed.

Overall, this study aims to gain more insight into the signaling of Nogo-A in hippocampal neurons and how it regulates excitation, inhibition, synaptic plasticity and ultimately, learning and memory processes.

Materials and Methods

2.1. Materials

2.1.1. Chemicals

All chemicals used in this thesis were acquired from AppliChem, Invitrogen, Roth, Tocris, Merck Millipore or Sigma if not stated otherwise.

2.1.2. Buffers and solutions

ACSF, pH 7.4	
NaCl	125 mM
KCl	2.5 mM
$NaH_2PO_4*H_2O$	1.25 mM
$MgCl_2*6H_2O$	2 mM
$NaHCO_3$	26 mM
D+ Glucose (water free)	25 mM
$CaCl_2$ $2H_2O$	2 mM

Extracellular imaging medium (single particle tracking), pH 7.4	
NaCl	145 mM
KCl	2.5 mM
$MgCl_2*6H_2O$	2 mM
HEPES	10 mM
D+ Glucose (water free)	10 mM
$CaCl_2$ $2H_2O$	2 mM

GBSS	
$CaCl_2*2H_2O$	1.5 mM
KCl	5 mM
KH_2PO_4	0.22 mM

$MgCl_2$*6H2O	1 mM
$MgSO_4$*7H2O	0.28 mM
NaCl	137 mM
$NaHCO_3$	2.7 mM
NaH_2PO_4	0.86 mM
D-Glucose	5.5 mM

Diluted in dH_2O and sterile filtered (stored at 4°C)

Glucose solution (50 %)

Glucose	50 g
H_2O	50 mL

Solution was sterile filtered and stored at -20°C.

Hank's balanced salt solution (HBSS)

10x HBSS (Gibco/life technologies)	50 ml
NaHCO3	175 mg
CaCl2*2H2O	147 mg
Glucose	1351 mg

Filled up to 500 mL with H2O (MilliQ)

Hippocampal slice culture preparation solution

GBSS	98 mL
Kynurenic acid	1 mL
Glucose solution (50 %)	1 mL

pH was adjusted to 7.2 and stored at 4°C.

Internal solution (EPSCs), pH 7.3, 290 ± 10 mOsm

K-gluconate	126 mM
KCl	4 mM
HEPES	10 mM
Mg ATP	4 mM
Na GTP	0.3 mM
Na_2 phosphocreatine	10 mM

Internal solution (IPSCs), pH 7.3, 290 ± 10 mOsm

K-gluconate	70 mM
KCl	70 mM
HEPES	10 mM
Mg ATP	4 mM
Na GTP	0.4 mM
Na_2 phosphocreatine	4 mM

Kynurenic acid solution

Kynurenic acid (Sigma)	946 mg
1 M NaOH	5 mL
dH_2O	45 mL

Kynuric acid was diluted in 1 M NaOH & dH_2O, sterile filtered & stored at -20°C.

Lysogeny Broth (LB) Medium

diluted Trypton	10 g/L
NaCl	10 g/L
Yeast extract	5 g/L
Agar	15 g/L
If required:	
Ampicillin	100 µg/mL
Kanamycin	50 µg/mL

Müller-Kultur-Medium (medium for organotypic hippocampal cultures)

BME medium (Invitrogen)	100 mL
HBSS (Invitrogen)	50 mL
Horse serum (Hyclone)	50 mL
L-Glutamin (200 mM, Sigma)	1 mL
Glucose solution (50 %)	2 mL

Stored at 4°C

Mitosis inhibitor solution

Uridin (Sigma)	1 M
Cytosin-ß-D-Arabinofuranosid-Hydrochlorid	1 M
5-Fluoro-2‘-Deoxyuridin	1 M

Diluted in dH2O, sterile filtered and stored at -20°C.

PBS (10X), pH 7.3

NaCl	1.37 M
KCl	27 mM
KH_2PO_4	15 mM
Na_2HPO_4	80 mM

pH7.3

RIPA buffer, pH 7.5

TRIS	50 mM
NaCl	150 mM
EGTA	2 mM
Triton X-100	1 %
DOC	0.25 %

4x SDS protein sample buffer

TRIS-HCl (pH 7.6)	375 mM
SDS	2 %
Glycerol (87 %)	12 %
Bromophenol blue	0.05 %
β-Mercaptoethanol	10 %

Semidry blot running buffer, pH 8.6

TRIS	25 mM
Glycine	192 mM
SDS	0.1 %

Sucrose medium (synaptosome isolation)

Sucrose	0.32 M

HEPES (pH 7.5)	5 mM
EDTA (pH 8.0)	1 mM

1 cOmplete protease inhibitor pellet was added per 50 ml

Tank blot running buffer

TRIS	25 mM
Glycine	190 mM
SDS	0.05 %
Methanol	20 %

10x TBS, pH 7.6

TRIS	0.2 M
NaCl	1.37 M

10x TBS-T

TBS	10x TBS
Tween-20	0.1 %

10x TBS-X

TBS	10x TBS
Triton X-100	0.1 %

TRIS-HCl buffer, pH 7.5

TRIS	0.01 M

Diluted in H_2O

X-ray film developer

Roentogen	150 ml
H_2O	700 ml

X-ray film fixing solution

Manual Fixing Bath G354	150 ml
H_2O	750 ml

2.1.3. Primary antibodies

Antibody	description	Manufacturer	Dilution
α-Nogo-A	Mouse IgG1	Gift from Prof. Martin Schwab, ETH and University of Zürich, Switzerland	5 µg/ml
α-Nogo-A H300	Rabbit polyclonal	Santa Cruz, sc-25660	1:400
α-Nogo Receptor 1	Goat polyclonal	R&D Systems, AF1440	5 µg/ml
α-Parvalbumin	Rabbit polyclonal	Swant, PV 27	1:5,000
α-Parvalbumin	Mouse monoclonal	Swant, PV 235	1:5,000
α-Synapsin 1/2	Chicken polyclonal	Synaptic Systems, 106006	1:1,000
α-$GABA_A$ receptor γ2	Rabbit polyclonal	Synaptic Systems, 224003	1:500
α-$GABA_A$ receptor γ2	Rabbit polyclonal	Abcam, ab170224	1:500
α-GluR1	Rabbit polyclonal	Merck Millipore, AB1504	1:1,000
α-GAPDH	Rabbit polyclonal	Sigma-Aldrich, G9545	1:15,000
α-VGAT (lumenal) Oyster® 550	Rabbit polyclonal	Synaptic Systems, 131103C3	1:200

2.1.4. Secondary antibodies

Antibody	Manufacturer	Dilution
α-Rabbit Cy2	Jackson, 111-225-144	1:500
α-Rabbit Cy3	Jackson, 111-165-144	1:500
α-Rabbit Cy5	Jackson, 711-175-152	1:500
α-Chicken Alexa Fluor® 488	Jackson, 703-545-155	1:500
α-Rabbit HRP	Sigma-Aldrich, A0545	1:20,000
α-Mouse HRP	Sigma-Aldrich, A9044	1:20,000

2.1.5. Mouse strains

All experiments included in this thesis were authorized by the animal welfare representative of the TU Braunschweig and the LAVES (Oldenburg, Germany, Az. §4 (02.05) TSchB TU BS). Animals were housed in standardized cages exposed to a 12 h light/dark cycle. If not stated otherwise, all mice used were in a C57Bl/6 background. To examine the physiological role of Nogo-A in spatial learning, conventional Nogo-A knockout (Nogo-A KO) mice were used, in which parts of the *nogo* exons 2 and 3 and the intron in between were exchanged for a *pgk-neo* (phosphoglycerate kinase-neomycin resistance) gene (Simonen et al., 2003; Dimou et al., 2006). Further, conditional knock-out (cKO) mice were used in which Nogo-A was partially deleted in excitatory (CaMKII-cre/Nogo-$A^{flox/flox}$) or inhibitory parvalbumin-positive (PV^+) interneurons (PV-cre/Nogo-$A^{flox/flox}$). In brief, the exon 3 of the *rtn4* gene is flanked by flox sites (Vajda et al., 2015, produced by TaconicArtemis, Cologne, Germany) and removed by CaMKII- (B6.Cg-Tg(Camk2a-cre)T29-1Stl/J, Tsien et al., 1996) or PV- (B6;129P2-Pvalbtm1(cre)Arbr/J, Hippenmeyer et al., 2005) dependent expression of the cre recombinase, respectively. Single particle tracking and calcium imaging experiments were performed on primary neurons derived from Wistar rats.

2.2 Methods

2.2.1. Cell culture techniques

2.2.1.1. Preparation of primary mouse hippocampal cultures

Primary hippocampal cultures were prepared from C57Bl/6 mice at embryonic day 18 as previously described (Kellner et al., 2014; Zagrebelsky et al., 2018). Upon removal from the uterus, mouse embryos were decapitated and the upper half of the brain was dissected under sterile conditions and kept in ice-cold Gey's balanced salt solution (GBSS, pH 7.2) supplemented with glucose. Hippocampal neurons were dissociated by incubation with trypsin/EDTA at 37°C for 30 minutes and by subsequent mechanical dissociation. The neurons were plated at a density of $3.5x10^4$ cells per well on poly-L-lysine coated coverslips. The cells were kept in neurobasal medium (NB^-, #21103049, Thermo Fisher) supplemented with 2 % B27, 11 % N_2 and 0.5 mM Glutamax (NB^+) at 37°C, 5 % CO_2 and 99 % humidity.

2.2.1.2. Preparation of primary rat hippocampal cultures

Primary rat hippocampal cultures were prepared from Wistar rats at embryonic day 18 as described previously (Banker, 1980; Frischknecht et al., 2008). After extraction of the brain the hippocampi were dissected and dissociated with trypsin. Cell suspensions were plated onto poly-L-lysine-coated (Sigma) 18 mm glass coverslips (Menzel-Gläser, Braunschweig, Germany) at a density of $3x10^4$ cells per coverslip. The coverslips were incubated in Dulbecco's Modified Eagle Medium (DMEM) plus fetal bovine serum at 37°C for 1-2 hours. Subsequently, coverslips were placed into a 35 mm petri dish (5 coverslips per dish) containing a 70-80 % confluent monolayer of astrocytes in neurobasal medium supplemented with 2 % B27 and 5 mM glutamine. The cultures were kept in a humidified incubator at 37°C. After 3 days *in vitro* 1.4 µM AraC was added to the cultures to control the number of astrocytes.

2.2.1.3. Preparation of organotypic hippocampal slice cultures

Organotypic hippocampal cultures (OHC) were prepared from postnatal day 5 (P5) C57Bl/6 mice of either sex as described previously (Michaelsen-Preusse, 2014; Stoppini et al., 1991). The mice were rapidly decapitated and the hippocampi were dissected in ice-cold sterile Gey's balanced salt solution (GBSS). Transversal slices were cut using a tissue chopper (McIlwain) at a thickness of 400 µm. The slices were placed on Millicells CM membrane inserts (Millipore, 0.4 µm pore size) and cultivated at 37°C, 5 % CO_2 and 99 % humidity in a medium containing 50 % BME (Eagle, with Hanks salts without glutamine), 25 % Hank's Buffered Salt Solution (HBSS), 1 % glucose, 25 % donor equine serum (HyClone), and 0.5 % L-glutamine. Three days after preparation, a mixture of antimitotic drugs (cytosine arabinoside, uridine, and fluorodeoxyuridine; 1 to 0.1 µM each) was applied for 24 h followed by a 100 % medium exchange. For preservation, 50 % of the medium was exchanged every week.

2.2.2. Preparation of acute hippocampal slices

Acute hippocampal slices were prepared from 6-8 weeks old C57BL/6 mice. After being euthanized with CO_2, the mice were decapitated, the brain was dissected and incubated for 3 min in 4°C carbogenated (95 % O_2, 5 % CO_2) artificial cerebrospinal fluid (ACSF). The hippocampi were dissected and 400 µm thick transversal slices were cut with a Tissue Slicer (Stoelting). Before

treatment the slices were maintained at room temperature for at least 90 min in a submerged storage chamber with carbogenated ACSF.

2.2.3. Single-cell DNA electroporation

Neurons localized in the *stratum pyramidale* in the CA3 region of 18-20 DIV organotypic hippocampal slice cultures were chosen for transfection. Electroporation was performed with an Axoporator 800A (Axon Instruments, Molecular Devices) under an upright fluorescence microscope (Zeiss) equipped with a 40x objective (water, NA 0.8, Zeiss) and a video camera as previously described (Michaelsen-Preusse et al., 2014). The DNA (eGFP-F expression plasmid) was used at a concentration of 150 ng/µl, diluted in HBSS 24 h before electroporation and centrifuged right before use at 13,000 g for 10 min. The slices were kept in prewarmed, sterile HBSS throughout the procedure. Pipettes were pulled with a PC-10 pipette puller (Narishige) and filled with DNA solution. The electrode (GC150F-10, O.D. 1.5 mm x I.D. 0.86 mm, Harvard Apparatus (Kent): tip diameter 1-2 µm) had a resistance of 5-10 MΩ dependent on the proximity to the cell body at a pressure of 10-20 mbar generated by a pressure gauge (GDH200, Greisinger). To increase visibility and to selectively approaching single cells the differential interference contrast (DIC) was enhanced. The neurons were electroporated using pulses of 5 V, 1 mA at 200 Hz. The slice cultures were imaged 24-48 h after electroporation. Only completely labeled pyramidal neurons without any sign of degeneration were chosen for the experiments.

2.2.4. Loss- and gain-of-function treatments

Loss-of-function for Nogo-A signaling was achieved by application of the following inhibitors: a monoclonal anti-Nogo-A function blocking antibody against an 18 amino acids peptide part of the most active region of the protein (mouse IgG1, 11C7; Liebscher et al., 2005; Maier et al., 2009; Oertle et al., 2003; gift from Martin Schwab, ETH, Zürich); an antagonist of the sphingosine-1-phosphate receptor 2 (S1PR2), JTE-13 (Tocris); a function-blocking antibody against the Nogo receptor 1 (anti-NgR1, goat anti-Nogo receptor affinity-purified IgG; R&D Systems). A mouse anti-BrdU IgG1 antibody was used as control for the Nogo-A and NgR1 neutralization experiments. All antibodies and peptides were diluted to a concentration of 5 µg/ml. The gain-of-function for Nogo-A was achieved by application of the active peptide NiGΔ20 that was also used

to generate the 11C7 anti-Nogo-A antibody (Oertle et al., 2003) at a concentration of 300 nM. All antibodies and peptides were solved in either H_2O, PBS or DMSO and an equal amount of solvent was used as control.

2.2.5. Patch clamp electrophysiology

Whole-cell patch clamp recording was performed on visually identified CA3 pyramidal neurons in organotypic mouse hippocampal slice cultures at DIV 21-25 (Figure 5). During the experiments the slices were kept in an open imaging chamber perfused with carbogenated ACSF (1 ml/min) at 32°C supplemented with 1µM tetrodotoxin and 20 µM CNQX (miniature inhibitory postsynaptic currents, mIPSC) or 10 µM bicuculline (miniature excitatory postsynaptic currents, mEPSC),

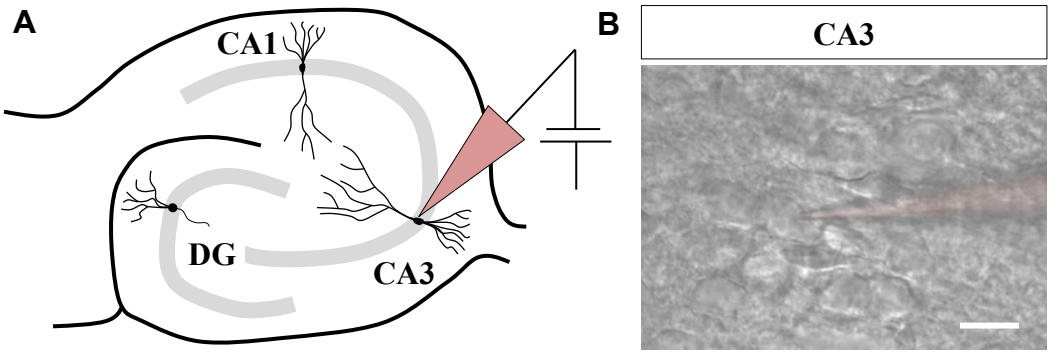

Figure 5: Whole-cell patch clamp electrophysiology.

(A) Schematic representation of patch clamp in CA3 neurons in an organotypic hippocampal slice culture. (B) Image of the CA3 area approached by the patch pipette (colored in red for visibility). Scale bar is 20 µm

respectively. Before starting the experiments the slices were transferred to the imaging chamber and let to rest and adapt to the ACSF for 20 min. Glass pipettes were pulled with a vertical micropipette puller (PC-10, Narishige) from borosilicate capillaries (1.5 mm) and filled with the respective internal solution (see section: buffers and media; resistance: 4.0-7.0 MΩ). Recordings were performed under an upright Axioskop 2 FS Plus microscope (Zeiss) with a 40X water-immersion objective (0.8 NA, Zeiss). The neurons were voltage-clamped at -70 mV and inhibitory or excitatory currents were recorded every 5 min for 120 seconds up to 25 min after membrane break-in of the patch pipette. Throughout the recordings, series resistance (R_s) and input resistance (R_{in}) were monitored and neurons exhibiting unstable resistances (R_s > 25 MΩ, R_{in} < 100 MΩ) were excluded from the analysis. The recordings were amplified with a MultiClamp 700B amplifier

and digitized with a Digidata 1322A digitizer (both Molecular Devices). Current detection was performed using Mini Analysis software (Justin Lee, Synaptosoft). Statistical analysis was performed in Prism 5 (GraphPad) using a Two-Way repeated measures ANOVA followed by a Bonferroni post hoc test for multiple comparisons.

2.2.6. Live-cell labeling and immunocytochemistry

Surface $GABA_A$ receptors were labeled on living primary mouse hippocampal neurons at DIV 21-25 (Figure 6). To this purpose, the neurons were incubated with anti-$GABA_AR$ γ2 (1:500, Synaptic Systems) in NB^- containing 1 % BSA for 10 minutes in a humidified incubator at 37°C, 5 % CO_2 and 99 % humidity followed by the respective loss-of-function treatments (Nogo-A antibody, JTE013, NgR1 antibody) for 10 minutes under the same conditions. Subsequently, the cultures were washed and rapidly fixed with 4 % paraformaldehyde (PFA) in PBS for 10-15 min followed by cell permeabilization using 0.3 % Triton X-100 in PBS for 5 min. Unspecific binding of

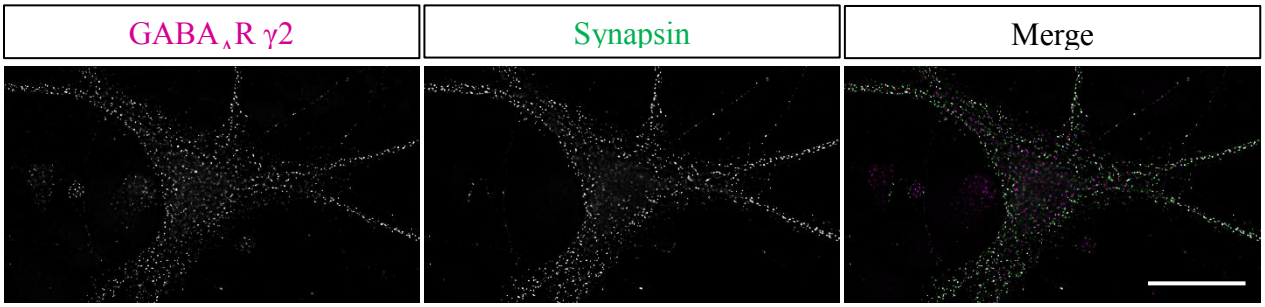

Figure 6: **$GABA_AR$ live-cell labeling and synapsin immunocytochemistry.**

Example images of a primary hippocampal neuron live-labeled for $GABA_AR$ γ2 (left, magenta), immunocytochemically labeled for synapsin (center, green) and their colocalization (right). Scale bar is 20 µm.

antibodies was blocked by incubation with 2 % BSA in PBS for 30 min. Presynaptic terminals were labeled with anti-synapsin 1/2 (1:1,000, Figure 6) diluted in PBS containing 2 % BSA for 1 h at RT followed by incubation with the secondary antibodies anti-chicken Alexa Fluor® 488 (1:500) and anti-rabbit Cy3 (1:500) in PBS for 40 min at RT. Finally, the coverslips were incubated in a quenching solution containing 50 mM NH_4Cl_2 in PBS for 10 min at RT and mounted onto glass slides using Fluoro-Gel (Electron Microscopy Sciences).

2.2.7. Widefield fluorescence imaging and analysis of synaptic proteins

2D widefield fluorescence imaging was used to image $GABA_AR$ γ2 and synapsin positive cluster. In detail, randomly chosen primary dendrites belonging to isolated, fluorescently labeled neurons were imaged using an upright Axio Imager M2 microscope (Zeiss) equipped with a 63x oil-immersion objective (NA 1.4) and a CCD camera. The same sub-saturation exposure time was used for imaging all cells belonging to each culture preparation. Background fluorescence was measured independently for $GABA_AR$ and synapsin puncta in ImageJ (National Institutes of Health) by placing 10 defined regions of interest (ROIs) on the dendrite between the synaptic puncta where no fluorescent clusters were visible. The averaged mean gray value of these ROIs was defined as background. SynPAnalysis (Danielson and Lee, 2014; Figure 7) was used to determine the number, fluorescence intensity and size of synaptic $GABA_AR$ and synapsin puncta

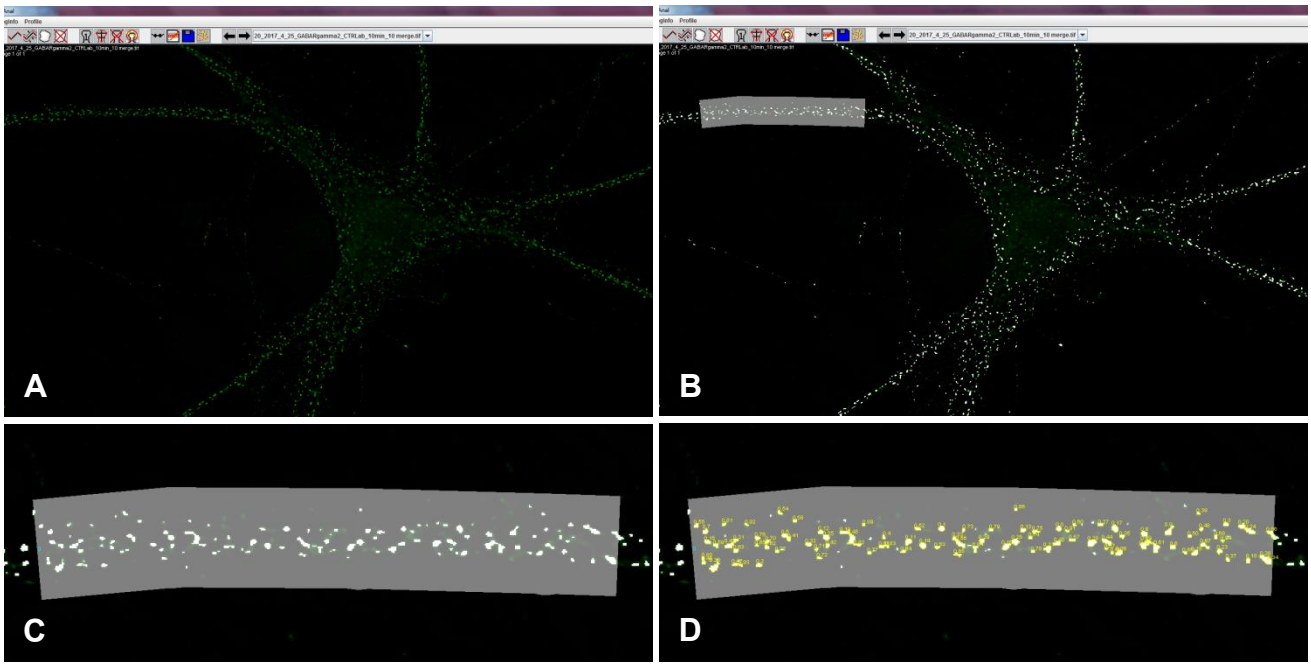

Figure 7: **Synaptic puncta analysis in SynPAnalysis.**

(A) 2D widefield fluorescence image showing a primary neuron labeled for synapsin opened in SynPAnalysis. (B, C) After background subtraction, the dendrite of interest was outlined (grey area) and automatic puncta detection (yellow ROIs) was performed (D).

after two-fold subtraction of the background. Colocalization of $GABA_AR$ and synapsin puncta was assessed in ImageJ and defined by overlap of at least 1 pixel after two-fold subtraction of the respective background (here the background was subtracted 2 times to increase specificity of the analysis). Statistical analysis was performed in Prism 5 (GraphPad) using a Student's t-test.

2.2.8. Single particle tracking and Fluo-4 imaging

Single particle tracking was performed using a quantum dot- (QD-) based approach. $GABA_AR$ primary antibodies were tagged with QDs by mixing anti-$GABA_AR$ antibodies (1:10, Synaptic Systems), F(ab')2-goat anti-rabbit IgG Qdot655 (1:10, #Q11422MP, Thermo Fisher) and 10x casein solution (1:10, #SP-5020, Vector Laboratories) in PBS (Figure 8). The mix was vortexed for 10 min at RT. Meanwhile, 10-14 DIV primary rat hippocampal neurons were incubated with a fluorescently labeled (Oyster® 550) anti-VGAT antibody (lumenal domain, 1:200) in extracellular imaging medium containing 0.5 % BSA for 30 min at 37°C followed by incubation with the QD-$GABA_AR$ antibody mix (1:200) diluted in extracellular imaging medium containing 0.5 % BSA for 5 min at 37°C. Before imaging the neurons were briefly washed with extracellular imaging medium containing 0.5 % BSA. Coverslips were moved to a closed imaging chamber filled with extracellular imaging medium at 37°C and recording was performed under an upright Olympus BX61 microscope equipped with a spinning disk (Yokogava) and a 100x oil-immersion objective (NA 1.4), using the 561 nm laser line and appropriate emission filters to record consecutive images of synapse labeling and QD tagged $GABA_ARs$. Images were captured by an EMCCD camera (iXon+ 897, Andor Technology) and the imaging system was controlled by the Andor iQ2 software. Image sequences of 1,000 frames and acquisition rate of 33 Hz were recorded for QD labelled $GABA_ARs$ and 100 frames (33 Hz) were acquired for VGAT labelled synapses. The QD-$GABA_AR$ tracking was repeated every 5 min for up to 20 min. VGAT fluorescence was averaged over 100 frames, background fluorescence was measured by placing ROIs in spots where no dendrites were visible, finally subtracted and VGAT positive areas were marked as synaptic compartments using MetaMorph software (Universal Imaging). The PalmTracer plugin for MetaMorph was used to track individual QD-$GABA_ARs$. Localization and trajectory reconnection of QDs were carried out using a wavelet-based algorithm and trajectories of QD-tagged $GABA_ARs$ were reconstructed by a simulated annealing algorithm (Izeddin et al., 2012). The diffusion coefficient (D) was determined by a linear fit of the first 4 points of the mean square displacement (MSD) over time using $MSD(t) = \langle r2 \rangle (t) = 4Dt$. Only trajectories longer than 8 points were included in the analysis. For the reconstruction of trajectories > 8 points the blinking of QDs was not taken into consideration. MSD plots were created by using the MSDs generated from trajectories with ≥ 34 points (~1 second) and the confinement area of $GABA_ARs$ in the membrane was calculated by fitting the MSD according to the procedure described earlier (Kusumi et al. 1993). Statistical significance within a group over time was assessed with a Friedman test followed

by a Dunn's post-hoc test while statistical significance between groups was tested with a Two-Way repeated-measures ANOVA followed by a Bonferroni post-hoc test.

The mean explored surface of QD-GABA$_A$Rs was quantified using ImageJ. To this purpose, maximum projections of single recordings (1000 frames) before and 10 minutes after control or Nogo-A neutralizing antibody application were generated. After background calculation and subtraction achieved by placing single ROIs in regions where no trajectories were visible, the projections were binarized and the function "Analyze Particles" (0.1-inf μm^2, no circularity) was used to assess the exploration area. The data are then presented as normalized mean explored surface area. Statistical differences were assessed using a Student's t-test.

In experiments where single particle tracking of GABA$_A$Rs was paired with Ca^{2+} imaging, the primary neurons were incubated with the calcium indicator Fluo-4 AM (1:200, #F14201, Thermo Fisher) together with the QD-GABA$_A$R mix in extracellular imaging medium containing 0.5 % BSA for 5 min at 37°C. Fluo-4 signal was imaged in sequences of 1,000 frames at 33 Hz before as well as 5 and 10 minutes after Nogo-A neutralizing antibody application. Fluo-4 fluorescence was averaged over 1,000 frames after subtraction of the background. The normalized fluorescence intensities (F/F_0), where F is the fluorescence intensity after 5 or 10 minutes and F_0 is the fluorescence intensity before treatment start, were assessed by normalization to the first time point of each experiment. Statistical analysis was performed in Prism using a Two-Way repeated-measures ANOVA followed by a Bonferroni post hoc test. A Spearman test was used to check for correlation between diffusion dynamics and Fluo-4 intensity of single cells.

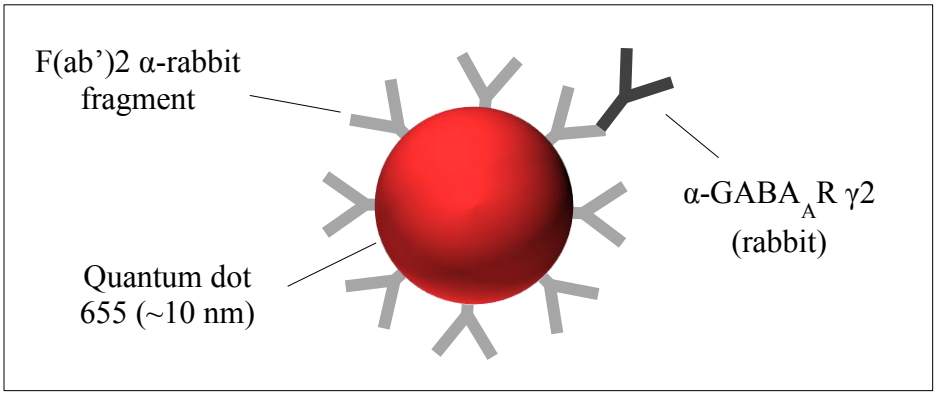

Figure 8: **Quantum dot presenting F(ab')2 fragments is tagged with anti-GABA$_A$R antibodies.**

The fluorescently active quantum dots (red, emission at 655 nm) were incubated with anti-GABA$_A$R antibodies that bind the F(ab')2 fragments located on their outer shell.

2.2.9. Synaptosome isolation and Bradford assay

This protocol was adapted from a publication in Bio Protocols (Suresh and Dunaevsky, 2015). Acute hippocampal slices were prepared as described (2.2.2). After resting in ACSF for 90 min at RT, slices were treated with either control antibody, Nogo-A neutralizing antibody (5 µg/ml) or high KCl concentration (55 mM). Subsequently, slices were transferred into an Eppendorf tube with 300 µl sucrose medium containing 0.32 M sucrose, 5 mM HEPES (pH 7.5), 0.1 mM EDTA (pH 8.0) and cOmplete protease inhibitor cocktail (1 tablet per 50 ml). After homogenization with a hand-held homogenizer (DWK Life Sciences) on ice for 1 min the samples were centrifuged at 1,500 rpm at 4°C for 10 min followed by a subsequent centrifugation of the supernatant containing suspended synaptosomes at 13,500 rpm at 4°C for 20 min. The pellet was resuspended and lysed in a volume of RIPA buffer depending on the pellet size on a rotor at 4°C for 30-40 min. Protein concentration was determined by Bradford assay. In brief, ascending concentrations of a BSA stock solution (1 mg/ml in PBS) were used as standard with a range from 10 µg/ml to 200 µg/ml. 20 µl of the standard concentration and different protein sample dilutions (ranging from 1:100 to 1:1,000) were applied to a 96-well ELISA microplate (Nunc, Max-isorb) followed by adding 100 µl of Bradford reagent to each well. The plate was incubated for 5-10 min at RT. The extinction was measured at a wavelength of 595 nm using a microplate reader (Dynatech Laboratories) and the protein concentrations of the samples were calculated using linear regression analysis. Finally, protein samples were prepared for western blot analysis by adding SDS and β-mercaptoethanol. Finally, the samples were boiled at ~90°C for 10 min and stored at -20°C until use.

2.2.10. SDS PAGE and western blot analysis

Before use protein samples were thawed at 37°C. 20 µg of proteins were loaded on 4-12 % polyacrylamide gradient gels, produced by stacking 4 % and 20 % gels and separated with 10 mA (per gel), 240 V for 1 h. During the last minutes of the gel electrophoresis, nitrocellulose membranes and Whatman® papers were equilibrated in the respective blotting buffers (semidry or tank blot running buffer, see 2.1.2.). After assembling of the blotters, the proteins were transferred onto the nitrocellulose membranes with 100 mA, 40 V, 10 W for 1h (semidry blot) or 100 mA, 100 V, 10 W for 12 h at 4°C (tank blot). To avoid overheating, the tank blotter was placed in a box filled with ice and water and placed in the cold room overnight. After successful transfer, remaining unspecific binding sites were blocked by incubation with 5 % milk in TBS-T for 1 h at RT.

Subsequently, the membranes were incubated with the primary antibodies (anti-Nogo-A, 5 µg/ml; anti-GluR1, 1:1,000; anti-GAPDH, 1:15,000) diluted in TBS-T at 4 °C overnight. The next day, the membranes were washed 5-10x with TBS-T and incubated with the respective HRP-conjugated secondary antibodies (anti-mouse HRP and anti-rabbit HRP, both 1:20,000) followed by washing 5-10x with each TBS-T, TBS-X and water. After removing the remaining water with Whatman® paper, the membranes were incubated with Luminata™ to start the enzymatic reaction for 2 min at RT. The X-Ray film development was achieved by placing an undeveloped film onto the membrane for different amounts of time (ranging from 10 seconds to 5 minutes). The film was developed in developer solution for 2 min, briefly washed with water and fixed with fixing solution for 1 min (see buffers and media section 2.1.2.). HeroLab EASY RH was used to image the developed film and densitometry analysis was performed in Easywin32. A student's t-test was used to assess the statistical significance of the differences between the treatments.

2.2.11. Time-lapse imaging and analysis of CA3 apical dendrites in OHCs

CA3 neurons of organotypic hippocampal slice cultures were electroporated to express eGFP-F as described above. Slices were transferred to an open imaging chamber (Series 20 Chamber RC-22; width: 8 mm, Warner Instruments) maintained at 32°C and continuously perfused with ACSF (1 ml/min). Before imaging, the slices were let to adapt for 30 minutes. To avoid movement, the slices were held down with a harp (Warner Instruments). Imaging was performed under an Olympus BX61W1 confocal microscope equipped with a 60x water immersion objective (NA 1.0) and controlled by the FluoView 1,000 software. eGFP-F was excited with an Argon laser (488 nm) and images were acquired every hour for 3 h. Right after the first image, control antibody or Nogo-A neutralizing antibody (5 µg/ml) with or without TTX (1 µM) were applied. To examine dendritic spine morphology, z stacks of second order apical dendritic branches of CA3 pyramidal neurons were imaged at 0.35 µm per z-section with a zoom of 6 to a final pixel size of 0.047 µm. Confocal images underwent deconvolution in AutQuantX2 (Media Cybernetics Inc.) and dendritic spine density, spine head size and spine length were quantified in ImageJ: in detail, spine density was assessed using the "Multi-point Tool", head size was measured by placing straight lines on the diameter of the spine head and length was measured by placing segmented lines from the base of the neck (close to the dendrite) up to the tip of the spine head. All parameters were averaged per

dendrite. Statistical analysis was performed in Prism 5 using a Two-Way repeated measures ANOVA followed by a post hoc Tukey's Multiple Comparisons test.

2.2.12. Morris Water Maze (MWM) spatial learning paradigm

The Morris Water Maze task was used to test for spatial learning in mice. In this task rodents swim to escape a circular pool onto a safe platform by navigation via visual cues (Morris, 1981; Morris, 1984). In this thesis, wildtype and Nogo-A KO mice were trained to locate a hidden platform (10 cm in diameter) for 2 or 10 consecutive days in a pool (160 cm in diameter, 60 cm in height) filled

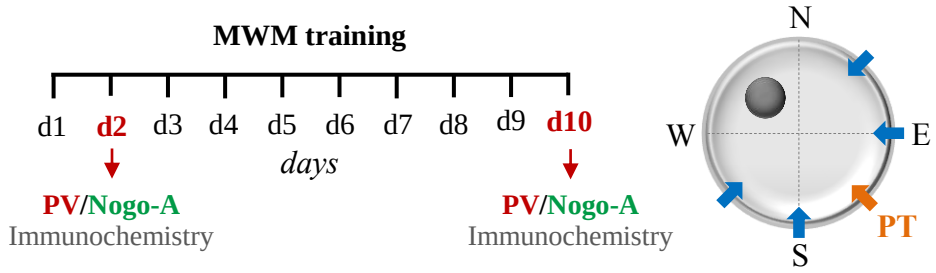

Figure 9: **Morris Water Maze experimental design and starting locations in the maze.**

Mice were trained for 2 or 10 days before immunohistochemistry was performed. At each day of the 10 days learning paradigm mice were put into the maze from 4 starting locations (blue arrows). The platform position was permanently located in the NW quadrant while the starting position of the probe trial (PT, orange) was located in the SE.

with opaque water (Titanium dioxide, Euro OTC Pharma) at ~22°C (Figure 9). In experiments where Nogo-A was conditionally knocked out (cKO) only in excitatory (CaMKII-cre/Nogo-$A^{flox/flox}$) or PV^{+} inhibitory neurons (PV-cre/Nogo-$A^{flox/flox}$), a modified paradigm was used where the mice were pre-trained for 3 days followed by 8 consecutive days of training. In all experiments three visual cues were set up around the pool for spatial navigation. The platform was localized in the NW quadrant and the mice were released into the pool from 4 different positions (SW, S, E, NE; Figure 9) whose order was changed daily. Each day consisted of 4 trials of each 60 seconds with an inter-trial interval of 5-10 min. The task was recorded by a camera above the pool and captured with the VideoMot2 tracking software (TSE Systems). The time from entering the pool to climbing onto the platform was measured and averaged per animal and day. In experiments where cKO mice were used (see section 3.4.) a probe trial (PT) was performed: in detail, on day 3 and day 9 the platform was removed from the pool and the mice swam for 60 seconds entering the

pool from the probe trial position (SE quadrant, Figure 9). The amount of time the mice spent in each of the four quadrants and the number of times they crossed the previous platform position were measured. Statistical differences of the latency over the training days were examined using a Two-Way repeated measures ANOVA and statistical differences of the amount of time spent in the different quadrants as well as the platform crossings during the probe trials were assessed using a Student's t-test.

2.2.13. Whole brain fixation

Fixation of the brain was achieved by transcardial perfusion with 4 % PFA. In brief, 2-4 month old male mice either untrained (swim controls), trained for 2 days or trained for 10 days in the MWM were euthanized with CO_2. The thorax was opened and heart was exposed before cutting the right atrium to let the blood escape the circulatory system. Immediately, the mouse was perfused with 4 % ice-cold PFA in PB through a butterfly needle placed into the left ventricle. Perfusion was maintained until the body of the mouse was completely stiff and the liver had lost its deep red color. Subsequently, the mouse was decapitated, the hippocampus was dissected and post-fixed in 4 % PFA in PB at 4°C for 2 h followed by dehydration in 30 % sucrose diluted in 0.1 M PB at 4°C overnight.

2.2.14. Cryotome sectioning and immunohistochemistry

Whole brain fixation was carried out as described above. After overnight dehydration, the hippocampi were embedded in Tissue-Tek© (Sakura), rapidly frozen at -80°C for 1 h and either immediately processed or stored at -20°C until use. The frozen hippocampi were attached to the cutting block using Tissue-Tek© and placed in the cryostat microtome (Leica, CM3050S) chamber maintained at -18°C. 30 µm hippocampal sections were cut and separated in 3 groups along the dorso-ventral axis (dorsal, mid and ventral) and collected in 12 well-plates filled with PBS. To prevent unspecific binding, the sections were incubated in blocking solution containing 0.3 % Triton X-100, 10 % goat serum and 1 % BSA in PBS for 1 h at RT. Subsequently, the sections were incubated with the primary antibodies (mouse anti-Nogo-A H300, 1:400; mouse anti-PV, 1:5,000) diluted in PBS containing 0.1 % Triton X-100 and 10 % goat serum at 4°C overnight. To prevent evaporation, the plates were sealed with Parafilm. The following day, the sections were

washed 6 times for 5 minutes with PBS and incubated with the respective secondary antibodies (anti-rabbit Cy2 and anti-mouse Cy3, both 1:500) diluted in PBS for 2 h at RT on a shaker. Again the sections were washed with PBS several times before they were mounted onto glass slides using Fluoro-Gel (Electron Miscroscopy Sciences).

2.2.15 Imaging and analysis of PV and Nogo-A immunofluorescence

Stained hippocampal cryosections were imaged using an Olympus BX61W1 confocal microscope equipped with a 40X oil immersion objective (UPlanFL N.A. 1.30) and the FluoView 1,000 software. The fluorophores were excited at wavelengths of 488 nm (Cy2) and 559 nm (Cy3). Z-stacks of the CA3 region were imaged with a step size of 2 µm, a pixel size of 0.621 µm for a final,

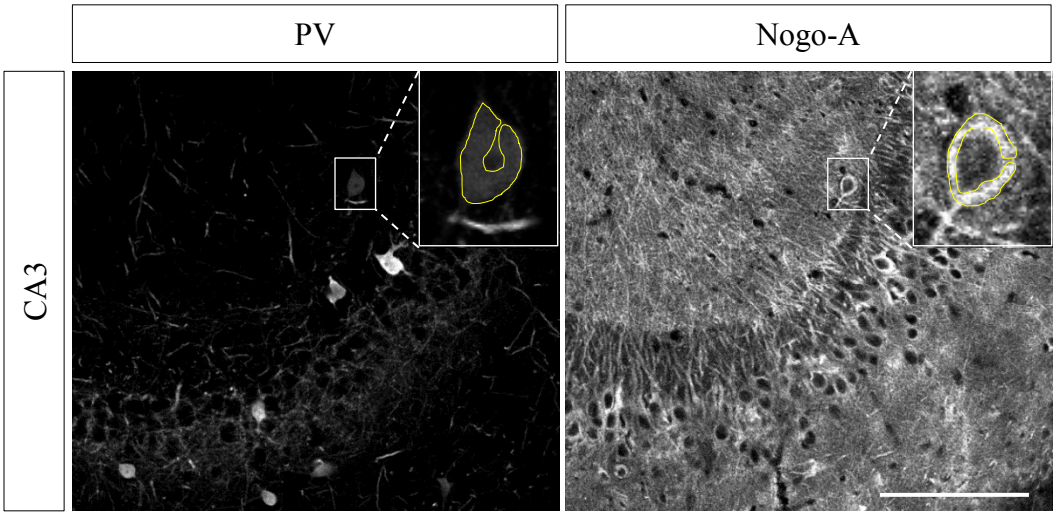

Figure 10: Analysis of Nogo-A and PV immunofluorescence in PV$^+$ interneurons.

Parvalbumin (left) and Nogo-A (right) immunofluorescence of PV$^+$ interneurons was determined by drawing ROIs around the somata and the mean grey value was quantified. Scale bar is 100 µm.

single image size of 496.8 x 496.8 µm (800 x 800 pixels). To reliably quantify changes in Nogo-A and PV immunofluorescence, an imaging and analysis protocol was adapted from (Donato et al., 2013; Çalişkan et al., 2016). In brief, laser power was set for individual sections in a way that < 20 % of the pixels belonging to the brightest PV/Nogo-A cells were saturated. Quantification of PV and Nogo-A fluorescence intensities was performed in ImageJ by manually drawing ROIs around the PV and Nogo-A immunofluorescence signal of the cell body of PV$^+$ interneurons crossing the focal plane at which the nucleus reached its biggest diameter (Figure 10). The background was measured in the same plane as the PV/Nogo-A immunofluorescence measuring ROIs within the

extracellular space of the *stratum radiatum* or *stratum oriens* and subtracted from the mean grey value individually for each cell. The PV^+ interneuron with the highest PV or Nogo-A fluorescence intensity was set to 100 % and the respective intensity values of the other PV^+ cells were normalized accordingly for each section (note that these can be two different PV^+ interneurons for PV and Nogo-A fluorescence, respectively). Further, the normalized PV and Nogo-A fluorescence intensities were grouped in 4 different sub-categories first described by Donato and colleagues (Donato et al., 2013): low (0-25 %), intermediate low (25-50 %), intermediate high (50-75 %) and high (75-100 %). For each animal, 3 sections per area (dorsal, mid, ventral) were imaged and analyzed. Statistical analysis was performed in Prism 5. Statistical differences between groups in their cumulative frequency distribution were assessed by a Kolmogorov-Smirnov test. Differences in the amount of the different sub-categories were analyzed by a One-Way ANOVA (inside one group) or by a Two-Way ANOVA (between groups) followed by a Bonferroni post hoc test.

Results

Learning and memory processes in the hippocampus are tightly regulated by the interplay between excitation and inhibition. To better understand the molecular mechanisms regulating this delicate balance, this thesis addresses the role of Nogo-A, a known inhibitor for synaptic plasticity, in the regulation of structural plasticity at dendritic spines as well as of both excitatory and inhibitory synaptic transmission in the hippocampus. Further, the involvement of Nogo-A in spatial learning and memory formation with special focus on its possible ability to regulate the parvalbumin interneuron network was examined.

3.1. Activity-dependent function and synaptic localization of Nogo-A

3.1.1. Activity-dependent regulation of dendritic spine architecture and number upon Nogo-A loss-of-function

Nogo-A signaling has been shown to control dendritic spine number and morphology in the hippocampus under basal conditions. For example, upon loss-of-function of Nogo-A or either of its receptors NgR1 and S1PR2 spine number and length of CA3 pyramidal neurons increased over the range of hours (Kellner et al., 2016). However, whether these changes occur in an activity-dependent manner remained obscure until now. Structural plasticity at dendritic spines was shown to be activity-dependent (for review see Butz et al., 2009). Therefore, in order to examine the relationship between neuronal activity and the regulatory mechanism of Nogo-A on dendritic spine architecture, changes in spine number and morphology of secondary branched, apical dendrites of CA3 pyramidal neurons were examined. Via live-imaging spine changes upon Nogo-A loss-of-function or control treatment in absence or presence of the sodium channel blocker tetrodotoxin (TTX) were monitored every hour for up to 3 hours.

Under control conditions spine density slightly decreased over time and reached a -3 % reduction after 3 hours while Nogo-A loss-of-function led to a regular increase in spine density up to +7 % 3 hours after antibody application that was significantly higher compared to the control treatment (Figure 11A and 11B, black vs. red: 1 h: $p < 0.05$, 2 h and 3 h: $p < 0.001$, Table 1). These results

are in line with recently published data from our group (Kellner et al., 2016). When TTX was added under both conditions, spine density remained unchanged over time upon control treatment (Figure 11A and 11B, blue, Table 1). Nogo-A loss-of-function led to a slight increase in spine number (+2 % after 3 hours, green) which was though not significantly different from control conditions (Figure 11A and 11B, Table 1). When comparing the control treatments with and without TTX, a significantly lower spine density was observed in the absence of TTX after 3 hours (Figure 11A and 11B, black vs. blue: 3 h: $p < 0.05$, Table 1). Interestingly, comparing the Nogo-A loss-of-function approaches, co-treatment with TTX led to a significantly lower increase in spine density over time (Figure 11A and 11B, red vs. green: 2 h: $p < 0.01$, 3 h: $p < 0.001$, Table 1).

Furthermore, dendritic spine length was found to remain unaltered under control conditions in absence of TTX over the time course of 3 hours (Figure 11A and 11C, black, Table 1). In contrast, upon Nogo-A loss-of-function a steady increase in spine length was observed that reached +12 % after 3 hours and which was significantly increased compared to the control treatment (Figure 11A and 11C, black vs. red: 1 h: $p < 0.01$, 2 h and 3 h: $p < 0.001$, Table 1). When TTX was added to both treatments, spine length remained unaltered under control conditions while Nogo-A loss-of-function resulted in a slight increase (+3 % after 2 and 3 hours) that was significantly different from the control treatment (Figure 11A and 11C, blue vs. green: 2 h and 3 h: $p < 0.05$, Table 1). Similarly to the change in spine density, TTX application resulted in a significantly lower increase in spine length upon Nogo-A loss-of-function (Figure 11A and 11C, red vs. green: 2 h: $p < 0.01$, 3 h: $p < 0.001$, Table 1).

Finally, dendritic spine head width was not altered under all analyzed conditions over the time course of 3 hours (Figure 11A and 11D, Table 1). Altogether, these results indicate that while the alterations in dendritic spine number upon Nogo-A loss-of-function require neuronal activity, the changes in spine morphology observed under these conditions are only partially dependent on neuronal activity.

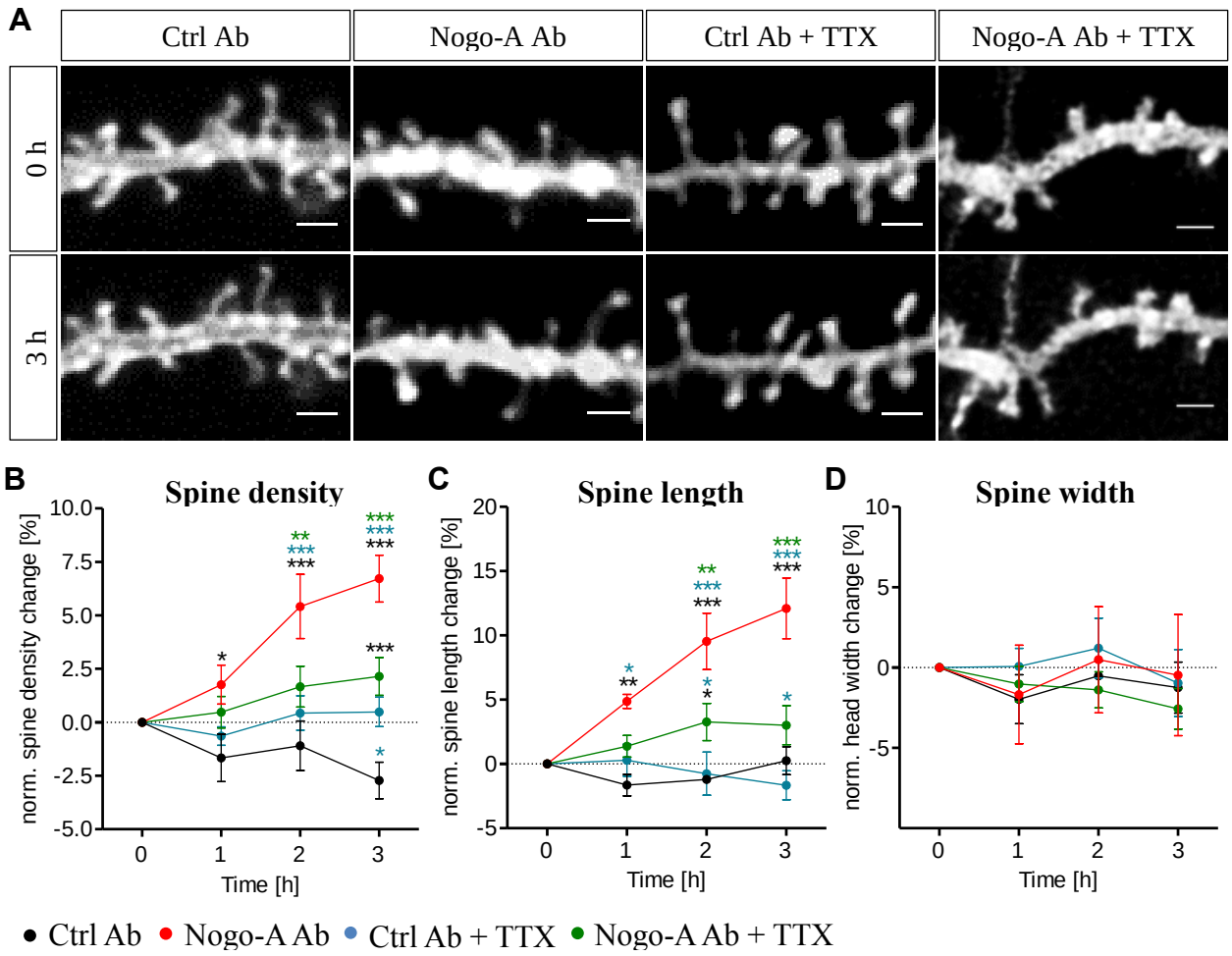

Figure 11: Alterations in dendritic spine architecture and number upon Nogo-A loss-of-function are in part activity-dependent.

(A) Representative secondary branched apical dendrites before (0h, upper panel) and 3 h after control antibody or Nogo-A neutralizing antibody application with and without TTX (3h, lower panel). Scale bars are 2 µm. (B-D) Normalized dendritic spine density (B), length (C) and width changes (D) upon control antibody application without (black) or with TTX (blue) and Nogo-A neutralizing antibody application without (red) or with TTX (green). All data are presented as mean ± SEM. *p < 0.05, **p < 0.01, ***p < 0.001.

3.1.2. Activity-dependent localization of Nogo-A at synapses

The previous findings suggest that the activity of Nogo-A on dendritic spine architecture and number requires in part neuronal activity (chapter 3.1). This raises the question whether the localization of Nogo-A itself at synapses is regulated in an activity-dependent manner. Therefore, acute hippocampal slices were prepared from 2-4 months old C57BL/6 WT mice, treated with 55 mM KCl to increase neuronal activity and the synaptosomal fractions were isolated. Western blot analysis revealed that the amount of Nogo-A protein decreased by ~40 % when the slices were treated with KCl compared to control conditions (Figure 12A, Ctrl: 1.000 ± 0.031; KCl: 0.582 ± 0.062; $p < 0.01$), indicating that synaptic Nogo-A is regulated in an activity-dependent manner.

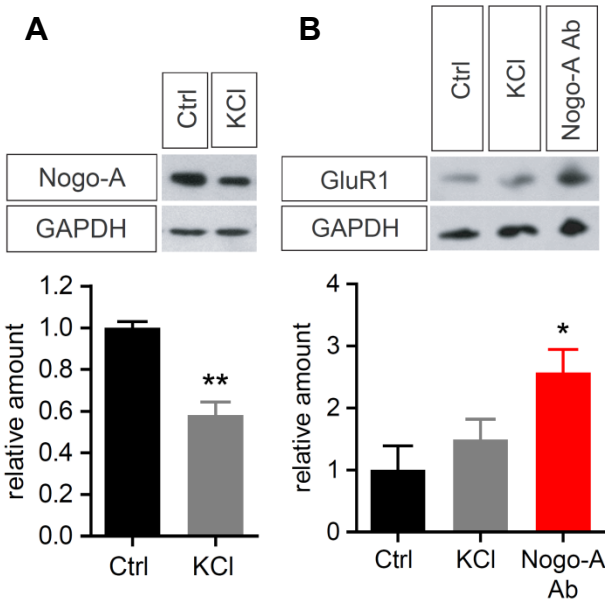

Figure 12: **Activity-dependent localization of Nogo-A at synapses.**

(A) Western blot (above) for Nogo-A and GAPDH in synaptosomes from acute hippocampal slices treated (n = 4) or not (n = 4) with 55 mM KCl. The graph shows quantification for the relative protein abundance (below). (B) Western blot (above) for GluR1 and GAPDH in synaptosomes from acute hippocampal slices with either control antibody (n = 5), 55 mM KCl (n = 5) or Nogo-A function blocking antibody (n = 3) and quantification for the relative protein amount (below). All data are presented as mean ± SEM. *$p < 0.05$, **$p < 0.01$.

3.2. Role of Nogo-A in regulating synaptic transmission in the hippocampus

3.2.1. Nogo-A regulates AMPAR localization at synapses and AMPAR-mediated excitatory synaptic currents in the hippocampus

Nogo-A and its receptor NgR1 have been shown to regulate AMPAR localization at synapses and their insertion into the postsynaptic membrane (Jitsuki et al., 2016; Kellner et al., 2016). However, this has been shown either by patch clamp electrophysiology after knockdown of NgR1 for one week (Jitsuki et al., 2016) or via live imaging of postsynaptic AMPAR clusters upon acute Nogo-A loss-of-function (Kellner et al., 2016). To directly examine rapid changes in AMPAR protein levels at synapses, the subunit GluR1 was quantified in synaptosomes upon loss-of-function for

Nogo-A. While increasing neuronal activity via application of 55 mM KCl slightly increased GluR1 protein levels as frequently reported (for review see Kessels and Malinow, 2009), blocking Nogo-A signaling led to a ~2.5-fold increase in GluR1 at synapses (Figure 12B, Ctrl: 1.000 ± 0.390; KCl: 1.489 ± 0.331; Nogo-A Ab: 2.571 ± 0.378, $p < 0.05$) suggesting a role of Nogo-A in modulating excitatory synaptic transmission as described in (Kellner et al., 2016). Further, whole-cell patch clamp of CA3 hippocampal neurons in 21-24 DIV organotypic mouse hippocampal slice cultures was performed to record miniature excitatory postsynaptic currents (mEPSCs) to investigate whether the regulation of AMPARs by Nogo-A resulted in a change in excitatory transmission. Indeed, Nogo-A loss-of-function resulted in a rapid increase in the amplitude of mEPSCs by ~15 % already after 10 minutes compared to control conditions (Figures 13A and 13B, 10 min: $p < 0.0001$, 15 min: $p < 0.05$, Table 2) without affecting mEPSC frequency (Figures 13A and 13C, Table 2).

In summary, these results indicate that Nogo-A regulates AMPAR localization at synapses and, ultimately, AMPAR-mediated excitatory synaptic transmission at CA3 pyramidal neurons on a fast time scale.

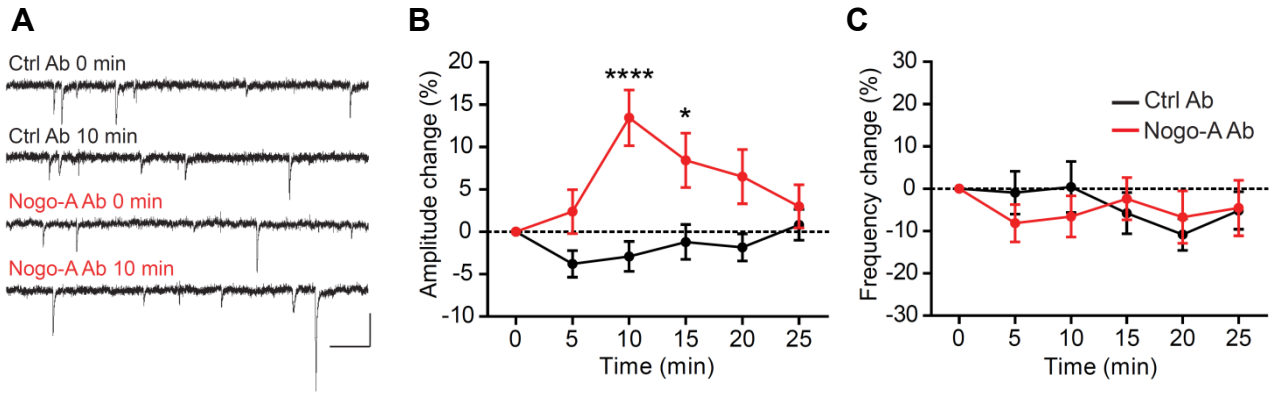

Figure 13: **Nogo-A restricts excitatory synaptic transmission in CA3 hippocampal neurons.**

(A) Example mEPSC recordings before and 10 minutes after application of either control or Nogo-A function blocking antibody. Scale bars are 20 pA and 200 ms. (B, C) mEPSC amplitude (left) and frequency (right) percent change upon control (black, n = 10) or Nogo-A blocking antibody (red, n = 11, ANOVA treatment $p < 0.01$ $F_{1,19} = 14.13$). All data are presented as mean ± SEM. *$p < 0.05$, **** $p < 0.0001$.

3.2.2. Nogo-A strengthens inhibitory synaptic transmission at CA3 pyramidal neurons via the S1PR2

The above findings and other recent studies (Jitsuki et al., 2016; Kellner et al., 2016) found that Nogo-A is involved in the regulation of excitatory synaptic transmission. However, it has been reported that Nogo-A is abundantly expressed in a subtype of inhibitory neurons in the hippocampus, namely the parvalbumin-positive interneurons (Zagrebelsky et al., 2016). This observation raised the question of whether Nogo-A is not only involved in the regulation of excitatory but also inhibitory, GABAergic synaptic transmission. Therefore, whole-cell patch clamp of CA3 pyramidal neurons was performed to record miniature inhibitory synaptic currents (mIPSCs). Nogo-A loss-of-function resulted in a rapid decrease in mIPSC amplitude beginning 5 minutes after antibody application and reaching a reduction of ~15 % compared to control antibodies (Figures 14A and 14E, 5 min: $p < 0.05$; 10-20 min: $p < 0.0001$, Table 2). The mIPSC frequency was also significantly reduced by ~10 % 10 and 15 minutes after antibody application (Figures 14A and 14I, 10 and 15 min: $p < 0.05$, Table 2).

To further analyze the regulation of inhibitory transmission by Nogo-A, a gain-of-function approach was used for the Nogo-A NiG-Δ20 domain by application of the soluble Δ20 inhibitory peptide. After infusion of the Δ20 peptide, mIPSC amplitude was significantly increased relative to the control treatment (Figures 14B and 14F, 5 min: $p < 0.05$, Table 2) without affecting the mIPSC frequency (Figures 14B and 14J, Table 2), confirming the observed regulation of inhibitory synaptic transmission through Nogo-A signaling.

Next, to assess whether the regulation of inhibition by Nogo-A is mediated by its signaling via the S1PR2, NgR1 or both, loss-of-function approaches for either of the two receptors were applied and examined. On the one hand, treatment with the S1PR2 antagonist JTE013 resulted in a rapid, significant decrease in mIPSC amplitude starting at 5 and peaking at 15 minutes with a reduction of ~10 % relative to the control condition (Figures 14C and 14G, 10 min: $p < 0.01$; 15 min: $p < 0.05$, Table 2), comparable to the one observed upon blocking Nogo-A. Moreover, mIPSC frequency was significantly overall decreased (Figures 14C and 14K, Table 2). On the other hand, when a function-blocking antibody against NgR1 was used, no alterations could be observed in mIPSC amplitude (Figures 14D and 14H, Table 2) and frequency (Figures 14D and 14L, Table 2). In summary, these findings indicate that Nogo-A strengthens GABAergic inhibitory synaptic transmission in the hippocampus via its receptor S1PR2, suggesting a Nogo-A-Δ20 specific effect in this context.

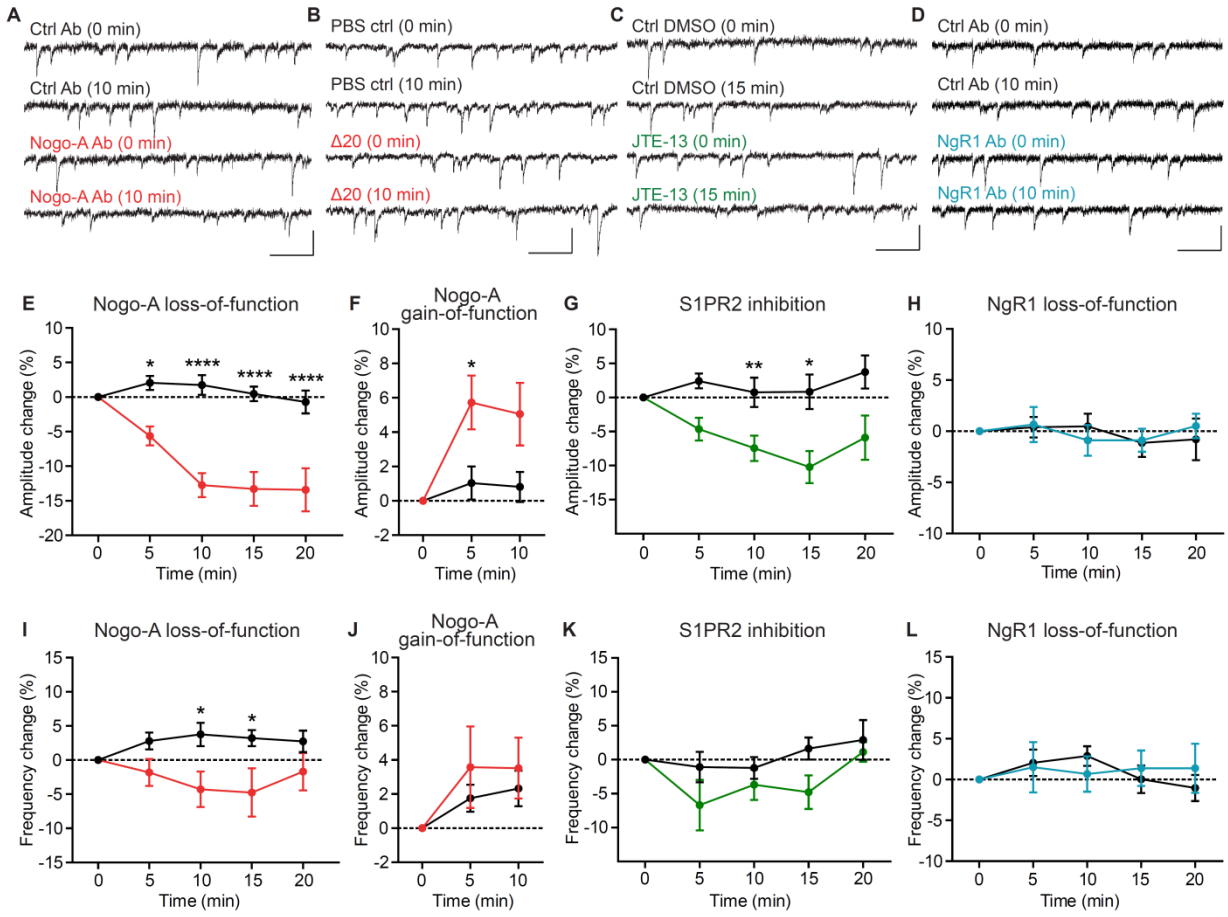

Figure 14: **Nogo-A strengthens inhibitory synaptic transmission in CA3 neurons via S1PR2.**

(A-D) Example mIPSC recordings in organotypic hippocampal slice cultures before and after Nogo-A loss-of-function (A, red), Nogo-A gain-of-function (B, red), S1PR2 loss-of-function (C, green), NgR1 loss-of-function (D, blue) and the respective controls (black). Scale bars are 20 pA vertical and 200 ms horizontal. (E-L) Normalized mIPSC amplitude (top) and frequency (bottom) change in percent upon Nogo-A loss-of-function (E, ANOVA treatment $p < 0.0001$ $F_{1,17} = 45.32$; I, ANOVA treatment $p < 0.05$ $F_{1,17} = 6.834$, n = 9, red), Nogo-A gain-of-function (F, ANOVA treatment $p < 0.05$ $F_{1,21} = 7.905$; J, n = 11, red), S1PR2 loss-of-function (G, ANOVA treatment $p < 0.001$ $F_{1,18} = 21.72$; K, ANOVA treatment $p < 0.05$ $F_{1,18} = 6.365$, n = 11, green), NgR1 loss-of-function (H and L, n = 12, blue) and respective controls (E and I, n = 10; F and J, n = 12; G and K, n = 9; H and L, n = 13, black). All data are presented as mean ± SEM. *$p < 0.05$, **$p < 0.01$, ****$p < 0.0001$.

3.2.3. Nogo-A signaling promotes $GABA_AR$ clustering at synapses via its receptor S1PR2

The strength and efficacy of inhibitory synaptic transmission has been shown to depend on the clustering of $GABA_ARs$ at GABAergic inhibitory synapses (Nusser et al., 1997; Kilman et al., 2002). Therefore, the number and the localization of $GABA_ARs$, particularly in spatial proximity

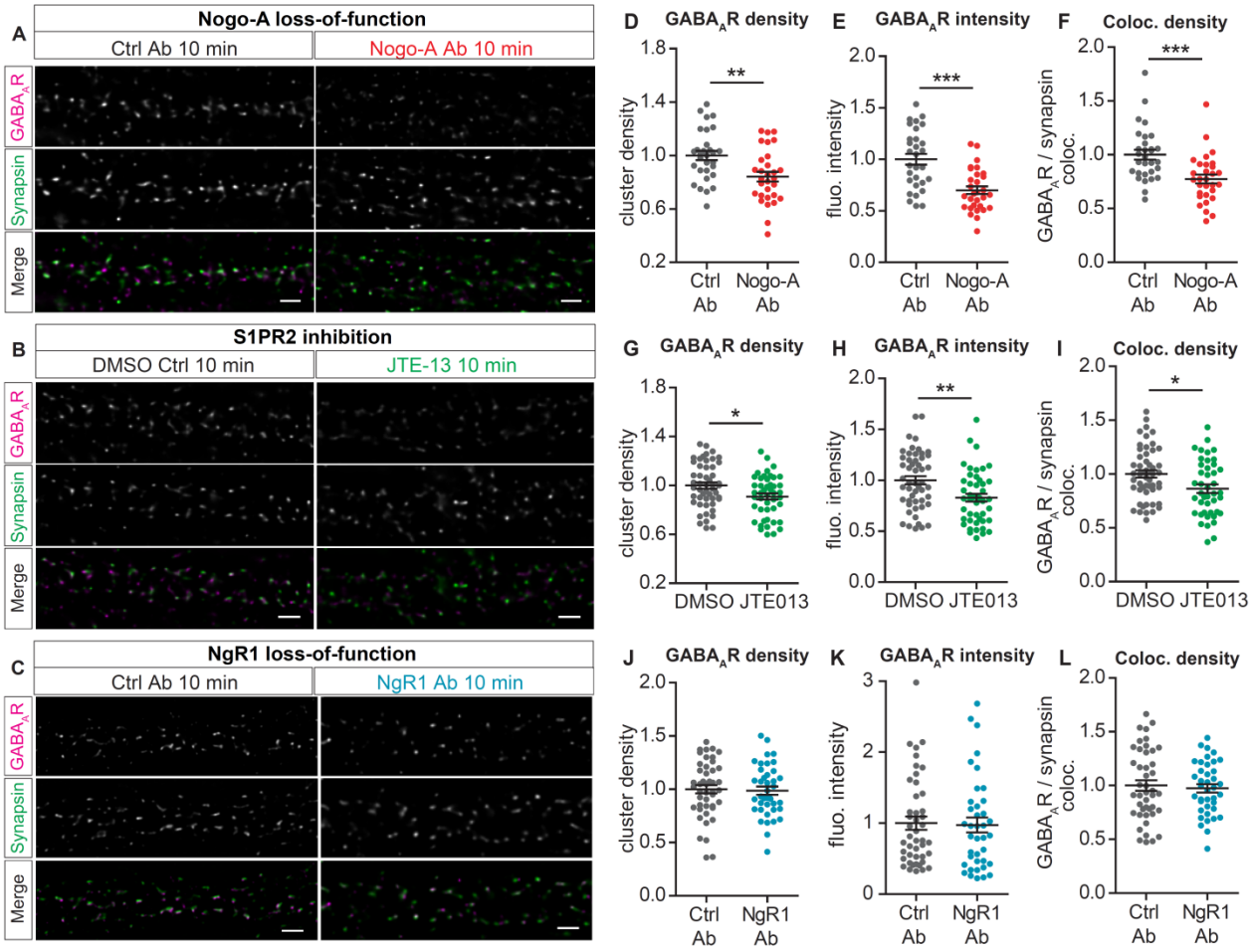

Figure 15: **Nogo-A signaling promotes $GABA_AR$ clustering at synapses via the S1PR2.**

(A-D) Live-cell immunolabeling of surface $GABA_ARs$ (magenta) and immunofluorescence for synapsin (green) treated for 10 minutes with control (A, left) or Nogo-A function blocking antibody (A, right), DMSO (B, left) or S1PR2 inhibitor JTE-13 (B, right), control (C, left) or NgR1 neutralizing antibody (C, right). For illustration, all images underwent deconvolution and were equally increased in brightness and contrast by the same absolute values for visibility. Scale bar is 2 µm. (D-L) Normalized $GABA_AR$ cluster density, fluorescence intensity and density of colocalized $GABA_AR$ and synapsin-positive puncta upon Nogo-A loss of function (D-F, red, n = 30; Ctrl Ab, grey n = 30), S1PR2 loss-of-function (G-I, green, n = 43; DMSO Ctrl, grey, n = 51) and NgR1 loss-of-function (J-L, blue, n = 39; Ctrl Ab, grey, n = 45). Data are presented as mean ± SEM. *p < 0.05, **p < 0.01, ***p < 0.001.

to presynaptic terminals, were examined upon acute blockade of Nogo-A signaling. To visualize surface receptors, live-cell immunolabeling against the extracellular part of the γ2 subunit of $GABA_AR$s was used in 21-25 DIV primary mouse hippocampal neurons (Figures 15A-C). Nogo-A loss-of-function via function blocking antibodies for 10 minutes resulted in a significant decrease in $GABA_AR$ cluster density of ~15 % (Figure 15D, $p < 0.01$, Table 3), fluorescence intensity of ~30 % (Figure 15E, $p < 0.001$, Table 3) and $GABA_AR$ colocalization with synapsin-positive puncta of ~20 % (Figure 15F, $p < 0.001$, Table 3) compared to the control condition. Moreover, S1PR2 inhibition via the application of the antagonist JTE013 for 10 minutes led to significant decreases in $GABA_AR$ cluster density of ~10 % (Figure 15G, $p < 0.05$, Table 3), fluorescence intensity of ~20 % (Figure 15H, $p < 0.01$, Table 3) and $GABA_AR$ colocalization with synapsin-positive puncta of ~15 % (Figure 15I, $p < 0.05$, Table 3) compared to a control treatment with DMSO. On the contrary, blocking the signaling via NgR1 with function blocking antibodies for 10 minutes did not alter either $GABA_AR$ cluster density (Figure 15J, Table 3), fluorescence intensity (Figure 15K, Table 3) or $GABA_AR$ colocalization with synapsin (Figure 15L, Table 3) compared to the control condition. Synapsin-positive puncta density (Figures 16A, 16E and 16C) and fluorescence intensity (Figures 16B, 16D and 16F) remained unaltered under all experimental conditions.

These findings indicate that synaptic $GABA_AR$ clustering is promoted by Nogo-A signaling via its receptor S1PR2.

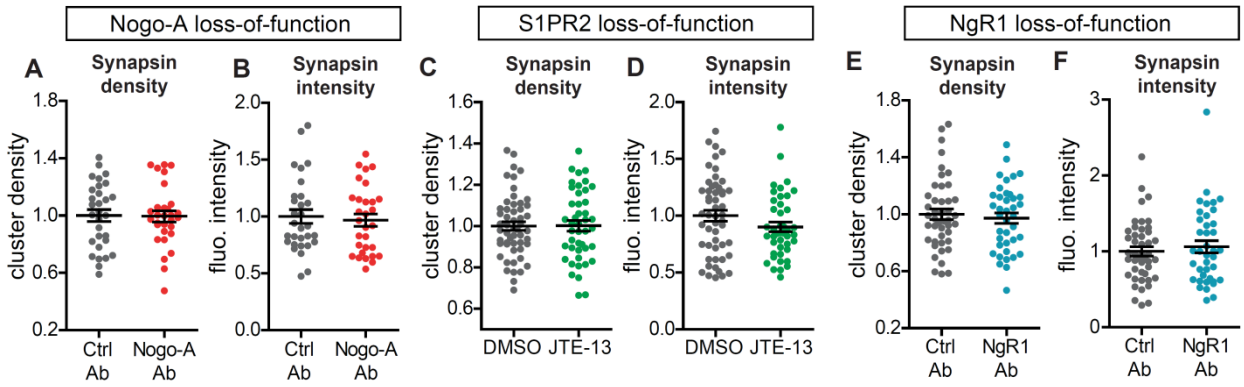

Figure 16: **Nogo-A signaling does not regulate presynaptic synapsin clustering.**

(A) Normalized synapsin density (A, C, E) and fluorescence intensity (B, D, F) upon Nogo-A NiG-Δ20 loss-of-function (A and B, Ctrl Ab, grey: n = 30; Nogo-A Ab, red: n = 30), S1PR2 inhibition (C and D, DMSO Ctrl, grey: n = 53; JTE-13, green: n = 44) and NgR1 loss-of-function (E and F, Ctrl Ab, grey: n = 45; NgR1 Ab, blue: n = 39). All data are presented as mean ± SEM.

3.2.4. Nogo-A loss-of-function increases $GABA_AR$ lateral diffusion dynamics

Inhibitory synaptic transmission is shaped by the localization and lateral mobility of $GABA_ARs$ along the neuronal plasma membrane. In particular, the regulation of the $GABA_AR$ exchange between intra- and extrasynaptic compartments influences the efficacy of inhibitory synaptic connectivity and, ultimately, synaptic strength. Thus, $GABA_AR$ diffusion dynamics were analyzed using a quantum dot-based single particle tracking approach (QD-SPT, Bannai et al., 2006) to examine whether Nogo-A signaling regulates $GABA_AR$ lateral movement. To this purpose, 10-14 DIV primary rat hippocampal neurons were tagged with anti-$GABA_AR$ γ2 antibodies bound to fluorescent QDs. Upon Nogo-A loss-of-function the average membrane surface explored by $GABA_AR$ diffusion was significantly increased 10 minutes after antibody application (Figure 17A, red trajectories, Nogo-A Ab 0 min: 1.000 ± 0.042; 10 min: 1.255 ± 0.104, $p < 0.05$) compared to the control condition (Figure 17A, black trajectories, Ctrl Ab 0 min: 1.000 ± 0.058; 10 min: 0.990 ± 0.072). Furthermore, while the increase in mean square displacement (MSD) of $GABA_ARs$ for neurons treated with control antibodies did not change over time, in neurons treated with Nogo-A blocking antibodies it increased significantly both at synaptic (Figures 18A and 18B, Table 6) and extrasynaptic compartments (Figures 18C and 18D, Table 6). Additionally, the MSD of all trajectories in synaptic and extrasynaptic locations was used (see Material and Methods section 2.2.8.) to calculate the diffusion coefficient (D [$\mu m^2/s$]) of labelled $GABA_ARs$ as a measure of their mobility. Labeled $GABA_ARs$ that had a diffusion coefficient below 0.004 $\mu m^2/s$ were considered immobile. Application of Nogo-A function blocking antibodies led to a significant decrease in the $GABA_AR$ immobile fractions both at synaptic (Figure 17D, 10 min: $p < 0.01$, Table 5) and extrasynaptic sites (Figure 17E, 10 min: $p < 0.05$, Table 5). At the same time, the size of mobile $GABA_AR$ fractions ($D > 0.004$ $\mu m^2/s$) was significantly increased at 5 and 10 minutes after Nogo-A blocking antibody application (Figures 17D and 17E, Table 5), relative to controls (Figures 17B and 17C, Table 5). Interestingly, while under control conditions no alterations in $GABA_AR$ mobility over time were observed (Figures 17F and 17G, Table 4), Nogo-A loss-of-function resulted in a rapid significant increase in the $GABA_AR$ diffusion coefficient at synaptic (Figure 17F, 10 min: $p < 0.05$, Table 4) as well as extrasynaptic compartments (Figure 17G, 10 min: $p < 0.01$; 15 min: $p < 0.05$, Table 4). It is notable that the increase in $GABA_AR$ diffusion coefficient peaked after 10 minutes and returned to baseline after 20 minutes of Nogo-A loss-of-function in comparison to control conditions (Figures 17F and 17G, Table 4).

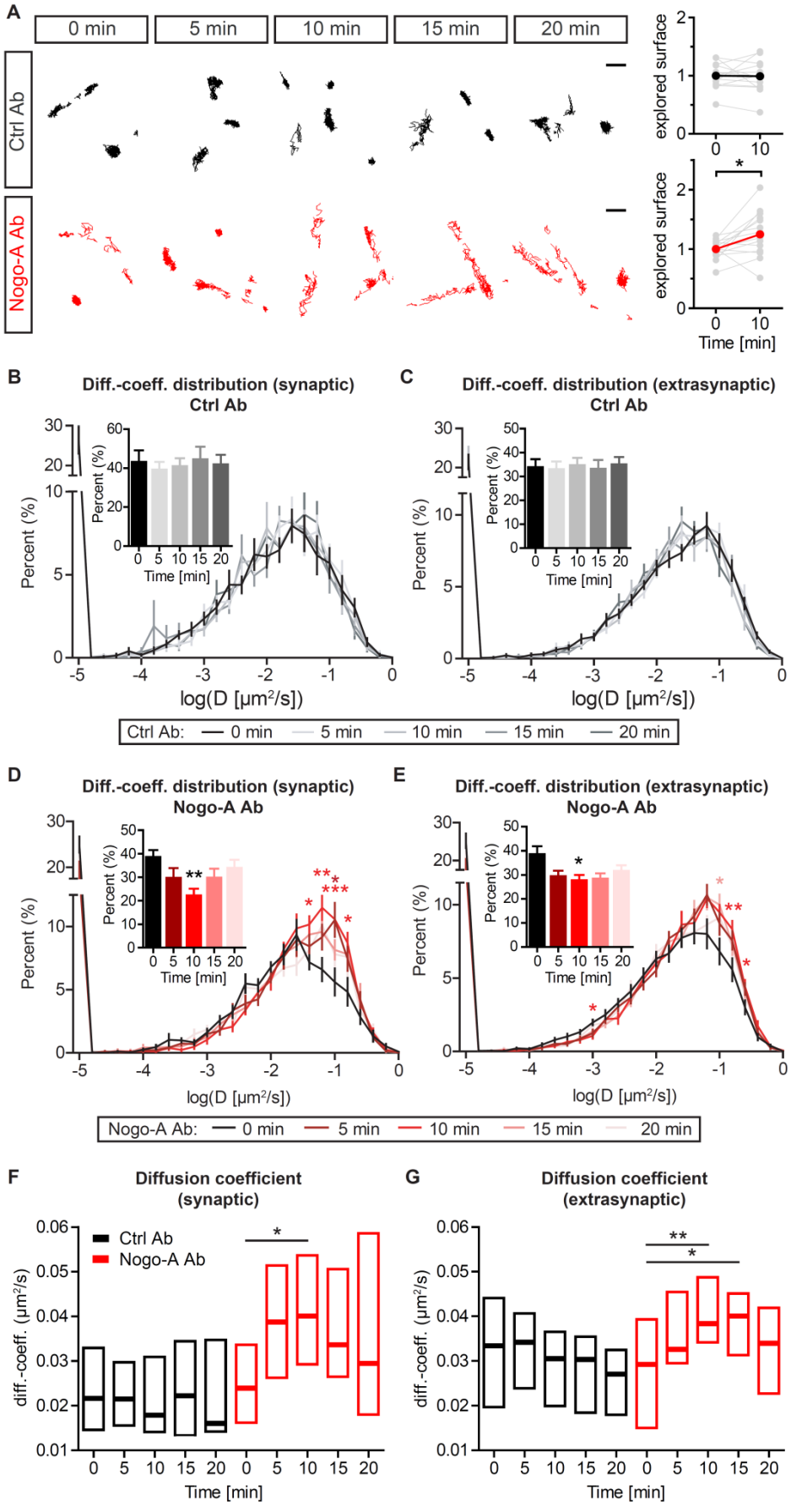
A
0 min
5 min
10 min
15 min
20 min
Ctrl Ab
Nogo-A Ab
explored surface
Time [min]
B
Diff.-coeff. distribution (synaptic)
Ctrl Ab
C
Diff.-coeff. distribution (extrasynaptic)
Ctrl Ab
Percent (%)
log(D [µm²/s])
Time [min]
Ctrl Ab: 0 min 5 min 10 min 15 min 20 min
D
Diff.-coeff. distribution (synaptic)
Nogo-A Ab
E
Diff.-coeff. distribution (extrasynaptic)
Nogo-A Ab
Nogo-A Ab: 0 min 5 min 10 min 15 min 20 min
F
Diffusion coefficient
(synaptic)
G
Diffusion coefficient
(extrasynaptic)
Ctrl Ab
Nogo-A Ab
diff.-coeff. (µm²/s)
Time [min]

Figure 17: **Nogo-A loss-of-function increases $GABA_AR$ diffusion dynamics**

(A, left) Example trajectories of $GABA_AR$-QDs recorded for 30 seconds in 5 minutes intervals up to 20 minutes in primary hippocampal neurons treated either with control (black trajectories) or Nogo-A blocking antibody (red trajectories). Scale bars are 2 µm. (A, right) Normalized average surface explored by QD-$GABA_AR$ upon control (above, black, n = 14) and Nogo-A blocking antibody (below, red, n = 14) at 0 and 10 minutes. (B-E) Percentage of fractions of the logarithmic diffusion coefficient (D, diff.-coeff.) of $GABA_AR$-QDs upon treatment with control (shades of grey) or Nogo-A blocking antibody (shades of red) at synaptic (B, D) and extrasynaptic sites (C, E) in 5 minute intervals and up to 20 minutes. Bar graphs show the percentage of the immobile $GABA_AR$-QD fraction (D < 0.004 µm2/s) over time (Ctrl Ab, n = 13; Nogo-A Ab, n = 14). (F, G) Median diffusion coefficients of QD-$GABA_ARs$ with interquartile ranges (IQR) upon control (black) or Nogo-A blocking antibody (red) at synaptic (F) and extrasynaptic sites (G). Overall 39137 trajectories from 14 different field of views (FOVs, 14 different coverslips from 4 different culture preparations) were analyzed in Nogo-A loss-of-function experiments (synaptic: 0 min = 2782, 5 min = 2664, 10 min = 2687, 15 min = 2253, 20 min = 1848; extrasynaptic: 0 min = 5582, 5 min = 5768, 10 min = 5703, 15 min = 5636, 20 min = 4214). Overall 35193 trajectories from 13 different FOVs (13 different coverslips from 4 different culture preparations) were analyzed in the control antibody treatment (synaptic: 0 min = 2579, 5 min = 2450, 10 min = 2471, 15 min = 2345, 20 min = 1904; extrasynaptic: 0 min = 5181, 5 min = 5052, 10 min = 4465, 15 min = 4895, 20 min = 3851). All data are presented as mean ± SEM if not stated otherwise. *p < 0.05, **p < 0.01, ***p < 0.001.

Furthermore, application of Nogo-A function blocking antibodies resulted in an increase in the confinement of $GABA_ARs$ opposed to the control condition (Figure 18E, Table 7). Taken together, these findings indicate that Nogo-A signaling rapidly modulates $GABA_AR$ diffusion dynamics to promote inhibitory synaptic transmission.

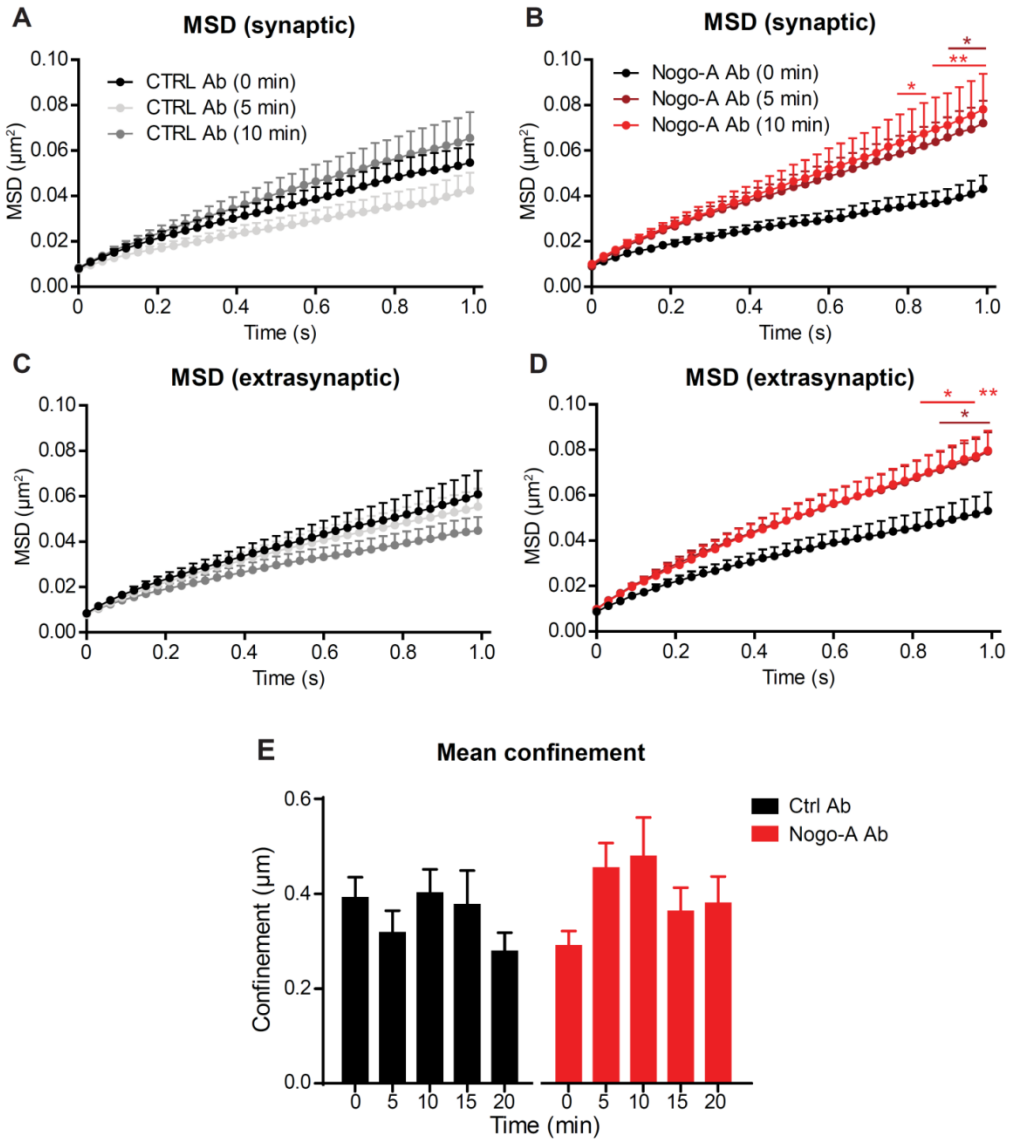

Figure 18: **Nogo-A loss-of-function increases mean square displacement (MSD) and confinement of GABA$_A$Rs in primary hippocampal neurons.**

(A-D) Mean square displacement (MSD) of QD-GABA$_A$Rs in µm^2 analyzed before (time point 0 minutes) and after application (time points 5 and 10 minutes) of control antibody (Ctrl Ab, shades of grey, n = 14) or Nogo-A blocking antibody (Nogo-A Ab, shades of red, n = 14) at synaptic (A and B) and extrasynaptic sites (C and D). (E) Mean confinement for QD-GABA$_A$Rs in µm analyzed before (time point 0 minutes) and after (time points 5 to 20 minutes) application of control antibody (Ctrl Ab, black, n = 11) or Nogo-A blocking antibody (Nogo-A Ab, red, ANOVA treatment x time $p < 0.05$ $F_{4,88} = 2.478$, n = 13). All data are presented as mean ± SEM. *p < 0.5, **p < 0.01.

3.2.5. Nogo-A loss-of-function increases Ca^{2+} dynamics in hippocampal neurons to promote $GABA_AR$ diffusion

Many different functions in neurons are regulated by, and are dependent on Ca^{2+} signaling, among them the transmission of the depolarizing signal and synaptic activity (Brini et al., 2014). Interestingly, Ca^{2+} dynamics and influx into neurons have been described to control $GABA_AR$ clustering and lateral diffusion in hippocampal cultures (Bannai et al., 2009; Bannai et al., 2015). Therefore, Fluo-4 based Ca^{2+} imaging and quantum dot single particle tracking (QD-SPT) of $GABA_ARs$ have been paired and performed within the same neuron in 10-14 DIV primary rat hippocampal cultures (Figure 19A). As expected, Nogo-A loss-of-function resulted in a fast increase in the diffusion coefficient of $GABA_ARs$ at synaptic compartments (Figure 19B, red bars, 5 min and 10 min: $p < 0.01$, Table 8) and showed a trend toward an increase at extrasynaptic sites (Figure 19C, red bars, Table 8) after 5 and 10 minutes opposed to the control condition (Figures 19B and 19C, Table 8). Interestingly, along with the increase in $GABA_AR$ diffusion, blocking Nogo-A signaling resulted in increased mean Fluo-4 intensity (F/F_0) in the dendrites of the imaged neurons (Figure 19D, 5 min: 1.553 ± 0.100; 10 min: 1.768 ± 0.146) that was significantly higher than the one observed for the control treatment after both 5 and 10 minutes (Figure 19D, 5 min: 1.114 ± 0.081, $p < 0.05$; 10 min: 1.315 ± 0.090, $p < 0.01$). When comparing the results per single neuron, a significant positive correlation could be found between the normalized change in $GABA_AR$ diffusion and the normalized change in Fluo-4 intensity upon Nogo-A loss-of-function (Figure 19E, red dots, $R_{Spearman} = 0.650$, $p = 0.022$). Under control treatment, there was a trend towards a positive correlation which was though not significant (Figure 19E, black dots, $R_{Spearman} = 0.429$, $p = 0.114$).

In summary, these data suggest the possibility that Nogo-A restricts Ca^{2+} dynamics in hippocampal neurons to limit $GABA_AR$ lateral mobility and might thereby, ultimately, promote their localization at synapses.

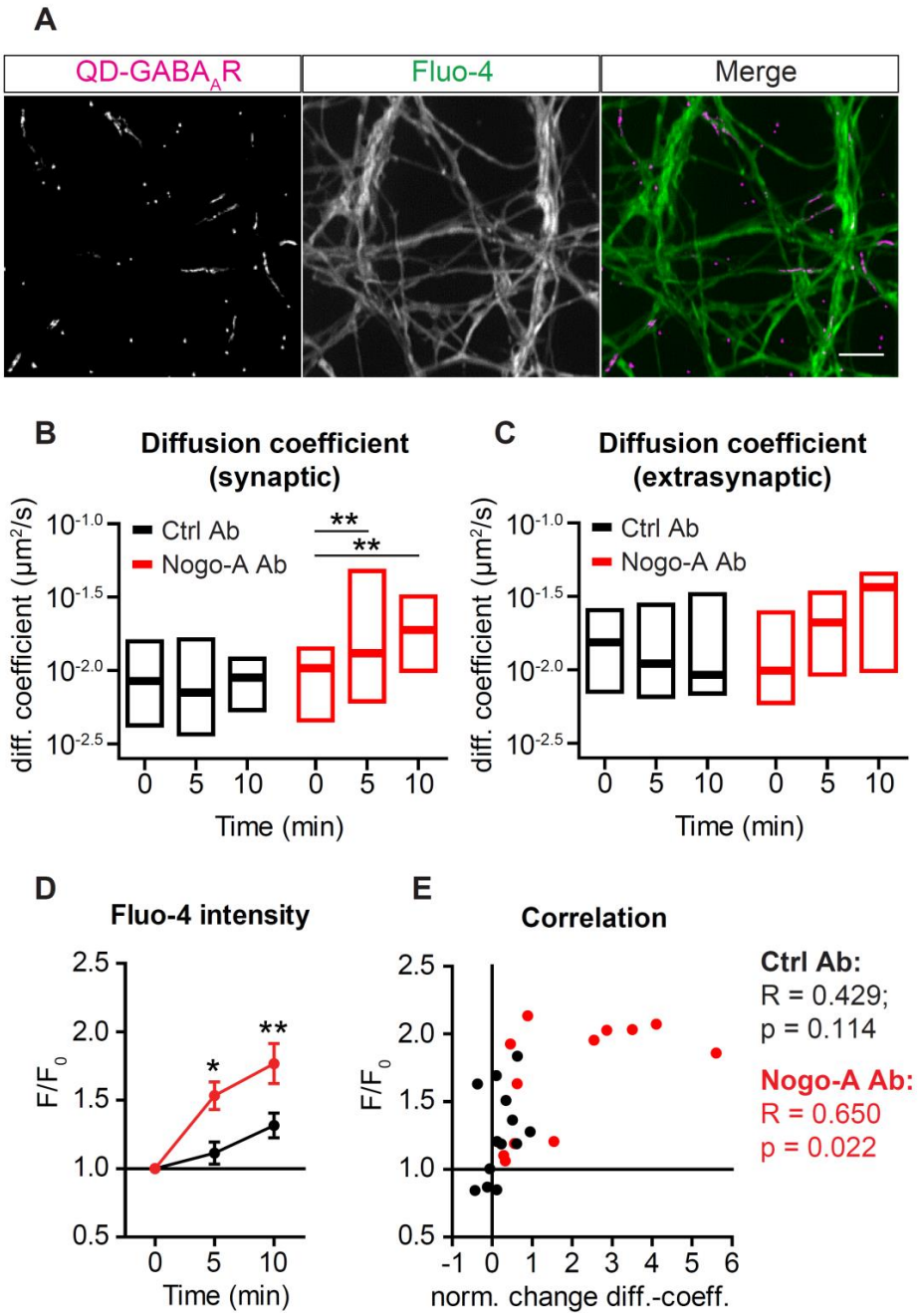

Figure 19: **Nogo-A restricts Ca^{2+} influx and $GABA_AR$ diffusion dynamics in hippocampal neurons.**

(D) $GABA_AR$-QD trajectories over 30 seconds and Fluo-4 fluorescence (maximum projection over 30 seconds) in primary hippocampal neurons. Scale bar is 5 µm. (B, C) Median diffusion coefficients with interquartile ranges (IQR) upon control antibody (B and C, black) or Nogo-A blocking antibody treatments (B and C, red) at synaptic (B) and extrasynaptic compartments (C). (D) Normalized Fluo-4 fluorescence intensity change over time (F/F_0) for control (black, n = 12) and Nogo-A function blocking antibody (red, ANOVA treatment $p < 0.001$ $F_{1,24} = 9.804$, n = 12). (E) Correlation between the peak value for the Fluo-4 fluorescence intensity change (F/F0) and the diffusion coefficient for control (black dots, n = 12) and Nogo-A function blocking antibody (red dots, n = 12). All data are presented as mean ±SEM if not mentioned otherwise. *p < 0.5, **p < 0.01.

3.3. Role of Nogo-A in regulating PV plasticity during learning

3.3.1. PV plasticity is unaltered in Nogo-A KO mice during spatial learning in the MWM

Learning and memory processes in the hippocampus have been shown to rely on changes in the neuronal activity of parvalbumin-positive (PV^+) inhibitory interneuron networks whose activity is mirrored by the expression pattern of PV, as high expression levels of this Ca^{2+}-binding protein are correlated to high inhibitory activity of the interneuron and *vice versa* (Donato et al., 2013; Donato et al., 2015; Karunakaran et al., 2016; for review see Caroni, 2015). Recent studies reported that targeted deletion of NgR1 in PV^+ interneurons is sufficient to retain ocular dominance (OD) plasticity in the visual cortex of mice into adulthood, usually restricted by the closure of the critical period (Stephany et al., 2014; Stephany et al., 2016) and enhances the erasure of fear memory in mice (Bhagat et al., 2016). Therefore, as Nogo-A was found to be abundantly expressed in PV^+ interneurons of the hippocampus (Zagrebelsky et al., 2016), PV plasticity during spatial learning in the Morris water maze (MWM) was examined comparing wildtype and Nogo-a KO mice. To this purpose, a learning paradigm established in the laboratory of Pico Caroni (Donato et al., 2013) was used in which mice were undergoing 4 training trials per day for 10 consecutive days without pre-training. Both WT and Nogo-A KO mice displayed spatial learning of the platform position over the whole training and reached a plateau around day 7-8 of ~7 seconds to locate the platform (Figure 20, Table 9). On days 2-4 WT mice performed slightly better compared to Nogo-A KO

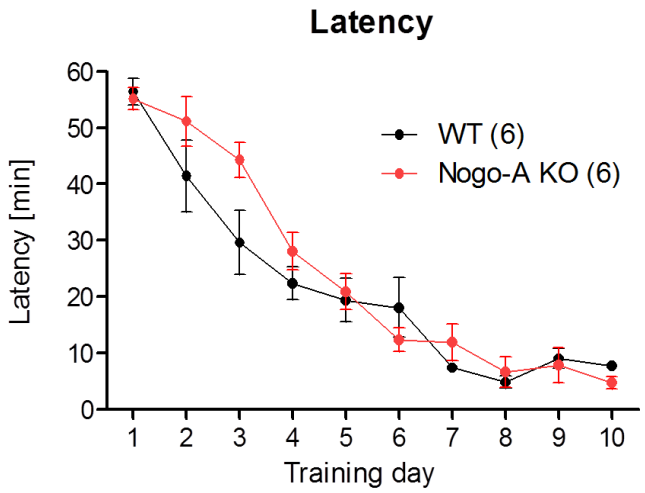

Figure 20: Spatial learning in the MWM is unaltered in Nogo-a KO mice.

Time either WT (black, n = 6) or Nogo-A KO mice (red, n = 6) needed to reach the hidden platform on the indicated day in the MWM. Data are presented as mean ± SEM.

mice. This difference was though not statistically significant (Figure 20, Table 9). Overall, a

reported improved spatial learning in Nogo-A KO mice (Zagrebelsky et al., 2016) could not be observed with the deployed protocol (Donato et al., 2013).

After either 2 or 10 days in the MWM, WT and Nogo-A KO mice were perfused and the dorsal, mid and ventral hippocampal sections were immunohistochemically stained for PV (Figures 21 and 23) and Nogo-A (Figure 23). As previously reported, changes in PV plasticity in the hippocampal CA3 area are crucial for spatial memory formation in the MWM (Donato et al., 2013). Therefore, PV plasticity was examined in the CA3 area. PV fluorescence analysis showed that PV

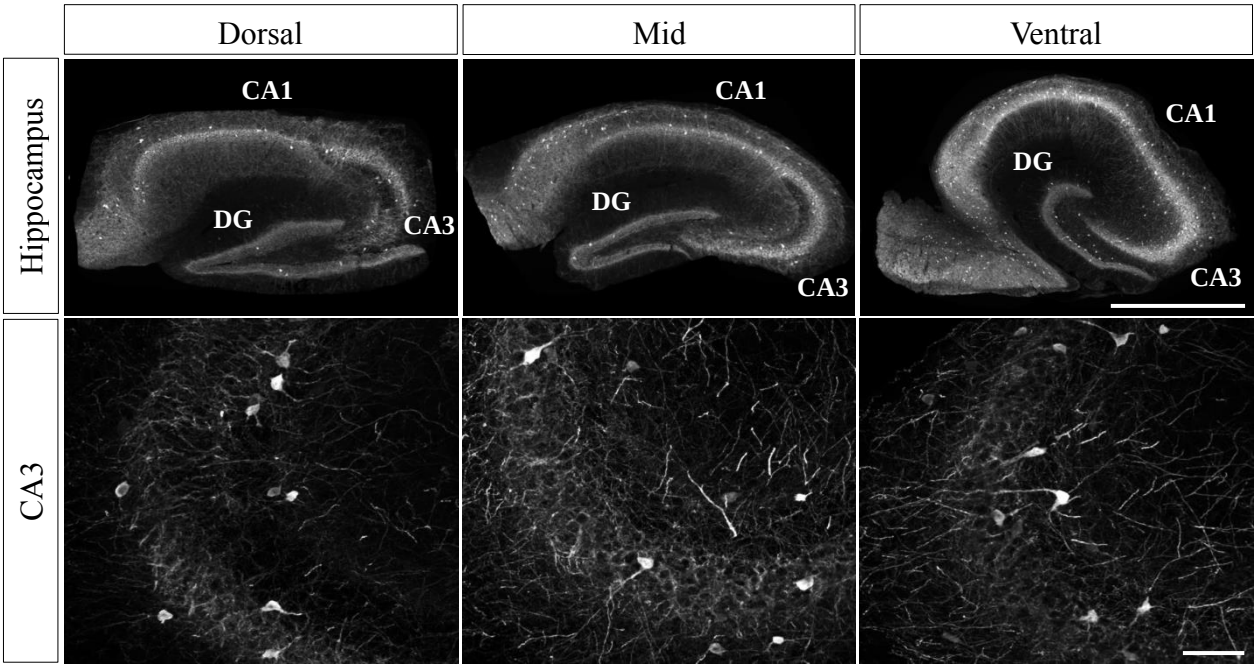

Figure 21: Distribution of parvalbumin$^+$ interneurons in the hippocampus

Hippocampal cryosections immunohistochemically stained for parvalbumin along the dorso-ventral axis (from left to right). Lower panels show example images of the CA3 area in the respective hippocampal regions. Scale bars are 500 µm (upper panels) and 50 µm (lower panels).

intensity was significantly decreased in the dorsal (Figure 22A, $p < 0.01$, Table 10) and ventral hippocampus (Figure 22C, $p < 0.001$, Table 10) with a trend for a decrease also in the mid hippocampus (Figure 22B, Table 10) in WT mice that were trained for 2 days compared to swim controls. Similarly, PV intensity of Nogo-A KO was mice significantly reduced in the dorsal and ventral hippocampus after 2 days of spatial learning (Figures 22D and 22F, dorsal and ventral: $p < 0.05$, Table 10), however the decrease appeared to be less pronounced compared to WTs (Figures 22C and 22F, Table 10). After 10 days of training in the MWM, PV intensity returned to baseline levels in the dorsal and ventral hippocampus (Figures 22D and 22F, Table 10) comparable to the PV intensity of the swim control group (Figures 22A and 22C, Table 10). However, in the mid-

section of the hippocampus a slight increase in PV intensity was observed in both WT and Nogo-A KO mice (Figures 22B and 22E, Table 10).

Taken together, the initial learning in the MWM induced a decrease in PV intensity in dorsal and ventral hippocampus of both WT and Nogo-A KO mice while it returned to baseline levels at the end of the learning paradigm when the memory was already consolidated. In summary, conventional deletion of Nogo-A in mice did not alter PV plasticity in the hippocampus upon spatial learning.

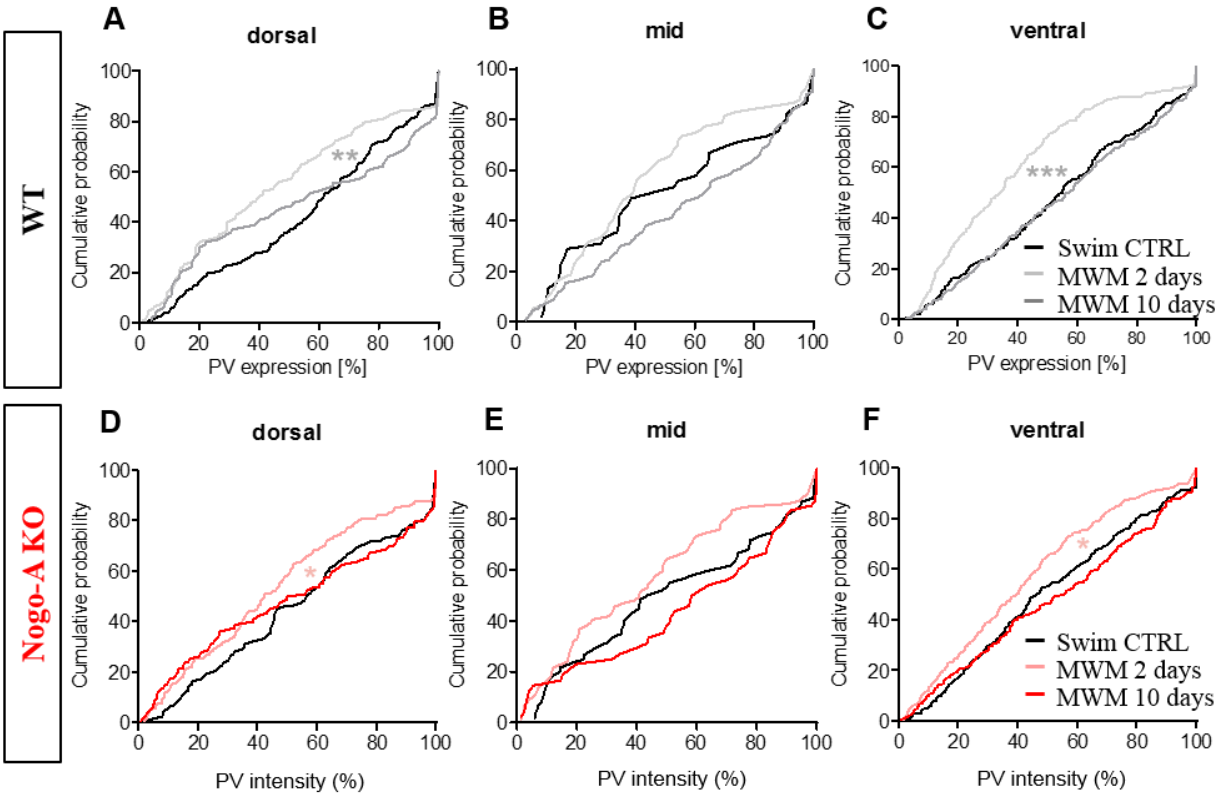

Figure 22: Spatial learning in the MWM induces PV plasticity in both WT and Nogo-A$^{-/-}$ mice.

(A-F) Cumulative probability distribution histograms showing the PV expression distribution in WT (A-C) and Nogo-A$^{-/-}$ mice (D-F) in CA3 of dorsal (A, D), mid (B, E) and ventral (C, F) hippocampus. Mice were either trained for 2 days (light grey, light red), 10 days (dark grey, dark red) or remained untrained (swim ctrl, black). Data are presented as cumulative frequency distribution. *$p < 0.05$, **$p < 0.01$, ***$p < 0.001$.

3.3.2. Spatial learning does not alter Nogo-A abundance in PV$^+$ interneurons

As reported previously, Nogo-A is abundantly expressed in PV$^+$ interneurons in the hippocampus (Zagrebelsky et al., 2016). Therefore, the relationship between the changes in PV plasticity and a potential regulation through Nogo-A have been examined by fluorescence intensity profile analysis of Nogo-A immunofluorescence inside PV$^+$ interneurons in the CA3 area of WT mice (Figure 23) upon spatial learning in the MWM. After both 2 and 10 days of training in the MWM Nogo-A intensity slightly decreased in all examined hippocampal regions compared to the control group

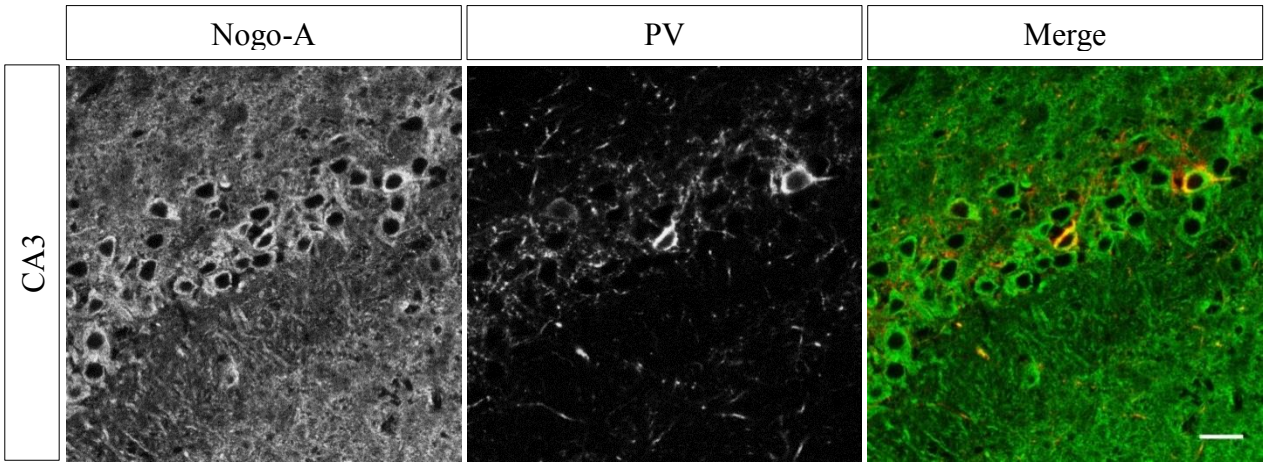

Figure 23: Nogo-A is expressed in PV$^+$ interneurons in the hippocampus

CA3 area of a hippocampal cryosection immunohistochemically stained for Nogo-A (green) and parvalbumin (red). Scale bar is 20 µm.

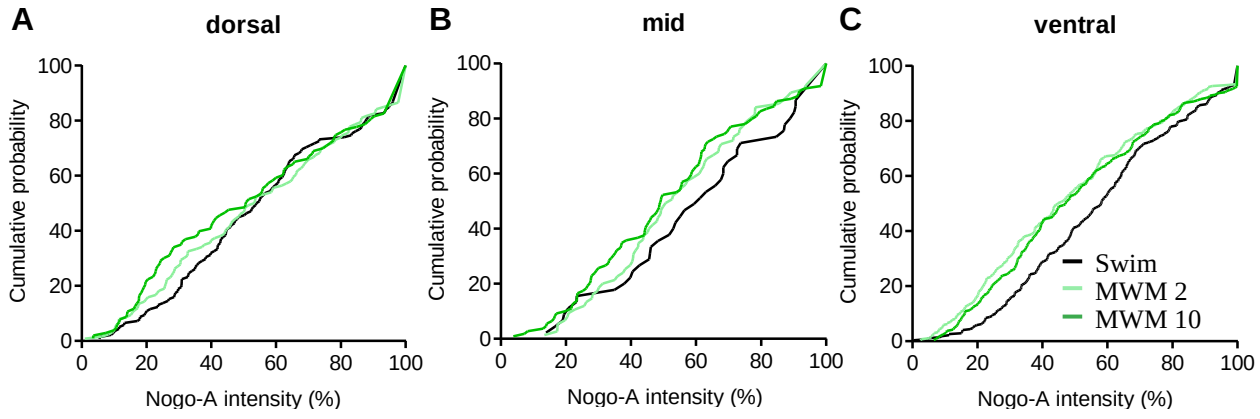

Figure 24: Spatial learning in the MWM does not alter Nogo-A expression in PV$^+$ interneurons

(A-C) Cumulative probability distribution histograms showing the Nogo-A expression distribution in PV$^+$ interneurons in WT mice in CA3 of dorsal (A), mid (B) and ventral hippocampus (C). Mice were either trained for 2 days (light green), 10 days (dark green) or remained untrained (swim ctrl, black). Data are presented as cumulative frequency distribution.

(Figure 24, Table 11). However, none of these changes were significantly different from the swim control. Taken together, Nogo-A immunofluorescence in PV^+ interneurons does not significantly change upon spatial learning in the MWM.

3.3.3. Fraction distribution analysis of PV plasticity in PV^+ interneurons

To further examine the changes in PV and Nogo-A immunofluorescence upon spatial learning in greater detail, the fluorescence intensities were divided into four fractions (see Material and Methods section 2.2.14.) as follows: 0-25 % = low, 25-50 % = intermediate low, 50-75 % intermediate high and 75-100 % = high (Figure 25); as described by Donato and colleagues (Donato et al., 2013). Fractioning revealed that 2 days of MWM training induced an increase in the low PV fractions in both dorsal (Figure 26A, $p < 0.05$, Table 12) and ventral hippocampus of WT mice (Figure 26B, $p < 0.001$, Table 12) which was absent in Nogo-A KO mice (Figures 26C and 26D, Table 12). In addition, 2 days of training also led to a significant decrease in the high PV fractions in the dorsal (Figure 26A, $p < 0.01$, Table 12) and ventral hippocampus of WT mice (Figure 26B, $p < 0.001$, Table 12) that was only present in the ventral (Figure 26D, $p < 0.01$, Table 12) but not

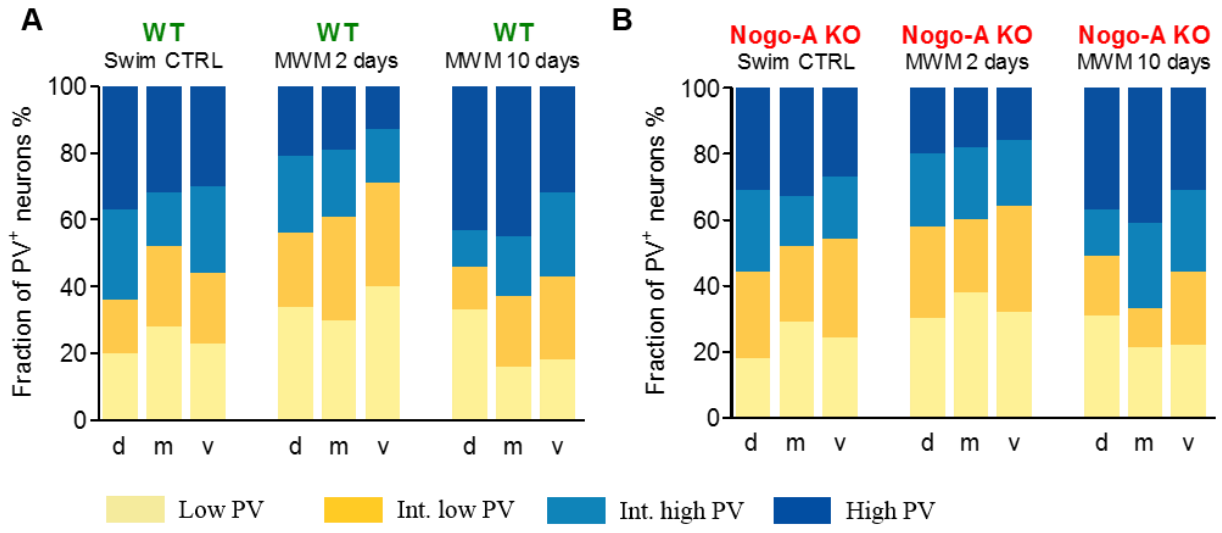

Figure 25: Spatial learning in the MWM alters fraction distribution of PV plasticity in WT and Nogo-A KO mice.

(A, B) PV fractions in the CA3 area of dorsal (d), mid (m) and ventral (v) hippocampus of WT (A) and Nogo-A KO mice (B) either untrained (swim ctrl) or trained for 2 or 10 days in the MWM. Data are presented as cumulative fractions of mean percent.

in the dorsal hippocampus in Nogo-A KO mice (Figure 26C, Table 12). After 10 days of spatial learning the low PV fractions in the ventral hippocampus of both WT and Nogo-A KO mice decreased significantly (Figures 26B and 26D, WT: $p < 0.001$; Nogo-A KO: $p < 0.05$, Table 12) while they remained unchanged in the dorsal hippocampus compared to only 2 days of training (Figures 26A and 26C, Table 12). Moreover, 10 days of MWM training resulted in an increase in the high PV fractions of both WT and Nogo-A KO mice in the dorsal (Figures 26A and 26C, WT: $p < 0.001$; Nogo-A KO: $p < 0.01$, Table 12) and ventral hippocampus compared to merely 2 days of spatial learning (Figures 26B and 26D, WT and Nogo-A KO: $p < 0.001$, Table 12).

When directly comparing the low and high PV fractions of WT and Nogo-A KO mice (Figure 27), there could not be found significant differences between genotypes in either the dorsal (Figures 27A and 27C) or the ventral hippocampus (Figures 27B and 27D, Table 12).

In summary, 2 days of spatial learning in the MWM induced a decrease in PV immunofluorescence intensity in the hippocampus of both WT and Nogo-A mice while at the end of the learning paradigm the PV intensity returned to baseline levels. Overall, however, the changes in PV plasticity were less pronounced in Nogo-A KO mice than in WT mice.

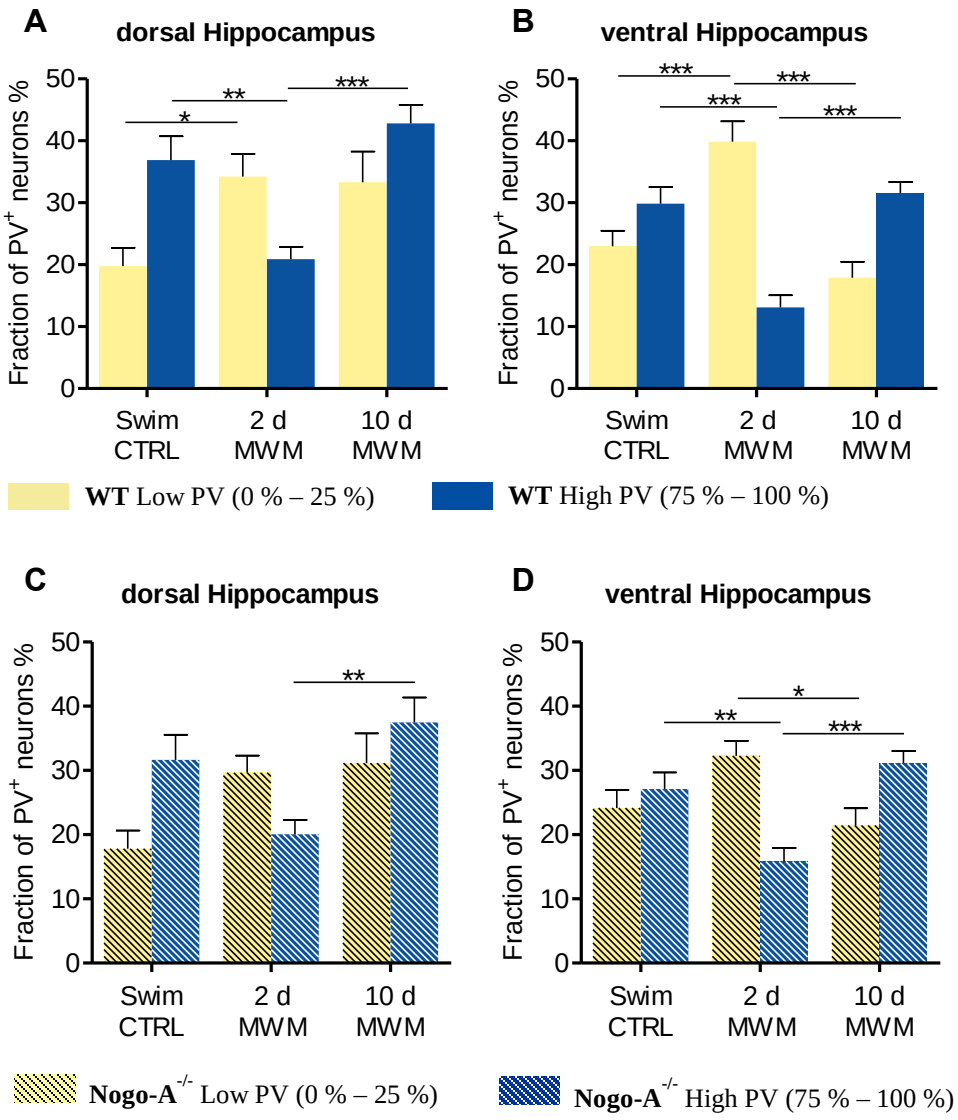

Figure 26: Spatial learning in the MWM alters low and high PV fraction distribution in the hippocampus

(A, B) Low (yellow) and high PV fractions (blue) in the CA3 area of the dorsal (A) and ventral hippocampus (B) of WT mice either untrained (swim ctrl) or trained for 2 or 10 days in the MWM. (C, D) Low (striped yellow) and high PV fractions (striped blue) in the CA3 area of the dorsal (C) and ventral hippocampus (D) of Nogo-A KO mice either untrained (swim ctrl) or trained for 2 or 10 days in the MWM. Data are presented as mean ± SEM. *p < 0.05, **p < 0.01, ***p < 0.001.

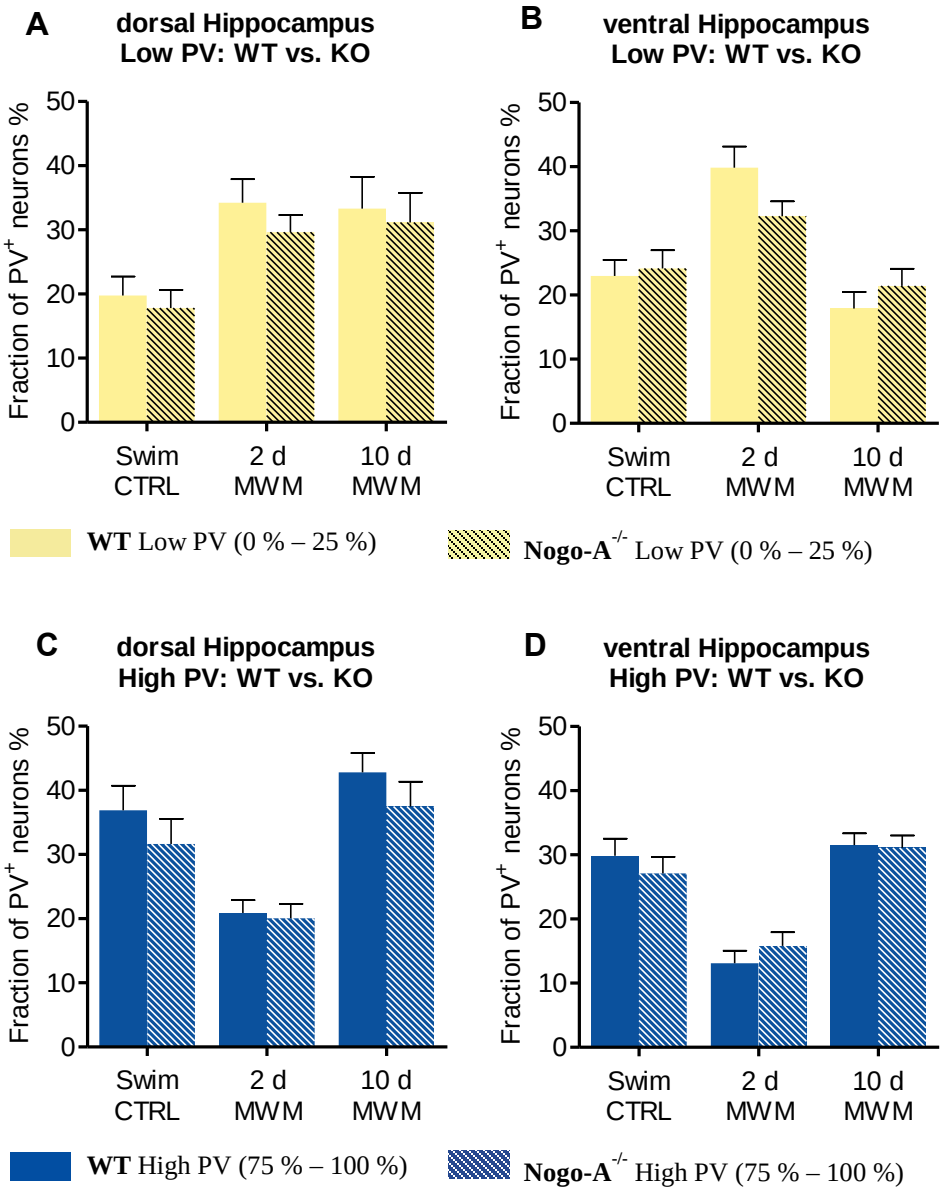

Figure 27: The percentages of low and high PV fractions upon spatial learning in the MWM are similar in WT and Nogo-A KO mice.

(A, B) Low PV fractions in the CA3 area of the dorsal (A) and ventral hippocampus (B) of WT (filled yellow bars) and Nogo-A KO mice (striped yellow bars) either untrained (swim ctrl) or trained for 2 or 10 days in the MWM. (C, D) High PV fractions in the CA3 area of the dorsal (C) and ventral hippocampus (D) of WT (filled blue bars) and Nogo-A KO mice (striped blue bars) either untrained (swim ctrl) or trained for 2 or 10 days in the MWM.

3.3.4. Fraction distribution analysis of Nogo-A immunofluorescence in PV$^+$ interneurons

To analyze the expression of Nogo-A in PV$^+$ interneurons in a comparable way, the fractioning method used above was also applied to the Nogo-A immunofluorescence in WT mice upon spatial learning. In section 3.3.2. Nogo-A fluorescence intensity was found to be slightly decreased in the dorsal, mid and ventral hippocampus after both 2 and 10 days of training in the MWM (Figure 24, Table 11). These results were mirrored by a rise in the low Nogo-A fractions that were significantly increased in the dorsal hippocampus after 10 days (Figure 28A, $p < 0.05$, Table 12) and in the

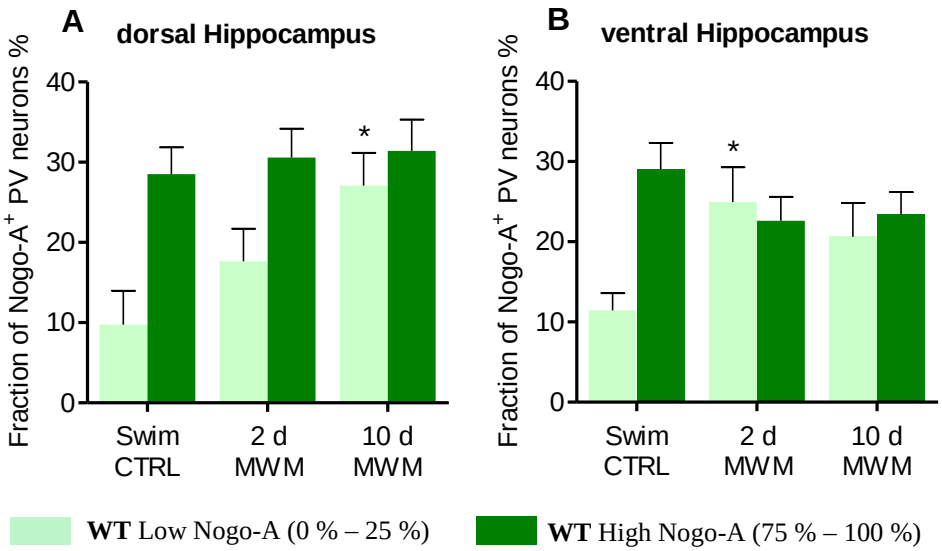

Figure 28: Spatial learning in the MWM does not alter Nogo-A expression in PV$^+$ interneurons

(A-F) Low (light green) and high (dark green) Nogo-A fractions in PV$^+$ interneurons in WT mice in the CA3 area of dorsal (A) and ventral (B) hippocampus for either swim controls or mice trained for 2 or 10 days in the MWM.

ventral hippocampus after 2 days of spatial learning (Figure 28B, $p < 0.05$, Table 12) compared to the swim control group. However, no alterations could be found in the high Nogo-A fractions upon MWM training (Figure 28, Table 12). These findings suggest that Nogo-A might be downregulated in PV$^+$ interneurons in the hippocampus during spatial learning in the MWM.

3.3.5. PV and Nogo-A immunofluorescence intensities correlate in the hippocampus

As spatial learning and memory formation has been shown to be regulated by both Nogo-A (Zagrebelsky et al., 2016) and PV plasticity (Donato et al., 2013), and as Nogo-A is highly enriched in PV$^+$ interneurons, it is possible that Nogo-A and PV abundance are correlated in single

interneurons. Indeed, when comparing the fluorescence intensity profiles of both proteins inside PV^+ interneurons, a strong positive correlation was found (Figure 29, $R_{Spearman} = 0.333$; $p < 0.001$). Taken together, these findings suggest that while Nogo-A does not seem to regulate PV plasticity upon spatial learning in the MWM, its abundance is positively correlated to PV in single interneurons and might therefore be correlated to its activity.

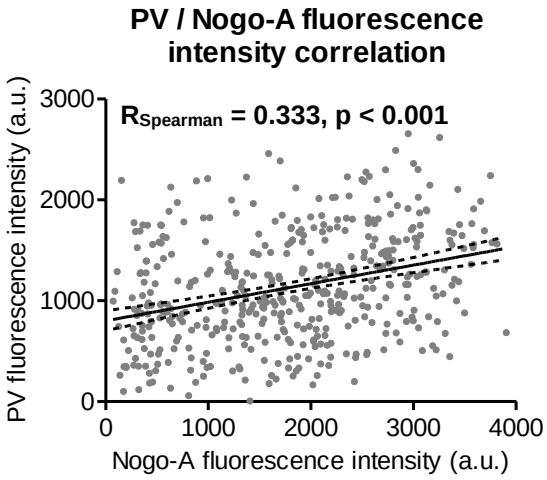

Figure 29: PV and Nogo-A fluorescence intensities in single PV^+ interneurons are positively correlated.

Correlation distribution of Nogo-A and PV immunofluorescence intensities from the entire hippocampus. Each dot represents a single PV^+ interneuron (n = 450). Linear regression slope: 0.184 ± 0.025, 95 % confidence interval: 0.135 to 0.233, $r^2 = 0.109$.

3.4. Cell-specific KO of Nogo-A in excitatory and PV^+ inhibitory neurons

Nogo-A has been reported to be expressed in both excitatory and inhibitory neurons throughout the hippocampus (Zagrebelsky et al., 2016). Together with the findings in this thesis that Nogo-A also controls inhibitory neuronal transmission, the question arises if and how it acts in different neuronal subpopulations. Hence, to knock out Nogo-A in a cell-specific manner, genetically modified Nogo-$A^{flox/flox}$ mice were crossed to either PV-cre or CaMKII-cre mice. Here, the exon 3 of the *rtn4* gene is flanked by flox sites and removed by either PV- or CaMKII-dependent expression of the cre recombinase, respectively.

3.4.1. Cell-specific KO of Nogo-A in PV^+ inhibitory interneurons in PV-cre/Nogo-$A^{flox/flox}$ mice

In order to visualize if and in which areas of the hippocampus and cortex Nogo-A was knocked out, immunohistochemistry for Nogo-A and PV was performed on cryosections of one hemisphere of PV-cre/Nogo-$A^{flox/flox}$ mice (Figure 30). In all evaluated regions (DG, CA1, CA3 and cortex) two different populations of PV^+ interneurons were present. On the one hand, PV^+ neurons could

be observed that showed regular immunofluorescence for Nogo-A (Figure 30, yellow arrowheads), as could be observed in WT mice (Figure 23, see also Zagrebelsky et al., 2016) while on the other hand PV^+ cells without any fluorescence signal for Nogo-A were observed (Figure 30, white arrowheads), indicating a complete knockout in these neurons. Hence, the genetic KO of Nogo-A seemed to be successful only in a subset of PV^+ interneurons in a yes / no fashion.

3.4.2. Cell-specific KO of Nogo-A in CaMKII-cre/Nogo-$A^{flox/flox}$ mice

To examine whether the deletion of Nogo-A in excitatory neurons was achieved, immunohistochemistry for Nogo-A and PV was used in cryosections of one hemisphere prepared from CaMKII-cre/Nogo-$A^{flox/flox}$ mice. Imaging of the hippocampus and cortex revealed that the knockout was region-dependent. While in the DG Nogo-A expression appeared unchanged, in the CA1 area Nogo-A immunofluorescence could not be observed in excitatory pyramidal neurons (Figure 31). Moreover, Nogo-A was still expressed in the complete CA2 area while in CA3 the deletion of Nogo-A seemed to be successful only in around half of the excitatory cells without a clear pattern in distribution (Figure 31). In contrast to PV-cre/Nogo-$A^{flox/flox}$ mice, in CaMKII-cre/Nogo-$A^{flox/flox}$ all of the PV interneurons displayed Nogo-A immunofluorescence throughout all evaluated regions (Figure 31).

In summary, in both mouse models the cell-specific KO of Nogo-A in either excitatory $CaMKII^+$ or PV^+ inhibitory neurons was either incomplete (PV-cre/Nogo-$A^{flox/flox}$) or region-dependent (CaMKII-cre/Nogo-$A^{flox/flox}$).

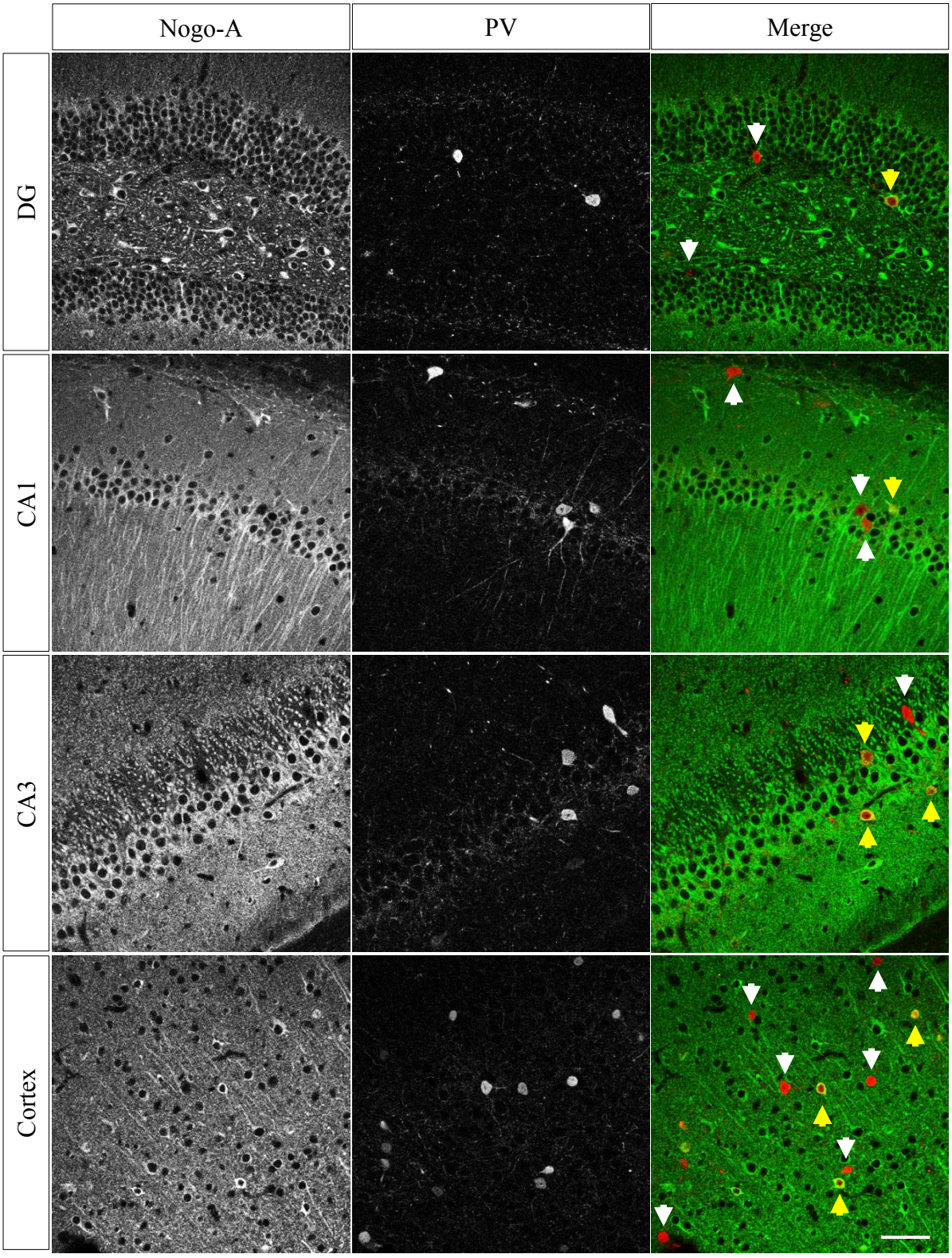

Figure 30: PV-cre/Nogo-A$^{flox/flox}$ mice display partial KO of Nogo-A in PV^{+} interneurons

Hippocampal cryosections of PV-cre/Nogo-A$^{flox/flox}$ mice immunohistochemically stained for Nogo-A and PV. White arrows indicate KO of Nogo-A in PV^{+} interneurons. Yellow arrows indicate incomplete or lack of KO in PV^{+} interneurons. Regions from top to bottom: DG, CA1, CA3 and cortex. Scale bar is 50 µm.

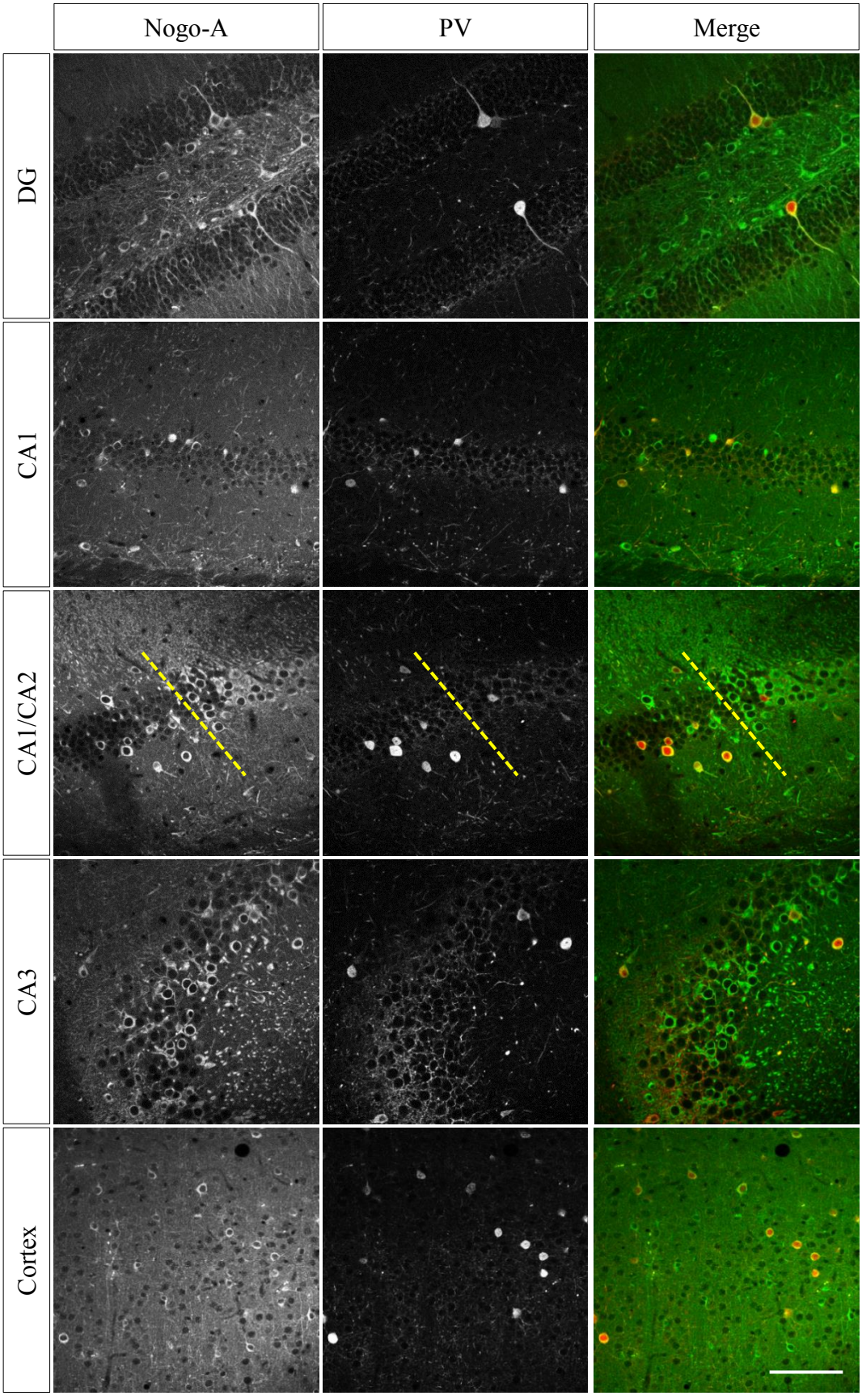
Nogo-A
PV
Merge
DG
CA1
CA1/CA2
CA3
Cortex

Figure 31: CaMKII-cre/Nogo-A$^{flox/flox}$ mice display an area-dependent KO of Nogo-A in excitatory neurons.

Hippocampal cryosections of CaMKII-cre/Nogo-A$^{flox/flox}$ mice immunohistochemically stained for Nogo-A and PV. Regions from top to bottom: DG, CA1, Ca1/2, CA3 and cortex. Yellow striped lines indicate the border between CA1 and CA2 area. Scale bar is 100 µm.

3.4.3. Spatial learning is unaltered in PV-cre/Nogo-A$^{flox/flox}$ and CaMKII-cre/Nogo-A$^{flox/flox}$ mice

Spatial learning and memory formation in the MWM have been shown to be improved in Nogo-A KO mice (Zagrebelsky et al., 2016). Therefore, both mouse models, PV-cre/Nogo-A$^{flox/flox}$ and CaMKII-cre/Nogo-A$^{flox/flox}$ were tested in an 8 days long spatial learning paradigm. Both genotypes performed similar to their respective controls (Nogo-A$^{flox/flox}$) and displayed a normal learning curve starting at ~30-35 seconds latency to find the platform at the first training day opposed to ~10 seconds latency at the last day in the MWM (Figures 32A and 32E, Table 13). Moreover, PV-cre/Nogo-A$^{flox/flox}$ and CaMKII-cre/Nogo-A$^{flox/flox}$ mice spent similar amounts of time in the target quadrant from where the platform has been removed from on probe trial day 3 (Figures 32B and 32F, Table 14) and day 9 (Figures 32C and 32G, Table 14) compared to Nogo-A$^{flox/flox}$ mice. Finally, all genotypes crossed the former platform position a comparable amount of times on probe trial day 3 and day 9 (Figures 32D and 32H, Table 14).

Taken together, cell-specific KO of Nogo-A in inhibitory or excitatory neurons using PV-cre/Nogo-A$^{flox/flox}$ and CaMKII-cre/Nogo-A$^{flox/flox}$ mice did not alter spatial learning in the MWM.

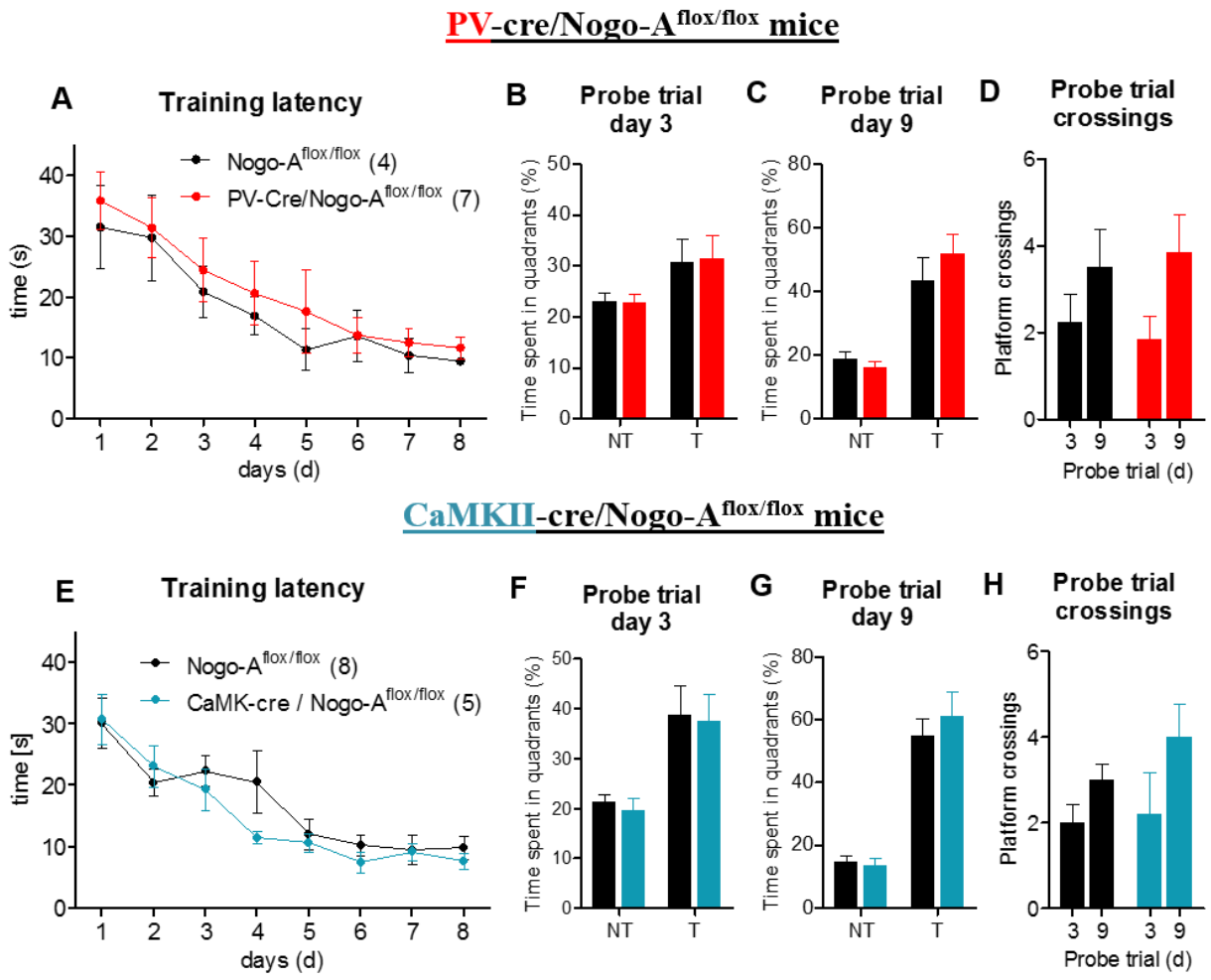

Figure 32: Spatial learning is unaltered in PV-cre/Nogo-A$^{flox/flox}$ and CaMKII-cre/Nogo-A$^{flox/flox}$ mice.

(A) Latency of PV-cre/Nogo-A$^{flox/flox}$ (red, n = 7) and control Nogo-A$^{flox/flox}$ mice (black, n = 4) to reach the hidden platform over 8 consecutive days of training in the MWM. (B, C) Percent of time PV-cre/Nogo-A$^{flox/flox}$ (red, n = 7) or Nogo-A$^{flox/flox}$ mice (black, n = 4) spent in the target quadrant opposed to the non-target quadrant on probe trial day 3 (B) and day 9 (C). (D) Number of times PV-cre/Nogo-A$^{flox/flox}$ (red, n = 7) and Nogo-A$^{flox/flox}$ mice (black, n = 4) crossed the position of the removed platform on probe trial day 3 and day 9. (E) Latency of CaMKII-cre/Nogo-A$^{flox/flox}$ (blue, n = 5) and control Nogo-A$^{flox/flox}$ mice (black, n = 8) to reach the hidden platform over 8 consecutive days of training in the MWM. (F, G) Percent of time CaMKII-cre/Nogo-A$^{flox/flox}$ (blue, n = 5) or Nogo-A$^{flox/flox}$ mice (black, n = 8) spent in the target quadrant opposed to the non-target quadrant on probe trial day 3 (F) and day 9 (G). (H) Number of times CaMKII-cre/Nogo-A$^{flox/flox}$ (blue, n = 5) and Nogo-A$^{flox/flox}$ mice (black, n = 8) crossed the position of the removed platform on probe trial day 3 and day 9. T = target quadrant, NT = non-target quadrant. All data are presented as mean ± SEM.

Discussion

Learning and memory processes in the adult brain depend on the plasticity of neurons and of the connections amongst them. The ability to modify and fine-tune these synaptic connections in a precise temporal manner is crucial to regulate their function. While it is necessary that synapses are plastic in order to gather and establish new information, the stabilization of synaptic connections is required to enable the long-term storage of data. A set of molecules has been identified to regulate this tight balance between plasticity and stability. This work addressed the role of Nogo-A in promoting the stability of the adult brain in the regulation of functional and structural synaptic plasticity in the hippocampus as well as in learning and memory formation.

One of the major regulatory mechanisms of network function and plasticity in the brain is inhibitory synaptic transmission. Adjustments in its strength represent a key mechanism to control processes such as learning and memory formation (Isaacson and Scanziani, 2011; Maffei, 2011; Barron et al., 2017). Hence, in this thesis the role of Nogo-A in inhibitory transmission was investigated. Nogo-A was found to promote inhibitory synaptic transmission by limiting the diffusion of the major inhibitory neurotransmitter receptor $GABA_AR$ and increasing its localization at synapses in a calcium-dependent manner.

Changes in the strength of synaptic transmission were described to shape neuronal morphology. Therefore, in this work, the regulatory mechanism of Nogo-A on structural plasticity at dendritic spines of CA3 hippocampal neurons was examined. It was observed that Nogo-A restricts spine number and length in an activity-dependent manner.

In the last part of this work, the role of Nogo-A in regulating spatial learning and memory formation was analyzed focusing especially on its function in either excitatory or inhibitory neurons. Here, particularly the role of Nogo-A on network plasticity of a subset of inhibitory neurons, the PV^+ interneurons was examined.

4.1. Nogo-A regulates functional and structural synaptic plasticity

4.1.1. Nogo-A bidirectionally regulates inhibitory and excitatory synaptic transmission on a fast time scale

While Nogo-A signaling was shown to rapidly modulate excitatory synaptic transmission in the hippocampus, the question whether it is involved in the regulation of inhibitory synaptic transmission remained obscure until now. For the first time in this study, Nogo-A signaling was found to promote inhibitory synaptic transmission on a fast time scale by regulating the synaptic localization and diffusion dynamics of $GABA_AR$s in hippocampal neurons. Indeed, interference with Nogo-A signaling by specifically blocking either the Nogo-A-Δ20 domain or inhibiting its receptor S1PR2 results in a fast decrease in mIPSC amplitude in CA3 hippocampal neurons as well as $GABA_AR$ cluster number and immunofluorescence intensity in primary hippocampal neurons. These effects are accompanied by a rapid increase in the $GABA_AR$ diffusion dynamics at synaptic and extrasynaptic compartments as shown by quantum dot-based single particle tracking in primary hippocampal neurons. Moreover, Nogo-A loss-of-function results in an increase in intracellular Ca^{2+} in these neurons within few minutes.

Inhibitory synaptic transmission has been shown to directly influence learning and memory processes (for a book review see Kumar et al., 2018) while changes in its strength are important to enable the initiation of learning (Caroni, 2015). Therefore, elucidating the mechanisms behind its rapid modulation is crucial to understand how inhibition affects learning and memory processes. The strength of inhibitory synaptic transmission underlies the number of $GABA_AR$s at inhibitory synapses (Moss and Smart, 2001; Kilman et al., 2002). While the number of $GABA_AR$s at synapses can be regulated by controlling the expression of $GABA_AR$ subunits for example via BDNF or CREB (Grabenstatter et al., 2012), their localization at synapses can also be modulated rapidly within minutes, e.g. by phosphorylation or dephosphorylation (for review see Nakamura et al., 2015). In this thesis, Nogo-A was found to strengthen inhibitory synaptic transmission by rapidly promoting the clustering of $GABA_AR$s at synapses. Indeed, already after 10 minutes of Nogo-A loss-of-function a significant decrease in the amplitude of inhibitory synaptic currents was observed, indicating a fast dispersal of $GABA_AR$ clusters. Synaptic clustering of $GABA_AR$s has been reported to depend on their confinement inside the synaptic compartment, on the rate of their insertion into and on their removal from the cell membrane as well as their lateral diffusion dynamics (Choquet and Triller, 2013). The findings in this thesis show that Nogo-A loss-of-

function results in a rapid increase in $GABA_AR$ lateral diffusion at both synaptic and extrasynaptic compartments. This is the result of an overall increase in the motility of $GABA_ARs$ and of the mobilization of previously immobile $GABA_ARs$ determining an overall higher exchange of receptors between synaptic and extrasynaptic compartments. The clustering of $GABA_ARs$ and their lateral diffusion have recently been described to be bidirectionally regulated by glutamate (Bannai et al., 2015). While low amounts of released glutamate induce $GABA_AR$ stabilization, higher amounts of glutamate result in increased $GABA_AR$ lateral diffusion and the dispersion of their synaptic clusters. Moreover, the lateral diffusion of $GABA_ARs$ along the membrane of hippocampal neurons has recently been revealed to rely on activity-dependent changes in intracellular Ca^{2+} concentration (Bannai et al., 2009; Bannai et al., 2015). Increased Ca^{2+} influx by stimulation of NMDA receptors resulted in an increase in $GABA_AR$ lateral diffusion within few minutes (Bannai et al., 2009). As reported in this thesis, the rapid increase in Ca^{2+} in hippocampal neurons as a result of Nogo-A loss-of-function was accompanied by and correlated to a simultaneous increase in $GABA_AR$ lateral diffusion within the same neurons. Moreover, recent results indicate that the increase in intracellular Ca^{2+} upon Nogo-A loss-of-function is required for the decrease in $GABA_AR$ clustering at synapses (Fricke, Metzdorf et al., in press). Further, the latter study also reports that the Ca^{2+} influx into neurons upon Nogo-A loss-of-function activates the Ca^{2+}-dependent phosphatase calcineurin (CaN) that dephosphorylates the γ2 subunit of $GABA_ARs$ at serine 327 (Figure 33). The dephosphorylation of this specific site was shown to be essential for Ca^{2+}-dependent dispersion of $GABA_ARs$ from synapses (Muir et al., 2010). The changes in $GABA_AR$ diffusion dynamics have been reported to rely on NMDAR-mediated influx of Ca^{2+} into neurons (Bannai et al., 2009; Muir et al., 2010). This suggests the possibility for the activation of an NMDAR-dependent downstream pathway upon Nogo-A loss-of-function leading to the observed increase in intracellular Ca^{2+}. This point however, remains to be elucidated.

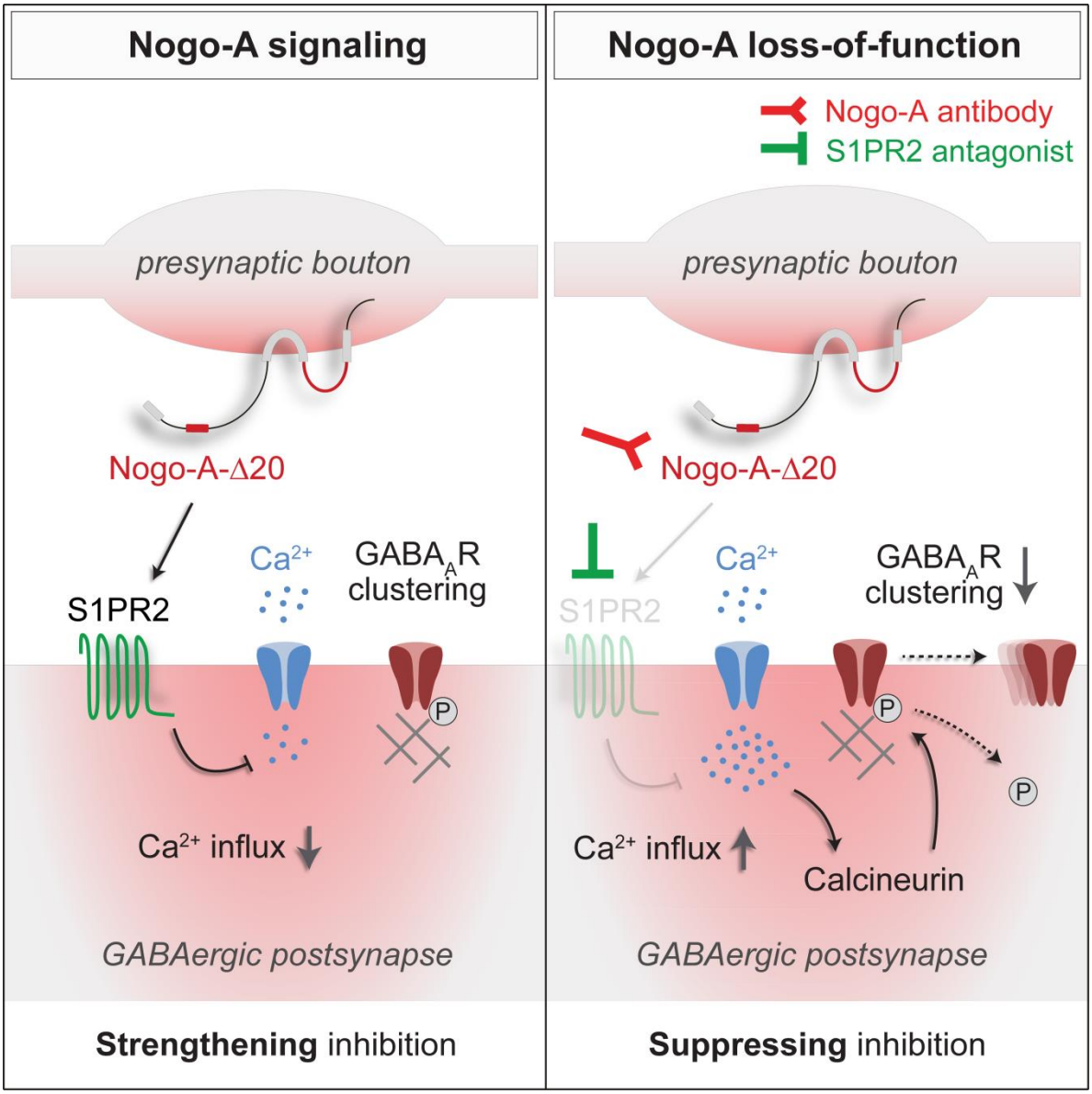

Figure 33: Nogo-A or S1PR2 loss-of-function decreases $GABA_AR$ clustering at inhibitory synapses in a Ca^{2+}- and calcineurin-dependent manner

(Left) Under basal conditions Nogo-A binds to S1PR2 which leads to the suppression of Ca^{2+} influx into the cell. (Right) However, when Nogo-A signaling is blocked by Nogo-A or S1PR2 loss-of-function the influx of Ca^{2+} is increased. The Ca^{2+}-dependent phosphatase calcineurin is activated and in turn dephosphorylates $GABA_A$ receptors at Ser327 of the γ2 subunit. This results in the mobilization and removal of $GABA_A$ receptors from inhibitory synapses (adapted from Fricke, Metzdorf et al., in press).

The results in this thesis also support the findings of previous studies reporting that Nogo-A loss-of-function led to an increase in excitatory synaptic transmission (Kellner et al., 2016; Berry et al., 2018) and to an increase in the number of AMPARs at synapses. Supporting this observation are

previous results indicating that while an increase in intracellular Ca^{2+} concentration is associated with an increase in $GABA_AR$ lateral diffusion, elevated intracellular Ca^{2+} concentration leads to a decrease in the mobility of AMPARs and their increased confinement at synapses (Borgdorff and Choquet, 2002; Heine et al., 2008). Therefore, the results in this work and of previous publications indicate that Nogo-A regulates both $GABA_AR$ and AMPAR localization at synapses in a reciprocal manner by controlling intracellular Ca^{2+} concentration and might hence represent a fast mechanism to adjust neuronal transmission in an activity-dependent manner. It is important to note that the effects on excitatory and inhibitory transmission occur simultaneously within 5 to 10 minutes after Nogo-A neutralization. Remarkably, this thesis shows that the localization of Nogo-A at synapses is reduced upon an increase in neuronal activity. Interestingly, the adhesion molecule Cadherin-10 was recently described to also regulate neuronal transmission in a reciprocal manner: Through interaction with different synaptic proteins Cadherin-10 limits inhibitory and promotes excitatory synaptic transmission, exerting thereby a bidirectional tuning of inhibition and excitation (Smith et al., 2017). However, in contrast to Nogo-A, Cadherin-10 directly binds to the synaptic clustering proteins PSD-95 and gephyrin in order to regulate the clustering of postsynaptic receptors. Nogo-A has been suggested to restrict AMPAR localization at postsynapses via modulating the actin cytoskeleton (Kellner et al., 2016) while it promotes $GABA_AR$ clustering at synapses indirectly via the second messenger Ca^{2+} (Fricke, Metzdorf et al., in press).

Taken together, the findings in this thesis show that Nogo-A regulates $GABA_AR$ and AMPAR localization at synapses on a fast time scale and is able to tune inhibitory as well as excitatory synaptic transmission within minutes. As fast modulation of neuronal transmission influences the fate of the underlying synaptic connections, these mechanisms might underlie changes in functional and structural synaptic plasticity.

4.1.2. Nogo-A regulates structural plasticity at dendritic spines

While various studies showed that knockout, knockdown or prolonged neutralization of Nogo-A or NgR1 resulted in increased axonal and dendritic complexity as well as in enhanced spine dynamics (Craveiro et al., 2008; Lee et al., 2008; Zagrebelsky et al., 2010; Akbik et al., 2013; Petrinovic et al., 2013; Zemmar et al., 2014), the consequences on neuronal architecture of an acute Nogo-A loss-of-function were less studied. However, recent findings show that acutely blocking Nogo-A signaling by interfering with either Nogo-A or either one of its receptors NgR1 or S1PR2,

resulted in a rapid increase in dendritic spine density and spine length of CA3 hippocampal neurons within 1-2 hours after treatment start (Kellner et al., 2016). Supporting these results, in this thesis, Nogo-A signaling was found to restrict structural plasticity at dendritic spines of CA3 hippocampal neurons at a time scale of few hours. Upon Nogo-A loss-of-function spine number and length were significantly increased within an hour and continued to rise continuously until up to 3 hours after function blocking antibody application. Structural plasticity at dendritic spines has been shown to occur in an activity-dependent manner (Butz et al., 2009), suggesting that the effect of Nogo-A in regulating structural plasticity at dendritic spines might depend on neuronal activity. The elongation of dendritic spines observed upon Nogo-A loss-of-function indicates that Nogo-A signaling might affect the maintenance of the mature architecture of dendritic spines as increased spine length was found to be associated with elevated spine motility (Zito et al., 2004) and electrical isolation of the spine heads to the dendrite (Yuste, 2013). When action potential generation was prevented via application of the sodium channel blocker TTX, Nogo-A loss-of-function resulted in an increase in dendritic spine length of CA3 hippocampal neurons without affecting spine number. However, the observed increase in spine length was significantly lower compared to a Nogo-A neutralization approach without TTX, suggesting that the regulation of structural plasticity at spines by Nogo-A signaling occurs, at least in part, in an activity-dependent manner. One hypothesis for the elongation of spines upon Nogo-A loss-of-function is that a compensatory effect causes the increases in spine length: The morphology of dendritic spines has been reported to regulate the biochemical and electrical compartmentalization of spines where an increase in spine length indicates an electrical isolation of the spine heads (Tønnesen et al., 2014). As reported in several studies, the intracellular Ca^{2+} concentration inside spines can be modulated independently of the parent dendrite (Andrews et al., 1988; Wickens, 1988; Guthrie et al., 1991; Gold and Bear, 1994; Segal, 1995). Therefore, spines might prevent Ca^{2+} surges from spreading into the dendrite and could thus act as neuroprotectants (Harris and Kater, 1994; Segal, 1995).

Furthermore, this thesis shows that the rapid increase in excitatory synaptic transmission due to the enhanced recruitment of AMPARs at synapses upon Nogo-A loss-of-function precedes the changes in dendritic spine structure. Interestingly, inhibitory synaptic transmission and GABAergic synapse remodeling shape excitatory synapses via the modulation of local Ca^{2+} concentration inside dendrites (Bar-Ilan et al., 2013) and inhibitory synapse and dendritic spine remodeling are tightly associated and spatially clustered (Chen et al., 2012). Hence, Nogo-A might control structural

plasticity at spines also via its modulatory function on inhibitory transmission and $GABA_AR$ clusters at synapses observed in the results of this thesis.

In this work, Nogo-A was found to be rapidly reduced in synaptosomes upon increased activity suggesting an activity-dependent regulation of Nogo-A itself. Indeed, both Nogo-A and NgR1 were found to be regulated by neuronal activity. Both running exercises and chemical stimulation via kainic acid injection decreased NgR1 mRNA in the rodent hippocampus (Josephson et al., 2003; Karlsson et al., 2017). Moreover, elevated neuronal activity also decreased NgR1 protein amounts in the rodent hippocampus (Karlen et al., 2009; Guo et al., 2013) and in the dendrites of cultured hippocampal neurons within few hours (Wills et al., 2012). While NgR1 mRNA and protein were decreased a few hours after enhanced neuronal activity, Nogo-A mRNA was found to be upregulated only in the dentate gyrus after kainic acid injection (Karlsson et al., 2017). The results in this thesis suggest that Nogo-A is removed from synapses within few minutes of increased neuronal activity. Hence, it could be speculated that while in the long run neuronal activity shapes the expression pattern of Nogo-A, neuronal activity might as well regulate the localization of Nogo-A on a fast time scale in order to control its function within minutes. However, whether Nogo-A is indeed rapidly relocated in an activity-dependent manner to control its function remains to be further investigated.

4.2. Nogo-A does not affect PV plasticity during spatial learning

Changes in dendritic spines and axonal boutons are not only correlated to functional changes at synapses (Yuste and Bonhoeffer, 2001) but are ultimately thought to underlie learning and memory processes (Caroni et al., 2012; Bailey et al., 2015). As Nogo-A is involved in the rapid regulation of synaptic transmission and structural plasticity in the hippocampus, this thesis further addressed the role of Nogo-A signaling in hippocampus-dependent learning and memory formation. Indeed, Nogo-A and its receptors NgR1 and S1PR2 have been shown to regulate long-term potentiation (LTP) in the hippocampus, which is considered one of the major cellular mechanisms that underlie learning and memory (Bliss and Collingridge, 1993). Moreover, Nogo-A signaling has been reported to be involved in experience-dependent morphological plasticity and learning in several behavioral tasks known to be associated with structural changes at dendritic spines (Akbik et al., 2013; Bhagat et al., 2015; Zemmar et al., 2014). Recently, Morris water maze (MWM) training of Nogo-A KO mice showed that spatial learning and memory formation in the hippocampus are

restricted by Nogo-A (Zagrebelsky et al., 2016). Spatial learning in the MWM has been reported to be dependent on the plasticity of PV^+ interneurons in the CA3 area (Donato et al., 2013). The results in this thesis show that after 2 days of training in the MWM PV expression is significantly reduced in both the dorsal and ventral hippocampus, which is in line with recent reports (Donato et al., 2013; Donato et al., 2015). Surprisingly, however, while it has been reported in these studies, that 10 days of spatial learning in the MWM induces a stark increase of PV expression in the dorsal and ventral hippocampus of WT mice, in the analysis of this thesis the PV expression only returns to the levels of the swim control group without increasing further. In an attempt to avoid methodological differences, the exact same protocols used in (Donato et al., 2013) for both MWM training and immunohistochemistry were applied in this thesis. However, especially concerning behavioral tasks, differences in experimental procedures can never be completely ruled out. While the protocols for the MWM training and the immunochemistry were adapted from said study, the imaging technique differed. Donato and colleagues set the critical values for imaging (laser power, exposure time) on the control samples, so that < 20 % of the pixels belonging to the brightest PV cells were saturated. These settings were then used for all of the tested conditions to be normalized for the control. However, given the high variance in PV immunofluorescence throughout all the experiments even within the same conditions, in this thesis another imaging technique adapted from (Çalişkan et al., 2015) was applied. In order to control for the increased variance, the laser power was set for each individual slice in a way that < 20 % of the pixels belonging to the brightest PV^+ interneurons were saturated. Çalişkan and colleagues report that PV immunofluorescence is significantly increased in the ventral hippocampus in response to contextual fear extinction, confirming that, with this imaging technique, elevated PV plasticity can indeed be detected. Nonetheless, it cannot be excluded that differences in imaging methods might cause that, in this thesis, 10 days of training in the MWM did not induce an increase in PV plasticity, in contrast to (Donato et al., 2013). While in the study from Donato and colleagues the mice improved every day in finding the platform in the MWM in this thesis it seems that learning reached a plateau after 7 days of training. Hence, it could also be speculated that due to the temporary changes in PV plasticity in response to spatial learning, the time window to observe the increase in PV immunofluorescence was missed. In order to control for this possibility, the experiments would have to be repeated and PV plasticity needed to be examined at days 7-8 in the MWM.

As PV^+ interneurons were found to highly express Nogo-A in the hippocampus (Zagrebelsky et al., 2016), in this thesis PV plasticity in response to spatial learning in the MWM was analyzed in

WT and Nogo-A KO mice. Changes in PV plasticity in response to spatial learning were found to be overall unaltered between WT and Nogo-A KO mice. As learning and memory formation in the MWM was found to be improved in Nogo-A KO mice (Zagrebelsky et al., 2016), the hypothesis for the experiments in this thesis was that Nogo-A might regulate spatial learning by controlling PV plasticity. However, in contrast to the results from (Zagrebelsky et al., 2016), Nogo-A KO mice did not show better performance in the MWM. In fact, Nogo-A KO mice performed even slightly worse over the first 4 days in the MWM. While in the study from 2016 the training protocol consisted of 3 days of pre-training with a visible platform followed by 8 consecutive days of training, a modified MWM protocol was used. In order to analyze PV plasticity and to compare the outcome directly to the experiments performed in (Donato et al., 2013), a 10 day training protocol without pre-training was applied. Although micro-RNA-mediated knockdown of Nogo-A in rats did not alter anxiety behavior (Tews et al., 2013) and chronic deletion of Nogo-A in rats even decreased anxiety (Petrasek et al., 2014), an effect on the early phase of spatial learning of Nogo-A KO mice due to the missing pre-training in this thesis cannot be ruled out. Taken together, it can be speculated that the slightly worse performance of Nogo-A KO mice over the first 4 days in the MWM resulted in the observed PV plasticity of Nogo-A KO mice that is not different from WT mice.

In addition to the PV expression, also the Nogo-A expression in PV^+ interneurons during the spatial learning in the MWM was quantified in this thesis. It was found that while overall Nogo-A expression was not changed at days 2 or 10 in the MWM compared to the controls, the fraction of PV^+ interneurons categorized as “low Nogo-A” expressing fraction was increased significantly after 2 days in the ventral and after 10 days in the dorsal hippocampus. These results suggest that, along with PV, Nogo-A expression might be regulated in PV^+ interneurons upon spatial learning in the MWM.

Interestingly, upon quantification of the PV and Nogo-A immunofluorescence in the same PV^+ interneurons of untrained WT mice, a strong positive correlation of PV and Nogo-A expression was found. This would suggest either a parallel regulation of both proteins or the regulation of one by the other. However, to gain more insight into the regulation and possible interdependence of both PV and Nogo-A expression in PV^+ neurons, especially during experience-dependent learning, additional experiments need to be performed. While the regulation of spatial learning in the MWM by Nogo-A and its dependence on PV plasticity have been previously reported, different behavioral tests might help to understand the role of Nogo-A in this context. For example, it was shown that

Nogo-A and NgR1 promote the persistence of fear memory during extinction training after contextual fear conditioning (Bhagat et al., 2015). Moreover, the study shows that deletion of NgR1 specifically in PV^+ interneurons is sufficient to induce these effects. Thus, a promising approach would be to apply contextual fear learning and examine the changes in PV and Nogo-A as well as their relation in the regulation of fear memory.

In order to investigate the action of Nogo-A in PV^+ inhibitory interneurons as well as its role in excitatory pyramidal neurons in the hippocampus additional tools to independently examine these actions would aid greatly to the understanding of the role of Nogo-A on a cellular level. One of these approaches is the specific genetic deletion of Nogo-A in these different neuronal subpopulations.

4.3. Cell-specific KO of Nogo-A in inhibitory PV^+ and excitatory neurons

As presented in this thesis, Nogo-A was found to exert different functions depending on its localization. While it strengthens inhibitory synaptic transmission, it limits excitatory transmission. Therefore, the question was raised whether its actions in inhibitory interneurons and excitatory neurons have different effects on synaptic plasticity and, hence, learning and memory processes. In order to get insight into the role of Nogo-A in different cellular subpopulations, transgenic mouse lines were generated with cell-specific deletion of Nogo-A in PV^+ inhibitory interneurons and excitatory pyramidal neurons. In a top-down approach, spatial learning and memory formation of the generated mice were tested in the MWM.

4.3.1. Spatial learning in PV-cre/Nogo-$A^{flox/flox}$ and CaMKII-cre/Nogo-$A^{flox/flox}$ mice

As previously reported, conventional Nogo-A KO mice display improved hippocampus-dependent learning and memory formation in the MWM (Zagrebelsky et al., 2016). In this study, while cell-specific KO of Nogo-A in inhibitory PV^+ interneurons did not alter spatial learning in the MWM, mice with a cell-specific deletion of Nogo-A in excitatory $CaMKII^+$ pyramidal neurons displayed a trend towards an improved spatial learning curve. While these results are preliminary and require an increase in the number of tested animals per genotype, these results might hint at that Nogo-A regulates spatial learning by controlling the actions in excitatory neurons. As it has been reported

that Nogo-A signaling in PV^+ interneurons regulates fear memory persistence in mice, the results in this thesis would rather point towards an important role of Nogo-A in pyramidal neurons in a hippocampus-dependent spatial learning paradigm. However, the deletion of Nogo-A in the hippocampus of both transgenic mice was only partially successful or region-dependent. Therefore, the impact of both conditional Nogo-A KOs on learning and memory processes in the hippocampus remains inconclusive. In order to further examine the role of Nogo-A in inhibitory and excitatory neurons and their action on spatial learning, new transgenic mouse lines that display complete deletion of Nogo-A in either inhibitory or excitatory neurons would aid greatly to analyze its actions in a more detailed fashion.

4.3.2. Cell-specific KO of Nogo-A in PV^+ interneurons

For PV^+ cell-specific KO of Nogo-A homozygous Nogo-$A^{flox/flox}$ mice were crossed with heterozygous PV-cre mice (B6;129P2-Pvalbtm1(cre)Arbr/J, Hippenmeyer et al., 2005). Immunohistochemistry for Nogo-A and PV revealed that the cell-specific KO of Nogo-A in PV^+ interneurons of PV-cre/Nogo-$A^{flox/flox}$ mice was incomplete. Around half of the PV^+ cells showed a clear absence of Nogo-A while the other half displayed normal Nogo-A expression. Several studies using this PV-cre mouse line reported a successful and complete cre-dependent KO of their gene of interest in PV^+ interneurons throughout the brain (Stephany et al., 2014; Donato et al., 2015; Stephany et al., 2016; Sun et al., 2017). However, it has been found that various conditional KO mice underlying the cre/loxP system show vagaries in their expression pattern (Matthaei, 2007; Schmidt-Supprian et al., 2007; Heffner et al., 2012). One example of these issues is inconsistent mosaicism which might have resulted in the two different PV^+ cell populations observed in this thesis. For immunohistochemical detection of Nogo-A an antibody corresponding to amino acids 701-1000 inside the ~ 800 amino acids long exon 3 was applied. Therefore, a positive immunofluorescence for Nogo-A in PV^+ interneurons would suggest an unsuccessful genetic deletion. However, to verify these results, further immunohistochemical staining should be performed using another α-Nogo-A antibody that corresponds to a region inside exon 3, e.g. the Nogo-A neutralizing antibody 11C7 that was described earlier in this thesis. Altogether, the cell-specific KO of Nogo-A in PV^+ interneurons was only successful in around half of the PV^+ cells in the hippocampus and cortex and needs to be examined genetically and immunohistochemically in further experiments.

4.3.3. Region-dependent cell-specific KO of Nogo-A in CaMKII^{+} excitatory neurons

For the cell-specific deletion of Nogo-A in excitatory neurons homozygous Nogo-A$^{flox/flox}$ mice were crossed with heterozygous CaMKII-cre mice (B6.Cg-Tg(Camk2a-cre)T29-1Stl/J, Tsien et al., 1996). Immunohistochemical staining for Nogo-A revealed that the KO of Nogo-A was dependent on the region: While the whole CA1 showed a clear lack of Nogo-A in pyramidal neurons, the CA3 area displayed a mosaic expression pattern. Indeed, this transgenic mouse line was described to express cre in the hippocampus in the pyramidal cell layer predominantly in the CA1 area, which is in line with the observed expression pattern.

4.4 Conclusions & outlook

In this work, Nogo-A signaling was found to promote inhibitory synaptic transmission and restrict excitatory synaptic transmission by regulating the localization of $GABA_AR$ and AMPARs at synapses of hippocampal neurons within few minutes. Moreover, the results indicate that Nogo-A limits structural plasticity at dendritic spines of CA3 hippocampal neurons in an activity-dependent manner. The findings in this thesis further suggest that Nogo-A does not control the expression of PV in PV^{+} interneurons and therefore does not seem to regulate their activity during spatial learning. Finally, cell-specific deletion of Nogo-A in either excitatory or PV^{+} inhibitory interneurons seems not to alter spatial learning of mice in the MWM. Taken together, this study provides a newly described role of Nogo-A in bidirectionally regulating and fine-tuning excitatory and inhibitory synaptic transmission within minutes. Further results in this thesis show that Nogo-A restricts structural plasticity at dendritic spines in an activity-dependent manner within hours possibly as a consequence of the rapid changes in synaptic transmission.

While this work describes that Nogo-A is present at excitatory synapses, results that are supported by previous findings (Lee et al., 2008), it is so far unclear whether Nogo-A is also located at inhibitory synapses. To this purpose, the specific localization of Nogo-A needs to be confirmed by super-resolution or electron microscopy in order to connect its localization to its function at synapses. Moreover, it remains obscure whether Nogo-A acts at synapses via *trans* and/or *cis* signaling as recently proposed (Vajda et al., 2014). In this thesis, Nogo-A was found to restrict inhibitory synaptic transmission and $GABA_AR$ localization at synapses via its receptor S1PR2, but

not via NgR1. While this would indicate an S1PR2-specific mechanism via Nogo-A, an involvement of PirB signaling cannot be excluded. In order to rule out a PirB-dependent effect on inhibition and $GABA_AR$ localization at synapses, patch clamp experiments measuring the inhibitory postsynaptic transmission upon PirB loss-of-function could be performed. Further results in this work indicate that while Nogo-A promotes $GABA_AR$ clustering, it simultaneously restricts AMPAR insertion at synapses of hippocampal neurons. Here, it would be fascinating to examine the fast simultaneous changes in $GABA_AR$ and AMPAR clusters upon Nogo-A loss-of-function within a single neuron by co-labeling these surface receptors. In addition, excitatory synaptic transmission was shown to be rapidly increased upon Nogo-A loss-of-function. It still remains unclear whether this effect on excitatory synaptic transmission is mediated by NgR1 or S1PR2, demanding further loss- or gain-of-function experiments in this context.

The results in this thesis indicate that Nogo-A restricts dendritic spine number and length in CA3 hippocampal neurons under basal conditions supporting previous findings (Kellner et al., 2016). Moreover, this regulation seems to occur in an activity-dependent manner as indicated by blocking sodium channels via TTX. As the data in this work show that Nogo-A localization itself at synapses and therefore at dendritic spines is regulated in an activity-dependent fashion, further localization studies might shed light on whether its function on structural plasticity is activity-dependent. Here, live imaging of both dendritic spine morphology and fluorescently labeled Nogo-A in single spines of hippocampal neurons upon changes in activity by application of e.g. KCl, glutamate or TTX would aid greatly to the understanding of how Nogo-A localization is affected by activity and in turn regulates structural plasticity.

In the final part of this study, the role of Nogo-A in spatial learning with focus on its action on interneuron networks was analyzed. Previous studies showed that changes in the expression levels of PV and thus in the function of PV^+ neurons are crucial for spatial learning and memory formation of mice in the MWM (Donato et al., 2013; Donato et al., 2015). Decreased PV expression during learning would indicate less inhibition and therefore more plasticity of the excitatory synaptic connections while increased PV expression during the end of the learning phase would suggest a high inhibition and therefore stabilization of newly formed synaptic connections. While this work could reproduce the decrease in PV levels observed previously during the first 4 days in the MWM, its increase at the end of the learning task was not observed, in contrast to recent literature (Donato et al., 2013). This might be due to the timing of analysis. At the latest time point where the PV expression was analyzed in this thesis, the mice did not show an improvement in their spatial

learning for 3 days, indicating that the consolidation of the spatial memory might have been already concluded and the time window for increased PV expression might have been missed. In order to confirm these results it would be best to repeat this experiment and analyze the PV expression in the hippocampus at each day in the MWM, ensuring that the time window for consolidation is not missed. Furthermore, the results in this thesis suggest that conventional KO of Nogo-A does not affect the changes in PV expression upon spatial learning in the MWM indicating that Nogo-A does not regulate PV expression. However, as a high positive correlation between Nogo-A and PV expression in the hippocampus of untrained WT mice was present, a regulation or interdependence of Nogo-A and PV cannot be ruled out. In addition, as Nogo-A KO mice did not show an improvement in their spatial learning compared to WT mice, in contrast to recent data (Zagrebelsky et al., 2016), it might be speculated that an effect on PV levels might only have been present upon improved learning.

In order to gain more insight into the regulation of Nogo-A in different cell-types the effects of the cell-specific KO of Nogo-A in PV^+ inhibitory interneurons and excitatory pyramidal neurons on spatial learning in the MWM were examined with no significant differences found between genotypes. As these results are preliminary and as mice lacking Nogo-A in excitatory neurons show a trend towards improved spatial learning the experiments should be repeated to increase the animal number. In addition to spatial learning in the MWM, the effect of cell-specific KO of Nogo-A in PV^+ neurons on contextual fear learning might be tested as PV^+ interneurons have been described to regulate contextual fear memory (Donato et al., 2013; Ognjanovski et al., 2017). Moreover, as the cell-specific KO of Nogo-A in PV^+ interneurons and excitatory pyramidal neurons was not successful in the entirety of the respective cells, more efficient transgenic mouse models might be useful for further experiments.

Finally, Nogo-A may act as a regulator of functional and structural synaptic plasticity by exerting different functions at inhibitory and excitatory synapses to ultimately control learning and memory. In this regard, it would be interesting to closer examine the rapid changes in neuronal activity of excitatory neurons along the impact on inhibitory neurons, especially PV^+ interneurons, upon Nogo-A gain- and loss-of-function approaches.

References

Akbik, F. V., Bhagat, S. M., Patel, P. R., Cafferty, W. B., & Strittmatter, S. M. (2013). Anatomical plasticity of adult brain is titrated by Nogo Receptor 1. Neuron, 77(5), 859-866.

Aloy, E. M., Weinmann, O., Pot, C., Kasper, H., Dodd, D. A., Rülicke, T., ... & Schwab, M. E. (2006). Synaptic destabilization by neuronal Nogo-A. Brain cell biology, 35(2-3), 137-157.

Alvarez, P., & Squire, L. R. (1994). Memory consolidation and the medial temporal lobe: a simple network model. Proceedings of the national academy of sciences, 91(15), 7041-7045.

Andersen, P., Bliss, T. V. P., & Skrede, K. K. (1971). Lamellar organization of hippocampal excitatory pathways. Experimental brain research, 13(2), 222-238.

Andrews, S. B., Leapman, R. D., Landis, D. M., & Reese, T. S. (1988). Activity-dependent accumulation of calcium in Purkinje cell dendritic spines. Proceedings of the National Academy of Sciences, 85(5), 1682-1685.

Bailey, C. H., Kandel, E. R., & Harris, K. M. (2015). Structural components of synaptic plasticity and memory consolidation. Cold Spring Harbor perspectives in biology, 7(7), a021758.

Banker, G. A. (1980). Trophic interactions between astroglial cells and hippocampal neurons in culture. Science, 209(4458), 809-810.

Bannai, H., Lévi, S., Schweizer, C., Dahan, M., & Triller, A. (2006). Imaging the lateral diffusion of membrane molecules with quantum dots. Nature protocols, 1(6), 2628.

Bannai, H., Lévi, S., Schweizer, C., Inoue, T., Launey, T., Racine, V., ... & Triller, A. (2009). Activity-dependent tuning of inhibitory neurotransmission based on GABAAR diffusion dynamics. Neuron, 62(5), 670-682.

Bannai, H., Niwa, F., Sherwood, M. W., Shrivastava, A. N., Arizono, M., Miyamoto, A., ... & Mikoshiba, K. (2015). Bidirectional control of synaptic GABAAR clustering by glutamate and calcium. Cell reports, 13(12), 2768-2780.

Bar-Ilan, L., Gidon, A., & Segev, I. (2013). The role of dendritic inhibition in shaping the plasticity of excitatory synapses. Frontiers in neural circuits, 6, 118.

Barron, H. C., Vogels, T. P., Behrens, T. E., & Ramaswami, M. (2017). Inhibitory engrams in perception and memory. Proceedings of the National Academy of Sciences, 114(26), 6666-6674.

Berry, S., Weinmann, O., Fritz, A. K., Rust, R., Wolfer, D., Schwab, M. E., ... & Ster, J. (2018). Loss of Nogo-A, encoded by the schizophrenia risk gene Rtn4, reduces mGlu3 expression and causes hyperexcitability in hippocampal CA3 circuits. PloS one, 13(7), e0200896.

Bhagat, S. M., Butler, S. S., Taylor, J. R., McEwen, B. S., & Strittmatter, S. M. (2016). Erasure of fear memories is prevented by Nogo Receptor 1 in adulthood. Molecular psychiatry, 21(9), 1281.

Bliss, T. V., & Collingridge, G. L. (1993). A synaptic model of memory: long-term potentiation in the hippocampus. Nature, 361(6407), 31.

Bliss, T. V., & Lømo, T. (1973). Long-lasting potentiation of synaptic transmission in the dentate area of the anaesthetized rabbit following stimulation of the perforant path. The Journal of physiology, 232(2), 331-356.

Bonhoeffer, T., & Yuste, R. (2002). Spine motility: phenomenology, mechanisms, and function. Neuron, 35(6), 1019-1027.

Borgdorff, A. J., & Choquet, D. (2002). Regulation of AMPA receptor lateral movements. Nature, 417(6889), 649.

Bourne, J., & Harris, K. M. (2007). Do thin spines learn to be mushroom spines that remember?. Current opinion in neurobiology, 17(3), 381-386.

Bourne, J. N., Chirillo, M. A., & Harris, K. M. (2013). Presynaptic Ultrastructural Plasticity Along CA3→ CA1 Axons During Long-Term Potentiation in Mature Hippocampus. Journal of Comparative Neurology,521(17), 3898-3912.

Brini, M., Calì, T., Ottolini, D., & Carafoli, E. (2014). Neuronal calcium signaling: function and dysfunction. Cellular and molecular life sciences, 71(15), 2787-2814.

Buffo, A., Zagrebelsky, M., Huber, A. B., Skerra, A., Schwab, M. E., Strata, P., & Rossi, F. (2000). Application of neutralizing antibodies against NI-35/250 myelin-associated neurite growth inhibitory proteins to the adult rat cerebellum induces sprouting of uninjured purkinje cell axons. Journal of Neuroscience, 20(6), 2275-2286.

Burgess, N., Maguire, E. A., & O'Keefe, J. (2002). The human hippocampus and spatial and episodic memory. Neuron, 35(4), 625-641.

Butz, M., Woergoetter, F., & van Ooyen, A. (2009). Activity-dependent structural plasticity. Brain research reviews, 60(2), 287-305.

Çalışkan, G., Müller, I., Semtner, M., Winkelmann, A., Raza, A. S., Hollnagel, J. O., ... & Meier, J. C. (2016). Identification of parvalbumin interneurons as cellular substrate of fear memory persistence. Cerebral Cortex, 26(5), 2325-2340.

Caroni, P. (2015). Regulation of Parvalbumin Basket cell plasticity in rule learning. Biochemical and biophysical research communications, 460(1), 100-103.

Caroni, P., Donato, F., & Muller, D. (2012). Structural plasticity upon learning: regulation and functions. Nature Reviews Neuroscience, 13(7), 478.

Cheatwood, J. L., Emerick, A. J., Schwab, M. E., & Kartje, G. L. (2008). Nogo-A expression after focal ischemic stroke in the adult rat. Stroke, 39(7), 2091-2098.

Chen, J. L., Villa, K. L., Cha, J. W., So, P. T., Kubota, Y., & Nedivi, E. (2012). Clustered dynamics of inhibitory synapses and dendritic spines in the adult neocortex. Neuron, 74(2), 361-373.

Choquet, D., & Triller, A. (2013). The dynamic synapse. Neuron, 80(3), 691-703.

Craveiro, L. M., Hakkoum, D., Weinmann, O., Montani, L., Stoppini, L., & Schwab, M. E. (2008). Neutralization of the membrane protein Nogo-A enhances growth and reactive sprouting in established organotypic hippocampal slice cultures. European Journal of Neuroscience, 28(9), 1808-1824.

Delekate, A., Zagrebelsky, M., Kramer, S., Schwab, M. E., & Korte, M. (2011). NogoA restricts synaptic plasticity in the adult hippocampus on a fast time scale. Proceedings of the National Academy of Sciences, 108(6), 2569-2574.

Deng, W., Aimone, J. B., & Gage, F. H. (2010). New neurons and new memories: how does adult hippocampal neurogenesis affect learning and memory?. Nature reviews neuroscience, 11(5), 339-350.

Dimou, L., Schnell, L., Montani, L., Duncan, C., Simonen, M., Schneider, R., ... & Schwab, M. E. (2006). Nogo-A-deficient mice reveal strain-dependent differences in axonal regeneration. Journal of Neuroscience, 26(21), 5591-5603.

Dodd, D. A., Niederoest, B., Bloechlinger, S., Dupuis, L., Loeffler, J. P., & Schwab, M. E. (2005). Nogo-A,-B, and-C are found on the cell surface and interact together in many different cell types. Journal of Biological Chemistry, 280(13), 12494-12502.

Donato, F., Chowdhury, A., Lahr, M., & Caroni, P. (2015). Early-and late-born parvalbumin basket cell subpopulations exhibiting distinct regulation and roles in learning. Neuron, 85(4), 770-786.

Donato, F., Rompani, S. B., & Caroni, P. (2013). Parvalbumin-expressing basket-cell network plasticity induced by experience regulates adult learning. Nature, 504(7479), 272.

Eichenbaum, H. (2004). Hippocampus: cognitive processes and neural representations that underlie declarative memory. Neuron, 44(1), 109-120.

Engert, F., & Bonhoeffer, T. (1999). Dendritic spine changes associated with hippocampal long-term synaptic plasticity. Nature, 399(6731), 66.

Evstratova, A., & Tóth, K. (2014). Information processing and synaptic plasticity at hippocampal mossy fiber terminals. Frontiers in cellular neuroscience, 8, 28.

Frischknecht, R., Fejtova, A., Viesti, M., Stephan, A., & Sonderegger, P. (2008). Activity-induced synaptic capture and exocytosis of the neuronal serine protease neurotrypsin. Journal of Neuroscience, 28(7), 1568-1579.

Fricke, S. (2015). The role of Nogo-A in regulating excitatory postsynaptic transmission in CA3 pyramidal neurons in the hippocampus: Is inhibition involved? (Master thesis)

Frisk, V., & Milner, B. (1990). The role of the left hippocampal region in the acquisition and retention of story content. Neuropsychologia, 28(4), 349-359.

Gold, J. I., & Bear, M. F. (1994). A model of dendritic spine Ca2+ concentration exploring possible bases for a sliding synaptic modification threshold. Proceedings of the National Academy of Sciences, 91(9), 3941-3945.

Gonzales, R. B., DeLeon Galvan, C. J., Rangel, Y. M., & Claiborne, B. J. (2001). Distribution of thorny excrescences on CA3 pyramidal neurons in the rat hippocampus. Journal of Comparative Neurology, 430(3), 357-368.

GrandPré, T., Nakamura, F., Vartanian, T., & Strittmatter, S. M. (2000). Identification of the Nogo inhibitor of axon regeneration as a Reticulon protein. Nature, 403(6768), 439.

Gulyás, A. I., Megıas, M., Emri, Z., & Freund, T. F. (1999). Total number and ratio of excitatory and inhibitory synapses converging onto single interneurons of different types in the CA1 area of the rat hippocampus. Journal of Neuroscience, 19(22), 10082-10097.

Guo, M. L., Xue, B., Jin, D. Z., Mao, L. M., & Wang, J. Q. (2013). Dynamic downregulation of Nogo receptor expression in the rat forebrain by amphetamine. Neurochemistry international, 63(3), 195-200.

Guthrie, P. B., Segal, M., & Kater, S. B. (1991). Independent regulation of calcium revealed by imaging dendritic spines.

Harris, K. M., & Kater, S. B. (1994). Dendritic spines: cellular specializations imparting both stability and flexibility to synaptic function. Annual review of neuroscience, 17(1), 341-371.

Harris, K. M., Jensen, F. E., & Tsao, B. (1992). Three-dimensional structure of dendritic spines and synapses in rat hippocampus (CA1) at postnatal day 15 and adult ages: implications for the maturation of synaptic physiology and long-term potentiation

[published erratum appears in J Neurosci 1992 Aug; 12 (8): following table of contents]. Journal of Neuroscience, 12(7), 2685-2705.

Heffner, C. S., Pratt, C. H., Babiuk, R. P., Sharma, Y., Rockwood, S. F., Donahue, L. R., ... & Murray, S. A. (2012). Supporting conditional mouse mutagenesis with a comprehensive cre characterization resource. Nature communications, 3, 1218.

Heine, M., Thoumine, O., Mondin, M., Tessier, B., Giannone, G., & Choquet, D. (2008). Activity-independent and subunit-specific recruitment of functional AMPA receptors at neurexin/neuroligin contacts. Proceedings of the National Academy of Sciences, 105(52), 20947-20952.

Hippenmeyer, S., Vrieseling, E., Sigrist, M., Portmann, T., Laengle, C., Ladle, D. R., & Arber, S. (2005). A developmental switch in the response of DRG neurons to ETS transcription factor signaling. PLoS biology, 3(5), e159.

Holtmaat, A., & Svoboda, K. (2009). Experience-dependent structural synaptic plasticity in the mammalian brain. Nature Reviews Neuroscience, 10(9), 647.

Hu, H., Gan, J., & Jonas, P. (2014). Fast-spiking, parvalbumin+ GABAergic interneurons: From cellular design to microcircuit function. Science, 345(6196), 1255263.

Huber, A. B., Weinmann, O., Brösamle, C., Oertle, T., & Schwab, M. E. (2002). Patterns of Nogo mRNA and protein expression in the developing and adult rat and after CNS lesions. Journal of Neuroscience, 22(9), 3553-3567.

Iobbi, C., Korte, M., & Zagrebelsky, M. (2017). Nogo-66 Restricts Synaptic Strengthening via Lingo1 and the ROCK2–Cofilin Pathway to Control Actin Dynamics. Cerebral cortex, 27(5), 2779-2792.

Isaacson, J. S., & Scanziani, M. (2011). How inhibition shapes cortical activity. Neuron, 72(2), 231-243.

Ishizuka, N., Cowan, W. M., & Amaral, D. G. (1995). A quantitative analysis of the dendritic organization of pyramidal cells in the rat hippocampus. Journal of Comparative Neurology, 362(1), 17-45.

Ishizuka, N., Weber, J., & Amaral, D. G. (1990). Organization of intrahippocampal projections originating from CA3 pyramidal cells in the rat. Journal of comparative neurology, 295(4), 580-623.

Izeddin, I., Boulanger, J., Racine, V., Specht, C. G., Kechkar, A., Nair, D., ... & Sibarita, J. B. (2012). Wavelet analysis for single molecule localization microscopy. Optics express, 20(3), 2081-2095.

Jitsuki, S., Nakajima, W., Takemoto, K., Sano, A., Tada, H., Takahashi-Jitsuki, A., & Takahashi, T. (2015). Nogo receptor signaling restricts adult neural plasticity by limiting synaptic AMPA receptor delivery. Cerebral cortex, 26(1), 427-439.

Josephson, A., Trifunovski, A., Schéele, C., Widenfalk, J., Wahlestedt, C., Brené, S., ... & Spenger, C. (2003). Activity-induced and developmental downregulation of the Nogo receptor. Cell and tissue research, 311(3), 333-342.

Kandel, E. R. (2001). The molecular biology of memory storage: a dialogue between genes and synapses. Science, 294(5544), 1030-1038.

Karlén, A., Karlsson, T. E., Mattsson, A., Lundströmer, K., Codeluppi, S., Pham, T. M., ... & Sherling, M. A. (2009). Nogo receptor 1 regulates formation of lasting memories. Proceedings of the National Academy of Sciences, 106(48), 20476-20481.

Karlsson, T. E., Smedfors, G., Brodin, A. T., Åberg, E., Mattsson, A., Högbeck, I., ... & Olson, L. (2016). NgR1: a tunable sensor regulating memory formation, synaptic, and dendritic plasticity. Cerebral cortex, 26(4), 1804-1817.

Karlsson, T. E., Wellfelt, K., & Olson, L. (2017). Spatiotemporal and long lasting modulation of 11 key nogo signaling genes in response to strong neuroexcitation. Frontiers in molecular neuroscience, 10, 94.

Karunakaran, S., Chowdhury, A., Donato, F., Quairiaux, C., Michel, C. M., & Caroni, P. (2016). PV plasticity sustained through D1/5 dopamine signaling required for long-term memory consolidation. Nature neuroscience, 19(3), 454.

Kasai, H., Matsuzaki, M., Noguchi, J., Yasumatsu, N., & Nakahara, H. (2003). Structure–stability–function relationships of dendritic spines. Trends in neurosciences, 26(7), 360-368.

Kellner, Y., Fricke, S., Kramer, S., Iobbi, C., Wierenga, C. J., Schwab, M. E., ... & Zagrebelsky, M. (2016). Nogo-A controls structural plasticity at dendritic spines by rapidly modulating actin dynamics. *Hippocampus*, *26*(6), 816-831.

Kellner, Y. P. (2014). The role of BDNF and Nogo-A signalling in modulating the architecture of mature hippocampal neurons (Doctoral dissertation).

Kellner, Y., Gödecke, N., Dierkes, T., Thieme, N., Zagrebelsky, M., & Korte, M. K. (2014). The BDNF effects on dendritic spines of mature hippocampal neurons depend on neuronal activity. Frontiers in synaptic neuroscience, 6, 5.

Kempf, A., & Schwab, M. E. (2013). Nogo-A represses anatomical and synaptic plasticity in the central nervous system. Physiology, 28(3), 151-163.

Kempf, A., Tews, B., Arzt, M. E., Weinmann, O., Obermair, F. J., Pernet, V., ... & Ristic, Z. (2014). The sphingolipid receptor S1PR2 is a receptor for Nogo-a repressing synaptic plasticity. PLoS biology, 12(1), e1001763.

Kilman, V., Van Rossum, M. C., & Turrigiano, G. G. (2002). Activity deprivation reduces miniature IPSC amplitude by decreasing the number of postsynaptic GABAA receptors clustered at neocortical synapses. Journal of Neuroscience, 22(4), 1328-1337.

Klausberger, T., & Somogyi, P. (2008). Neuronal diversity and temporal dynamics: the unity of hippocampal circuit operations. Science, 321(5885), 53-57.

Konorski, J. (1948). Conditioned reflexes and neuron organization. CUP Archive.

Kowiański, P., Lietzau, G., Czuba, E., Waśkow, M., Steliga, A., & Moryś, J. (2018). BDNF: a key factor with multipotent impact on brain signaling and synaptic plasticity. Cellular and molecular neurobiology, 38(3), 579-593.

Kubota, Y., Shigematsu, N., Karube, F., Sekigawa, A., Kato, S., Yamaguchi, N., ... & Kawaguchi, Y. (2011). Selective coexpression of multiple chemical markers defines discrete populations of neocortical GABAergic neurons. Cerebral cortex, 21(8), 1803-1817.

Kuhlman, S. J., Olivas, N. D., Tring, E., Ikrar, T., Xu, X., & Trachtenberg, J. T. (2013). A disinhibitory microcircuit initiates critical-period plasticity in the visual cortex. Nature, 501(7468), 543.

Kumar, K. (2018). Role of hippocampal GABAergic interneurons in learning and memory, March 2018. Publisher: LAP. ISBN: 978-613-9-57694-4

Kumar, A. (2011). Long-term potentiation at CA3–CA1 hippocampal synapses with special emphasis on aging, disease, and stress. Frontiers in aging neuroscience, 3, 7.

Kusumi, A., Sako, Y., & Yamamoto, M. (1993). Confined lateral diffusion of membrane receptors as studied by single particle tracking (nanovid microscopy). Effects of calcium-induced differentiation in cultured epithelial cells. Biophysical journal, 65(5), 2021-2040.

Lee, H., Raiker, S. J., Venkatesh, K., Geary, R., Robak, L. A., Zhang, Y., ... & Giger, R. J. (2008). Synaptic function for the Nogo-66 receptor NgR1: regulation of dendritic spine morphology and activity-dependent synaptic strength. Journal of Neuroscience, 28(11), 2753-2765.

Letzkus, J. J., Wolff, S. B., Meyer, E. M., Tovote, P., Courtin, J., Herry, C., & Lüthi, A. (2011). A disinhibitory microcircuit for associative fear learning in the auditory cortex. Nature, 480(7377), 331.

Li, X. G., Somogyi, P., Ylinen, A., & Buzsáki, G. (1994). The hippocampal CA3 network: an in vivo intracellular labeling study. Journal of comparative neurology, 339(2), 181-208.

Liebscher, T., Schnell, L., Schnell, D., Scholl, J., Schneider, R., Gullo, M., ... & Hamers, F. P. (2005). Nogo-A antibody improves regeneration and locomotion of spinal cord–injured rats. Annals of Neurology: Official Journal of the American Neurological Association and the Child Neurology Society, 58(5), 706-719.

Liu, Y. Y., Jin, W. L., Liu, H. L., & Ju, G. (2003). Electron microscopic localization of Nogo-A at the postsynaptic active zone of the rat. Neuroscience letters, 346(3), 153-156.

Maffei, A. (2011). The many forms and functions of long term plasticity at GABAergic synapses. Neural plasticity, 2011.

Maier, I. C., Ichiyama, R. M., Courtine, G., Schnell, L., Lavrov, I., Edgerton, V. R., & Schwab, M. E. (2009). Differential effects of anti-Nogo-A antibody treatment and treadmill training in rats with incomplete spinal cord injury. Brain, 132(6), 1426-1440.

Maletic-Savatic, M., Malinow, R., & Svoboda, K. (1999). Rapid dendritic morphogenesis in CA1 hippocampal dendrites induced by synaptic activity. Science, 283(5409), 1923-1927.

Matsuzaki, M., Honkura, N., Ellis-Davies, G. C., & Kasai, H. (2004). Structural basis of long-term potentiation in single dendritic spines. Nature, 429(6993), 761.

Matthaei, K. I. (2007). Genetically manipulated mice: a powerful tool with unsuspected caveats. The Journal of physiology, 582(2), 481-488.

Matus, A. (2000). Actin-based plasticity in dendritic spines. Science, 290(5492), 754-758.

Mdzomba, J. B., Rodriguez, L., Joly, S., Bretzner, F., & Pernet, V. (2018). Nogo-A inactivation promotes visual recovery and plasticity after retinal injury. Investigative Ophthalmology & Visual Science, 59(9), 5297-5297.

Meier, S., BRÄUER, A. U., Heimrich, B., Schwab, M. E., Nitsch, R., & Savaskan, N. E. (2003). Molecular analysis of Nogo expression in the hippocampus during development and following lesion and seizure. The FASEB journal, 17(9), 1153-1155.

Mi, S., Lee, X., Shao, Z., Thill, G., Ji, B., Relton, J., ... & Crowell, T. (2004). LINGO-1 is a component of the Nogo-66 receptor/p75 signaling complex. Nature neuroscience, 7(3), 221.

Michaelsen-Preusse, K., Kellner, Y., Korte, M., & Zagrebelsky, M. (2014). Analysis of actin turnover and spine dynamics in hippocampal slice cultures. In Laser Scanning Microscopy and Quantitative Image Analysis of Neuronal Tissue (pp. 189-217). Humana Press, New York, NY.

Mingorance, A., Fontana, X., Solé, M., Burgaya, F., Ureña, J. M., Teng, F. Y., ... & Schwab, M. E. (2004). Regulation of Nogo and Nogo receptor during the development of the entorhino-hippocampal pathway and after adult hippocampal lesions. Molecular and Cellular Neuroscience, 26(1), 34-49.

Mingorance-Le Meur, A., Zheng, B., Soriano, E., & del Río, J. A. (2006). Involvement of the myelin-associated inhibitor Nogo-A in early cortical development and neuronal maturation. Cerebral Cortex, 17(10), 2375-2386.

Mironova, Y. A., & Giger, R. J. (2013). Where no synapses go: gatekeepers of circuit remodeling and synaptic strength. Trends in neurosciences, 36(6), 363-373.

Moss, S. J., & Smart, T. G. (2001). Constructing inhibitory synapses. Nature Reviews Neuroscience, 2(4), 240.

Muir, J., Arancibia-Carcamo, I. L., MacAskill, A. F., Smith, K. R., Griffin, L. D., & Kittler, J. T. (2010). NMDA receptors regulate GABAA receptor lateral mobility and clustering at inhibitory synapses through serine 327 on the γ2 subunit. Proceedings of the National Academy of Sciences, 107(38), 16679-16684.

Nägerl, U. V., Eberhorn, N., Cambridge, S. B., & Bonhoeffer, T. (2004). Bidirectional activity-dependent morphological plasticity in hippocampal neurons. Neuron, 44(5), 759-767.

Nakamura, Y., Darnieder, L. M., Deeb, T. Z., & Moss, S. J. (2015). Regulation of GABAARs by phosphorylation. In Advances in pharmacology (Vol. 72, pp. 97-146). Academic Press.

Nash, M., Pribiag, H., Fournier, A. E., & Jacobson, C. (2009). Central nervous system regeneration inhibitors and their intracellular substrates. Molecular neurobiology, 40(3), 224-235.

Niederöst, B., Oertle, T., Fritsche, J., McKinney, R. A., & Bandtlow, C. E. (2002). Nogo-A and myelin-associated glycoprotein mediate neurite growth inhibition by antagonistic regulation of RhoA and Rac1. Journal of Neuroscience, 22(23), 10368-10376.

Niwa, F., Bannai, H., Arizono, M., Fukatsu, K., Triller, A., & Mikoshiba, K. (2012). Gephyrin-independent GABAAR mobility and clustering during plasticity. PLoS One, 7(4), e36148.

Nörenberg, A., Hu, H., Vida, I., Bartos, M., & Jonas, P. (2010). Distinct nonuniform cable properties optimize rapid and efficient activation of fast-spiking GABAergic interneurons. Proceedings of the National Academy of Sciences, 107(2), 894-899.

Nusser, Z., Cull-Candy, S., & Farrant, M. (1997). Differences in synaptic GABAA receptor number underlie variation in GABA mini amplitude. Neuron, 19(3), 697-709.

Oertle, T., van der Haar, M. E., Bandtlow, C. E., Robeva, A., Burfeind, P., Buss, A., ... & Kaupmann, K. (2003). Nogo-A inhibits neurite outgrowth and cell spreading with three discrete regions. Journal of Neuroscience, 23(13), 5393-5406.

Ognjanovski, N., Schaeffer, S., Wu, J., Mofakham, S., Maruyama, D., Zochowski, M., & Aton, S. J. (2017). Parvalbumin-expressing interneurons coordinate hippocampal network dynamics required for memory consolidation. Nature communications, 8, 15039.

O'Keefe, J., & Dostrovsky, J. (1971). The hippocampus as a spatial map: preliminary evidence from unit activity in the freely-moving rat. Brain research.

Park, J. B., Yiu, G., Kaneko, S., Wang, J., Chang, J., & He, Z. (2005). A TNF receptor family member, TROY, is a coreceptor with Nogo receptor in mediating the inhibitory activity of myelin inhibitors. Neuron, 45(3), 345-351.

Pelkey, K. A., Chittajallu, R., Craig, M. T., Tricoire, L., Wester, J. C., & McBain, C. J. (2017). Hippocampal GABAergic inhibitory interneurons. Physiological reviews, 97(4), 1619-1747.

Petrasek, T., Prokopova, I., Sladek, M., Weissova, K., Vojtechova, I., Bahnik, S., ... & Bartsch, D. (2014). Nogo-A-deficient transgenic rats show deficits in higher cognitive functions, decreased anxiety, and altered circadian activity patterns. Frontiers in behavioral neuroscience, 8, 90.

Petrinovic, M. M., Hourez, R., Aloy, E. M., Dewarrat, G., Gall, D., Weinmann, O., ... & Schwab, M. E. (2013). Neuronal Nogo-A negatively regulates dendritic morphology and synaptic transmission in the cerebellum. Proceedings of the National Academy of Sciences, 110(3), 1083-1088.

Raiker, S. J., Lee, H., Baldwin, K. T., Duan, Y., Shrager, P., & Giger, R. J. (2010). Oligodendrocyte-myelin glycoprotein and Nogo negatively regulate activity-dependent synaptic plasticity. Journal of Neuroscience, 30(37), 12432-12445.

Schwab, M. E. (2004). Nogo and axon regeneration. Current opinion in neurobiology, 14(1), 118-124.

Schwab, M. E. (2010). Functions of Nogo proteins and their receptors in the nervous system. Nature Reviews Neuroscience, 11(12), 799.

Schwab, M. E., & Strittmatter, S. M. (2014). Nogo limits neural plasticity and recovery from injury. Current opinion in neurobiology, 27, 53-60.

Scoville, W. B., & Milner, B. (1957). Loss of recent memory after bilateral hippocampal lesions. Journal of neurology, neurosurgery, and psychiatry, 20(1), 11.

Segal, M. (1995). Dendritic spines for neuroprotection: a hypothesis. Trends in neurosciences, 18(11), 468-471.

Segal, M. (1995). Imaging of calcium variations in living dendritic spines of cultured rat hippocampal neurons. The Journal of physiology, 486(2), 283-295.

Sheng, M., & Hoogenraad, C. C. (2007). The postsynaptic architecture of excitatory synapses: a more quantitative view. Annu. Rev. Biochem., 76, 823-847.

Simonen, M., Pedersen, V., Weinmann, O., Schnell, L., Buss, A., Ledermann, B., ... & Schwab, M. E. (2003). Systemic deletion of the myelin-associated outgrowth inhibitor Nogo-A improves regenerative and plastic responses after spinal cord injury. Neuron, 38(2), 201-211.

Smith, D. A., & Graesser, A. C. (1981). Memory for actions in scripted activities as a function of typicality, retention interval, and retrieval task. Memory & Cognition, 9(6), 550-559.

Smith, K. R., Jones, K. A., Kopeikina, K. J., Burette, A. C., Copits, B. A., Yoon, S., ... & Swanson, G. T. (2017). Cadherin-10 maintains excitatory/inhibitory ratio through interactions with synaptic proteins. Journal of Neuroscience, 37(46), 11127-11139.

Sorra, K. E., & Harris, K. M. (2000). Overview on the structure, composition, function, development, and plasticity of hippocampal dendritic spines. Hippocampus, 10(5), 501-511.

Spacek, J., & Harris, K. M. (1997). Three-dimensional organization of smooth endoplasmic reticulum in hippocampal CA1 dendrites and dendritic spines of the immature and mature rat. Journal of Neuroscience, 17(1), 190-203.

Stephany, C. É., Chan, L. L., Parivash, S. N., Dorton, H. M., Piechowicz, M., Qiu, S., & McGee, A. W. (2014). Plasticity of binocularity and visual acuity are differentially limited by nogo receptor. Journal of Neuroscience, 34(35), 11631-11640.

Stephany, C. É., Ikrar, T., Nguyen, C., Xu, X., & McGee, A. W. (2016). Nogo receptor 1 confines a disinhibitory microcircuit to the critical period in visual cortex. Journal of Neuroscience, 36(43), 11006-11012.

Squire, L. R. (2004). Memory systems of the brain: a brief history and current perspective. Neurobiology of learning and memory, 82(3), 171-177.

Stoppini, L., Buchs, P. A., & Muller, D. (1991). A simple method for organotypic cultures of nervous tissue. Journal of neuroscience methods, 37(2), 173-182.

Sun, Q., Sotayo, A., Cazzulino, A. S., Snyder, A. M., Denny, C. A., & Siegelbaum, S. A. (2017). Proximodistal heterogeneity of hippocampal CA3 pyramidal neuron intrinsic properties, connectivity, and reactivation during memory recall. Neuron, 95(3), 656-672.

Schmidt-Supprian, M., & Rajewsky, K. (2007). Vagaries of conditional gene targeting. Nature immunology, 8(7), 665.

Tews, B., Schönig, K., Arzt, M. E., Clementi, S., Rioult-Pedotti, M. S., Zemmar, A., ... & Kasper, H. (2013). Synthetic microRNA-mediated downregulation of Nogo-A in transgenic

rats reveals its role as regulator of synaptic plasticity and cognitive function. Proceedings of the National Academy of Sciences, 110(16), 6583-6588.

Thompson, C. L., Pathak, S. D., Jeromin, A., Ng, L. L., MacPherson, C. R., Mortrud, M. T., ... & Puchalski, R. B. (2008). Genomic anatomy of the hippocampus. Neuron, 60(6), 1010-1021.

Tønnesen, J., Katona, G., Rózsa, B., & Nägerl, U. V. (2014). Spine neck plasticity regulates compartmentalization of synapses. Nature neuroscience, 17(5), 678.

Tsien, J. Z., Chen, D. F., Gerber, D., Tom, C., Mercer, E. H., Anderson, D. J., ... & Tonegawa, S. (1996). Subregion-and cell type–restricted gene knockout in mouse brain. Cell, 87(7), 1317-1326.

Tukker, J. J., Lasztóczi, B., Katona, L., Roberts, J. D. B., Pissadaki, E. K., Dalezios, Y., ... & Somogyi, P. (2013). Distinct dendritic arborization and in vivo firing patterns of parvalbumin-expressing basket cells in the hippocampal area CA3. Journal of Neuroscience, 33(16), 6809-6825.

Turner, D. A., Li, X. G., Pyapali, G. K., Ylinen, A., & Buzsaki, G. (1995). Morphometric and electrical properties of reconstructed hippocampal CA3 neurons recorded in vivo. Journal of Comparative Neurology, 356(4), 580-594.

Vajda, F. (2014). The role of glial versus neuronal nogo-a in axonal regeneration in the mouse central nervous system (Doctoral dissertation, ETH Zurich).

Vajda, F., Jordi, N., Dalkara, D., Joly, S., Christ, F., Tews, B., ... & Pernet, V. (2015). Cell type-specific Nogo-A gene ablation promotes axonal regeneration in the injured adult optic nerve. Cell death and differentiation, 22(2), 323.

Van Harreveld, A., & Fifkova, E. (1975). Swelling of dendritic spines in the fascia dentata after stimulation of the perforant fibers as a mechanism of post-tetanic potentiation. Experimental neurology, 49(3), 736-749.

Vargha-Khadem, F., Gadian, D. G., Watkins, K. E., Connelly, A., Van Paesschen, W., & Mishkin, M. (1997). Differential effects of early hippocampal pathology on episodic and semantic memory. Science, 277(5324), 376-380.

Wang, K. C., Kim, J. A., Sivasankaran, R., Segal, R., & He, Z. (2002). P75 interacts with the Nogo receptor as a co-receptor for Nogo, MAG and OMgp. Nature, 420(6911), 74.

Wang, X., Chun, S. J., Treloar, H., Vartanian, T., Greer, C. A., & Strittmatter, S. M. (2002). Localization of Nogo-A and Nogo-66 receptor proteins at sites of axon–myelin and synaptic contact. Journal of Neuroscience, 22(13), 5505-5515.

Wickens, J. (1988). Electrically coupled but chemically isolated synapses: dendritic spines and calcium in a rule for synaptic modification. Progress in neurobiology, 31(6), 507-528.

Wills, Z. P., Mandel-Brehm, C., Mardinly, A. R., McCord, A. E., Giger, R. J., & Greenberg, M. E. (2012). The nogo receptor family restricts synapse number in the developing hippocampus. Neuron, 73(3), 466-481.

Wolff, S. B., Gründemann, J., Tovote, P., Krabbe, S., Jacobson, G. A., Müller, C., ... & Lüthi, A. (2014). Amygdala interneuron subtypes control fear learning through disinhibition. Nature, 509(7501), 453.

Xu, T., Yu, X., Perlik, A. J., Tobin, W. F., Zweig, J. A., Tennant, K., ... & Zuo, Y. (2009). Rapid formation and selective stabilization of synapses for enduring motor memories. Nature, 462(7275), 915.

Yazaki-Sugiyama, Y., Kang, S., Câteau, H., Fukai, T., & Hensch, T. K. (2009). Bidirectional plasticity in fast-spiking GABA circuits by visual experience. Nature, 462(7270), 218.

Yuste, R. (2013). Electrical compartmentalization in dendritic spines. Annual review of neuroscience, 36, 429-449.

Yuste, R., & Bonhoeffer, T. (2001). Morphological changes in dendritic spines associated with long-term synaptic plasticity. Annual review of neuroscience, 24(1), 1071-1089.

Zagrebelsky, M., Lonnemann, N., Fricke, S., Kellner, Y., Preuß, E., Michaelsen-Preusse, K., & Korte, M. (2017). Nogo-A regulates spatial learning as well as memory formation and modulates structural plasticity in the adult mouse hippocampus. *Neurobiology of learning and memory*, *138*, 154-163.

Zagrebelsky, M., Schweigreiter, R., Bandtlow, C. E., Schwab, M. E., & Korte, M. (2010). Nogo-A stabilizes the architecture of hippocampal neurons. Journal of Neuroscience, 30(40), 13220-13234.

Zemmar, A., Weinmann, O., Kellner, Y., Yu, X., Vicente, R., Gullo, M., ... & Rioult-Pedotti, M. (2014). Neutralization of Nogo-A enhances synaptic plasticity in the rodent motor cortex and improves motor learning in vivo. Journal of Neuroscience, 34(26), 8685-8698.

Zhou, Q., Homma, K. J., & Poo, M. M. (2004). Shrinkage of dendritic spines associated with long-term depression of hippocampal synapses. Neuron, 44(5), 749-757

Zito, K., Knott, G., Shepherd, G. M., Shenolikar, S., & Svoboda, K. (2004). Induction of spine growth and synapse formation by regulation of the spine actin cytoskeleton. Neuron, 44(2), 321-334.

Abbreviations

AMPAR	α-amino-3-hydroxy-5-methyl-4-isoxazolepropionic acid receptor
CA	*cornu ammonis*
CaMKII	Ca^{2+}/calmodulin-dependent protein kinase II
Cre	causes recombination
Ctrl	control
d, m, v	dorsal, mid, ventral
D	diffusion coefficient
DIV	days *in vitro*
DOC	2,5-dimethoxy-4-chloroamphetamine
eGFP-F	farnesylated enhanced green fluorescent protein
GABA	gamma-aminobutyric acid
GluR1	glutamate receptor subunit 1
KD	knockdown
KO	knockout
LTP	long-term potentiation
mEPSC	miniature excitatory postsynaptic current
mIPSC	miniature inhibitory postsynaptic current
MSD	mean square displacement
MWM	Morris water maze
NMDA	N-methyl-D-aspartate
OD	ocular dominance
OHC	organotypic hippocampal culture
P	postnatal day
PSD	postsynaptic density
PT	probe trial
PV	Parvalbumin

RT	room temperature
RNA	ribonucleic acid
S1PR2	Sphingosine 1-phosphate receptor 2
TTX	tetrodotoxin
WT	wildtype

Appendix

Table 1: related to Figure 11

	Spine architecture and density												
		CTRL			**CTRL + TTX**			**Nogo-A Ab**			**Nogo-A Ab + TTX**		
	Time (h)	Mean (%)	SEM	N	Mean (%)	SEM	N	Mean (%)	SEM	N	Mean (%)	SEM	N
Spine density	0	0	0	6	0	0	7	0	0	6	0	0	8
	1	-1.661	1.111	6	-0.641	0.434	7	1.762	0.912	6	0.474	0.740	8
	2	-1.097	1.158	6	0.435	0.801	7	5.417	1.504	6	1.666	0.953	8
	3	-2.722	0.854	6	0.488	0.693	7	6.716	1.093	6	2.147	0.882	8
Spine length	0	0	0	7	0	0	6	0	0	7	0	0	8
	1	-1.649	0.832	7	0.292	1.244	6	4.865	0.546	7	1.383	0.839	8
	2	-1.200	0.260	7	-0.760	1.675	6	9.535	2.197	7	3.267	1.450	8
	3	0.252	1.093	7	-1.654	1.122	6	12.103	2.356	7	3.012	1.519	8
Spine width	0	0	0	7	0	0	6	0	0	7	0	0	8
	1	-1.975	1.524	7	0.077	1.123	6	-1.680	3.071	7	-1.024	1.092	8
	2	-0.519	0.914	7	1.214	1.857	6	0.486	3.304	7	-1.391	1.128	8
	3	-1.251	1.589	7	-0.965	2.084	6	-0.472	3.771	7	-2.568	1.261	8

Table 2: related to Figures 13 and 14

	mIPSC amplitude						mIPSC frequency					
	Ctrl Ab			Nogo-A Ab			Ctrl Ab			Nogo-A Ab		
Time (min)	Mean (%)	SEM	N	Mean (%)	SEM	N	Mean (%)	SEM	N	Mean (%)	SEM	N
0	0	0	10	0	0	9	0	0	10	0	0	9
5	2.053	1.006	10	-5.626	1.365	9	2.795	1.240	10	-1.814	1.981	9
10	1.732	1.425	10	-12.740	1.731	9	3.751	1.712	10	-4.283	2.603	9
15	0.461	1.045	10	-13.283	2.445	9	3.211	1.174	10	-4.751	3.536	9
20	-0.716	1.656	10	-13.406	3.102	9	2.737	1.585	10	-1.698	2.740	9
	PBS Ctrl			Δ20			PBS Ctrl			Δ20		
Time (min)	Mean (%)	SEM	N	Mean (%)	SEM	N	Mean (%)	SEM	N	Mean (%)	SEM	N
0	0	0	12	0	0	11	0	0	12	0	0	11
5	1.037	0.964	12	5.728	1.564	11	1.756	0.789	12	3.577	2.390	11
10	0.813	0.874	12	5.052	1.822	11	2.327	1.041	12	3.517	1.786	11
	DMSO Ctrl			JTE013			DMSO Ctrl			JTE013		
Time (min)	Mean (%)	SEM	N	Mean (%)	SEM	N	Mean (%)	SEM	N	Mean (%)	SEM	N
0	0	0	9	0	0	11	0	0	9	0	0	11
5	2.416	1.089	9	-4.637	1.671	11	-1.091	2.256	9	-6.698	3.721	11
10	0.765	2.153	9	-7.445	1.869	11	-1.205	1.602	9	-3.676	2.270	11
15	0.844	2.521	9	-10.216	2.353	11	1.641	1.621	9	-4.783	2.477	11
20	3.747	2.446	9	-5.890	3.255	11	2.916	2.926	9	1.140	1.456	11
	Ctrl Ab			NgR1 Ab			Ctrl Ab			NgR1 Ab		
Time (min)	Mean (%)	SEM	N	Mean (%)	SEM	N	Mean (%)	SEM	N	Mean (%)	SEM	N
0	0	0	13	0	0	12	0	0	13	0	0	12
5	0.396	0.999	13	0.661	1.712	12	2.045	1.618	13	1.518	3.082	12
10	0.481	1.222	13	-0.895	1.502	12	2.880	1.203	13	0.678	2.162	12
15	-1.139	1.373	13	-0.885	1.118	12	0.034	1.680	13	1.385	2.158	12
20	-0.792	2.040	13	0.505	1.201	12	-1.039	1.595	13	1.381	3.010	12
	mEPSC amplitude						mEPSC frequency					
	Ctrl Ab			Nogo-A Ab			Ctrl Ab			Nogo-A Ab		
Time (min)	Mean (%)	SEM	N	Mean (%)	SEM	N	Mean (%)	SEM	N	Mean (%)	SEM	N
0	0	0	10	0	0	11	0	0	10	0	0	11
5	-3.782	1.579	10	2.376	2.590	11	-0.916	5.040	10	-8.142	4.435	11
10	-2.909	1.763	10	13.452	3.286	11	0.436	6.060	10	-6.552	4.860	11
15	-1.208	2.062	10	8.439	3.193	11	-5.767	4.881	10	-2.383	4.995	11
20	-1.835	1.594	10	6.508	3.204	11	-10.804	3.749	10	-6.708	6.181	11
25	0.822	1.816	10	2.998	2.545	11	-5.169	4.428	10	-4.548	6.576	11

Table 3: related to Figures 15 and 16

GABA$_A$R live-cell-labeling analysis										
		Density			Fluorescence intensity			Colocalization with synapsin		
		Mean	**SEM**	**N**	**Mean**	**SEM**	**N**	**Mean**	**SEM**	**N**
GABA$_A$R puncta	**Ctrl Ab**	1.000	0.035	30	1.000	0.052	30	1.000	0.045	30
	Nogo-A Ab	0.842	0.036	30	0.699	0.037	30	0.775	0.041	30
	DMSO ctrl	1.000	0.025	51	1.000	0.040	51	1.000	0.034	52
	JTE013	0.909	0.025	46	0.829	0.039	46	0.864	0.039	43
	Ctrl Ab	1.000	0.040	45	1.000	0.093	45	1.000	0.050	44
	NgR1 Ab	0.987	0.039	39	0.974	0.104	39	0.974	0.039	39
Synapsin puncta	**Ctrl Ab**	1.000	0.042	30	1.000	0.061	30			
	Nogo-A Ab	0.995	0.039	30	0.967	0.054	30			
	DMSO ctrl	1.000	0.021	53	1.000	0.048	52			
	JTE013	1.001	0.026	44	0.902	0.043	43			
	Ctrl Ab	1.000	0.038	45	1.000	0.061	45			
	NgR1 Ab	0.972	0.037	39	1.062	0.080	39			

Table 4: related to Figure 17

GABA$_A$R diffusion coefficient							
		Time [min]	0	5	10	15	20
Ctrl Ab	**Synaptic**	N (QDs)	2579	2450	2471	2345	1904
		N (FOV)	13	13	13	13	11
		25% Percentile	0.015	0.016	0.014	0.013	0.014
		Median	0.022	0.022	0.018	0.022	0.016
		75% Percentile	0.033	0.03	0.031	0.034	0.035
		Mean	0.023	0.025	0.023	0.022	0.023
		Std. Error	0.003	0.004	0.004	0.003	0.004
	Extrasynaptic	N (QDs)	5181	5052	4465	4895	3851
		N (FOV)	13	13	13	13	12
		25% Percentile	0.02	0.024	0.02	0.018	0.018
		Median	0.033	0.034	0.031	0.03	0.027
		75% Percentile	0.044	0.041	0.037	0.035	0.032
		Mean	0.034	0.033	0.029	0.03	0.027
		Std. Error	0.004	0.003	0.003	0.004	0.003
Nogo-A Ab	**Synaptic**	N (QDs)	2782	2664	2687	2253	1848
		N (Exp)	14	14	14	14	12
		25% Percentile	0.016	0.026	0.029	0.026	0.018
		Median	0.024	0.039	0.04	0.034	0.029
		75% Percentile	0.034	0.051	0.054	0.051	0.059
		Mean	0.027	0.039	0.041	0.038	0.036

		Std. Error	0.004	0.004	0.004	0.004	0.006
	Extrasynaptic	N (QDs)	5582	5768	5703	5636	4214
		N (Exp)	14	14	14	14	13
		25% Percentile	0.015	0.03	0.034	0.031	0.023
		Median	0.029	0.033	0.038	0.04	0.034
		75% Percentile	0.039	0.045	0.049	0.045	0.042
		Mean	0.03	0.038	0.041	0.041	0.034
		Std. Error	0.004	0.003	0.003	0.004	0.003

Table 5.1: related to Figure 17

Diffusion coefficient (frequency distribution histogram)															
	Ctrl Ab (synaptic)														
Time	**0 min**			**5 min**			**10 min**			**15 min**			**20 min**		
Bin	Mean	SEM	N	Mean	SEM	N	Mean	SEM	N	Mean	SEM	N	Mean	SEM	N
-5	26.324	3.363	13	24.317	2.287	13	26.798	2.738	13	27.082	3.097	13	26.443	2.373	11
-4.8	0.017	0.017	13	0.023	0.023	13	0.050	0.035	13	0.041	0.028	13	0.000	0.000	11
-4.6	0.055	0.046	13	0.088	0.088	13	0.142	0.079	13	0.000	0.000	13	0.092	0.065	11
-4.4	0.138	0.100	13	0.186	0.086	13	0.063	0.052	13	0.019	0.019	13	0.026	0.026	11
-4.2	0.403	0.193	13	0.169	0.103	13	0.258	0.120	13	0.048	0.048	13	0.090	0.065	11
-4	0.173	0.061	13	0.101	0.056	13	0.175	0.075	13	0.437	0.146	13	0.340	0.124	11
-3.8	0.451	0.188	13	0.532	0.152	13	0.366	0.167	13	1.902	1.512	13	0.550	0.159	11
-3.6	0.829	0.194	13	0.709	0.207	13	0.644	0.221	13	1.171	0.747	13	0.817	0.167	11
-3.4	1.387	0.214	13	0.805	0.180	13	0.809	0.285	13	1.427	0.620	13	0.703	0.225	11
-3.2	1.716	0.389	13	1.009	0.232	13	1.499	0.259	13	1.593	0.444	13	1.496	0.428	11
-3	2.359	0.356	13	2.727	0.474	13	1.763	0.416	13	1.713	0.283	13	1.738	0.338	11
-2.8	3.043	0.402	13	3.348	0.361	13	2.584	0.336	13	2.780	0.561	13	3.817	0.818	11
-2.6	4.396	0.842	13	3.369	0.384	13	3.580	0.575	13	3.161	0.460	13	4.052	1.003	11
-2.4	4.382	0.502	13	4.728	0.898	13	5.741	0.444	13	6.169	1.201	13	4.499	0.583	11
-2.2	6.216	0.917	13	5.600	0.530	13	5.833	0.503	13	4.953	0.610	13	5.668	0.748	11
-2	6.096	0.679	13	6.448	0.616	13	7.820	1.491	13	5.514	0.645	13	7.340	0.652	11
-1.8	6.481	0.702	13	7.821	0.676	13	6.678	0.934	13	8.241	0.846	13	6.667	0.877	11
-1.6	7.947	0.971	13	8.363	1.282	13	7.991	0.804	13	8.116	1.057	13	7.905	0.978	11
-1.4	7.478	1.064	13	7.251	1.074	13	7.904	0.951	13	7.679	1.128	13	8.622	1.263	11
-1.2	6.164	1.153	13	7.580	0.963	13	6.732	1.095	13	6.524	1.060	13	8.136	1.238	11
-1.0	5.694	0.907	13	5.869	0.943	13	5.780	0.949	13	4.950	1.028	13	4.821	0.862	11
-0.8	4.073	0.845	13	4.931	0.885	13	3.469	0.783	13	3.502	0.832	13	3.911	0.938	11
-0.6	3.020	0.521	13	2.853	0.380	13	2.538	0.550	13	1.940	0.563	13	1.632	0.460	11
-0.4	0.948	0.235	13	0.946	0.239	13	0.632	0.179	13	0.821	0.264	13	0.594	0.207	11
-0.2	0.179	0.059	13	0.230	0.172	13	0.152	0.065	13	0.217	0.071	13	0.026	0.026	11
0	0.031	0.031	13	0	0	13	0	0	13	0	0	13	0.015	0.015	11

Table 5.2: related to Figure 17

Diffusion coefficient (frequency distribution histogram)															
	Ctrl Ab (extrasynaptic)														
Time	**0 min**			**5 min**			**10 min**			**15 min**			**20 min**		
Bin	Mean	SEM	N	Mean	SEM	N	Mean	SEM	N	Mean	SEM	N	Mean	SEM	N
-5	21.426	1.836	13	21.291	1.998	13	23.352	1.974	13	22.061	2.167	13	22.504	1.610	12
-4.8	0.045	0.027	13	0.054	0.025	13	0.019	0.019	13	0.013	0.013	13	0.036	0.019	12
-4.6	0.069	0.050	13	0.074	0.031	13	0.064	0.031	13	0.043	0.024	13	0.046	0.031	12
-4.4	0.215	0.105	13	0.110	0.078	13	0.044	0.023	13	0.045	0.025	13	0.055	0.024	12
-4.2	0.066	0.036	13	0.080	0.047	13	0.073	0.035	13	0.178	0.087	13	0.133	0.043	12
-4	0.257	0.098	13	0.181	0.052	13	0.221	0.075	13	0.112	0.038	13	0.157	0.058	12
-3.8	0.314	0.091	13	0.254	0.071	13	0.316	0.071	13	0.219	0.056	13	0.309	0.122	12
-3.6	0.615	0.124	13	0.786	0.259	13	0.528	0.109	13	0.455	0.144	13	0.310	0.133	12
-3.4	0.767	0.138	13	0.756	0.139	13	0.929	0.181	13	0.431	0.105	13	0.714	0.248	12
-3.2	1.369	0.302	13	1.013	0.194	13	0.946	0.123	13	1.018	0.234	13	0.892	0.177	12
-3	1.512	0.229	13	1.599	0.225	13	1.668	0.193	13	1.472	0.219	13	1.645	0.295	12
-2.8	2.692	0.409	13	2.076	0.294	13	2.119	0.239	13	2.616	0.345	13	2.689	0.333	12
-2.6	3.119	0.283	13	3.242	0.337	13	2.730	0.265	13	3.136	0.408	13	3.912	0.550	12
-2.4	4.071	0.346	13	3.787	0.274	13	4.743	0.631	13	4.664	0.740	13	4.060	0.387	12
-2.2	5.119	0.273	13	4.581	0.337	13	5.446	0.211	13	5.304	0.299	13	5.951	0.582	12
-2	6.309	0.501	13	6.063	0.397	13	6.964	0.493	13	6.780	0.773	13	6.279	0.327	12
-1.8	6.907	0.538	13	7.392	0.476	13	7.665	0.540	13	8.250	0.860	13	7.803	0.664	12
-1.6	7.363	0.530	13	8.592	0.658	13	8.875	1.008	13	7.641	0.660	13	9.548	0.957	12
-1.4	8.588	0.584	13	8.510	0.675	13	7.753	0.936	13	8.086	0.840	13	8.855	0.647	12
-1.2	9.257	0.874	13	9.091	0.631	13	8.484	0.806	13	8.465	0.970	13	9.038	0.831	12
-1.0	7.858	0.796	13	8.725	0.667	13	8.054	0.777	13	7.663	0.902	13	6.445	0.702	12
-0.8	6.127	0.711	13	6.024	0.521	13	4.970	0.615	13	6.293	0.858	13	5.005	0.429	12
-0.6	3.836	0.387	13	4.388	0.711	13	2.604	0.587	13	3.487	0.485	13	2.557	0.457	12
-0.4	1.599	0.212	13	1.129	0.217	13	1.187	0.296	13	1.264	0.193	13	0.860	0.159	12
-0.2	0.476	0.074	13	0.189	0.065	13	0.220	0.075	13	0.293	0.112	13	0.198	0.060	12
0	0.024	0.016	13	0.013	0.013	13	0.026	0.017	13	0.012	0.012	13	0.000	0.000	12

Table 5.3: related to Figure 17

Diffusion coefficient (frequency distribution histogram)															
	Nogo-A Ab (synaptic)														
Time	**0 min**			**5 min**			**10 min**			**15 min**			**20 min**		
Bin	Mean	SEM	N	Mean	SEM	N	Mean	SEM	N	Mean	SEM	N	Mean	SEM	N
-5	24.975	1.750	14	18.912	2.327	14	14.690	1.831	14	19.027	2.286	14	22.045	2.187	13
-4.8	0.051	0.036	14	0.023	0.023	14	0.000	0.000	14	0.000	0.000	14	0.154	0.083	13
-4.6	0.000	0.000	14	0.107	0.049	14	0.063	0.043	14	0.055	0.041	14	0.000	0.000	13
-4.4	0.104	0.042	14	0.068	0.050	14	0.104	0.047	14	0.175	0.110	14	0.104	0.077	13
-4.2	0.047	0.026	14	0.059	0.042	14	0.101	0.083	14	0.074	0.040	14	0.199	0.091	13
-4	0.261	0.085	14	0.196	0.070	14	0.135	0.062	14	0.416	0.217	14	0.226	0.088	13
-3.8	0.457	0.172	14	0.228	0.094	14	0.127	0.054	14	0.418	0.127	14	0.273	0.107	13
-3.6	1.030	0.454	14	0.421	0.118	14	0.397	0.167	14	0.473	0.219	14	0.264	0.110	13
-3.4	0.998	0.162	14	0.742	0.157	14	0.233	0.091	14	0.515	0.142	14	0.769	0.179	13
-3.2	0.831	0.180	14	0.686	0.123	14	0.493	0.173	14	0.862	0.239	14	1.475	0.372	13
-3	1.622	0.294	14	1.525	0.263	14	1.036	0.307	14	1.232	0.341	14	1.844	0.291	13
-2.8	2.587	0.333	14	1.731	0.304	14	1.844	0.275	14	2.255	0.367	14	1.758	0.276	13
-2.6	3.245	0.484	14	3.367	0.505	14	2.079	0.371	14	3.014	0.448	14	2.190	0.418	13
-2.4	5.490	0.728	14	3.922	0.612	14	3.391	0.351	14	3.590	0.421	14	5.187	0.510	13
-2.2	5.354	0.492	14	4.251	0.464	14	4.798	0.479	14	4.762	0.560	14	5.067	0.525	13
-2	6.801	0.379	14	6.142	0.558	14	5.736	0.735	14	6.013	0.526	14	5.831	0.767	13
-1.8	7.790	0.767	14	7.592	0.928	14	8.211	0.510	14	7.890	0.662	14	6.711	0.601	13
-1.6	9.351	1.176	14	8.940	1.236	14	9.855	1.106	14	8.459	0.818	14	6.965	0.789	13
-1.4	7.168	0.561	14	8.444	0.889	14	10.171	0.656	14	9.374	0.933	14	8.152	0.621	13
-1.2	6.604	0.915	14	9.165	0.985	14	11.489	0.948	14	9.579	0.977	14	10.090	1.186	13
-1.0	5.612	1.071	14	10.526	1.349	14	10.574	1.134	14	8.160	0.755	14	7.812	1.143	13
-0.8	4.835	1.092	14	7.442	0.948	14	8.709	0.797	14	7.816	1.195	14	7.600	1.571	13
-0.6	2.835	0.549	14	4.148	0.665	14	3.915	0.466	14	4.239	1.217	14	3.307	0.701	13
-0.4	1.334	0.444	14	1.193	0.273	14	1.609	0.325	14	1.275	0.310	14	1.841	0.411	13
-0.2	0.521	0.195	14	0.145	0.056	14	0.223	0.079	14	0.301	0.128	14	0.136	0.072	13
0	0.098	0.098	14	0.025	0.025	14	0.016	0.016	14	0.029	0.029	14	0.000	0.000	13

Table 5.4: related to Figure 17

Diffusion coefficient (frequency distribution histogram)															
	Nogo-A Ab (extrasynaptic)														
Time	**0 min**			**5 min**			**10 min**			**15 min**			**20 min**		
Bin	Mean	SEM	N	Mean	SEM	N	Mean	SEM	N	Mean	SEM	N	Mean	SEM	N
-5	25.195	1.940	14	19.185	1.160	14	18.608	1.145	14	18.922	1.168	14	20.970	1.364	13
-4.8	0.040	0.019	14	0.013	0.013	14	0.013	0.013	14	0.012	0.012	14	0.038	0.027	13
-4.6	0.050	0.023	14	0.018	0.014	14	0.028	0.020	14	0.052	0.029	14	0.000	0.000	13
-4.4	0.025	0.017	14	0.024	0.020	14	0.069	0.039	14	0.111	0.072	14	0.173	0.073	13
-4.2	0.211	0.047	14	0.141	0.059	14	0.041	0.034	14	0.094	0.034	14	0.063	0.031	13
-4	0.183	0.039	14	0.115	0.049	14	0.111	0.040	14	0.081	0.033	14	0.166	0.058	13
-3.8	0.454	0.105	14	0.262	0.091	14	0.275	0.077	14	0.229	0.077	14	0.237	0.085	13
-3.6	0.788	0.142	14	0.514	0.109	14	0.372	0.073	14	0.465	0.100	14	0.327	0.087	13
-3.4	1.021	0.184	14	0.524	0.111	14	0.648	0.110	14	0.604	0.107	14	0.425	0.101	13
-3.2	1.323	0.142	14	0.870	0.135	14	0.781	0.175	14	0.857	0.132	14	0.983	0.117	13
-3	1.973	0.188	14	1.253	0.230	14	1.069	0.191	14	1.370	0.135	14	1.807	0.262	13
-2.8	2.515	0.294	14	2.142	0.212	14	2.205	0.213	14	1.833	0.177	14	1.980	0.222	13
-2.6	3.323	0.265	14	3.064	0.294	14	2.249	0.366	14	2.428	0.306	14	2.799	0.279	13
-2.4	4.106	0.411	14	3.682	0.410	14	3.659	0.303	14	3.358	0.268	14	4.368	0.437	13
-2.2	5.197	0.466	14	4.644	0.418	14	4.931	0.385	14	5.122	0.459	14	4.753	0.330	13
-2	6.314	0.482	14	5.530	0.414	14	5.995	0.455	14	6.178	0.275	14	6.735	0.524	13
-1.8	6.667	0.547	14	7.698	0.454	14	6.720	0.413	14	7.486	0.652	14	7.431	0.770	13
-1.6	7.748	0.620	14	8.278	0.350	14	8.650	0.881	14	7.755	0.628	14	7.939	0.651	13
-1.4	8.075	0.711	14	9.234	0.444	14	8.759	0.574	14	9.545	0.730	14	8.155	0.542	13
-1.2	8.012	0.988	14	10.687	0.671	14	10.427	0.585	14	10.487	0.804	14	8.647	0.584	13
-1.0	6.818	0.884	14	8.720	0.763	14	9.484	0.508	14	10.007	0.688	14	9.143	0.677	13
-0.8	5.572	0.786	14	7.566	0.631	14	8.330	0.581	14	7.303	0.719	14	7.186	0.683	13
-0.6	3.012	0.479	14	4.250	0.402	14	4.428	0.449	14	4.093	0.699	14	3.807	0.536	13
-0.4	0.979	0.214	14	1.287	0.232	14	1.745	0.308	14	1.350	0.166	14	1.523	0.264	13
-0.2	0.393	0.066	14	0.266	0.090	14	0.352	0.089	14	0.244	0.084	14	0.247	0.068	13
0	0.005	0.005	14	0.033	0.021	14	0.050	0.040	14	0.016	0.016	14	0.098	0.073	13

Table 5.5: related to Figure 17

Immobile fraction (%)							
		Time (min)	**0**	**5**	**10**	**15**	**20**
Ctrl Ab	**synaptic**	Mean (%)	43.665	39.71	41.467	45.048	42.391
		SEM	5.393	3.494	3.625	5.945	4.48
		N	13	13	13	13	11
	extra-synaptic	Mean (%)	34.336	33.409	35.13	33.638	35.448
		SEM	2.917	2.892	2.665	3.283	2.675
		N	13	13	13	13	12
Nogo-A Ab	**synaptic**	Mean (%)	39.046	30.154	22.68	30.22	34.39
		SEM	2.523	3.77	2.433	3.422	3.017
		N	14	14	14	14	13
	extra-synaptic	Mean (%)	38.988	29.788	28.167	28.789	31.999
		SEM	2.956	1.949	1.837	1.89	1.977
		N	14	14	14	14	13

Table 6.1: related to Figure 18

$GABA_AR$ mean sqaure displacement (MSD)									
	Ctrl Ab (synaptic)								
Time (min)	**0 min**			**5 min**			**10 min**		
Time (s)	Mean MSD	SEM	N	Mean MSD	SEM	N	Mean MSD	SEM	N
0.03	0.0080	0.0005	14	0.0075	0.0004	14	0.0084	0.0005	14
0.06	0.0108	0.0008	14	0.0095	0.0007	14	0.0112	0.0008	14
0.09	0.0131	0.0012	14	0.0112	0.0009	14	0.0136	0.0012	14
0.12	0.0151	0.0015	14	0.0127	0.0011	14	0.0161	0.0016	14
0.15	0.0170	0.0018	14	0.0140	0.0013	14	0.0181	0.0020	14
0.18	0.0187	0.0021	14	0.0152	0.0015	14	0.0200	0.0024	14
0.21	0.0203	0.0023	14	0.0162	0.0017	14	0.0222	0.0027	14
0.24	0.0218	0.0026	14	0.0171	0.0019	14	0.0240	0.0031	14
0.27	0.0233	0.0028	14	0.0181	0.0021	14	0.0258	0.0034	14
0.3	0.0248	0.0030	14	0.0191	0.0023	14	0.0277	0.0038	14
0.33	0.0260	0.0032	14	0.0198	0.0025	14	0.0294	0.0041	14
0.36	0.0275	0.0034	14	0.0210	0.0026	14	0.0311	0.0044	14
0.39	0.0287	0.0036	14	0.0220	0.0028	14	0.0329	0.0047	14
0.42	0.0301	0.0038	14	0.0230	0.0030	14	0.0343	0.0051	14
0.45	0.0314	0.0040	14	0.0240	0.0032	14	0.0363	0.0054	14
0.48	0.0326	0.0042	14	0.0247	0.0034	14	0.0377	0.0058	14
0.51	0.0338	0.0044	14	0.0256	0.0037	14	0.0398	0.0062	14
0.54	0.0349	0.0046	14	0.0265	0.0039	14	0.0415	0.0065	14
0.57	0.0361	0.0048	14	0.0273	0.0041	14	0.0429	0.0068	14
0.6	0.0375	0.0050	14	0.0282	0.0043	14	0.0448	0.0070	14
0.63	0.0386	0.0052	14	0.0293	0.0045	14	0.0464	0.0074	14
0.66	0.0400	0.0055	14	0.0303	0.0047	14	0.0475	0.0078	14
0.69	0.0414	0.0057	14	0.0313	0.0049	14	0.0493	0.0080	14
0.72	0.0428	0.0060	14	0.0323	0.0051	14	0.0507	0.0082	14
0.75	0.0443	0.0063	14	0.0330	0.0054	14	0.0522	0.0087	14
0.78	0.0458	0.0066	14	0.0340	0.0057	14	0.0544	0.0089	14
0.81	0.0473	0.0069	14	0.0350	0.0061	14	0.0553	0.0092	14
0.84	0.0485	0.0070	14	0.0355	0.0064	14	0.0567	0.0096	14
0.87	0.0498	0.0073	14	0.0362	0.0067	14	0.0586	0.0099	14
0.9	0.0506	0.0074	14	0.0368	0.0068	14	0.0595	0.0102	14
0.93	0.0514	0.0076	14	0.0379	0.0071	14	0.0608	0.0105	14
0.96	0.0521	0.0077	14	0.0397	0.0073	14	0.0622	0.0107	14
0.99	0.0533	0.0077	14	0.0413	0.0076	14	0.0635	0.0108	14
1.02	0.0547	0.0080	14	0.0426	0.0078	14	0.0655	0.0114	14

Table 6.2: related to Figure 18

$GABA_AR$ mean sqaure displacement (MSD)									
	Ctrl Ab (extrasynaptic)								
Time (min)	**0 min**			**5 min**			**10 min**		
Time (s)	Mean MSD	SEM	N	Mean MSD	SEM	N	Mean MSD	SEM	N
0.03	0.0084	0.0003	14	0.0078	0.0004	14	0.0082	0.0003	14
0.06	0.0115	0.0006	14	0.0107	0.0007	14	0.0105	0.0006	14
0.09	0.0141	0.0010	14	0.0131	0.0010	14	0.0124	0.0009	14
0.12	0.0164	0.0014	14	0.0153	0.0013	14	0.0142	0.0012	14
0.15	0.0185	0.0017	14	0.0172	0.0016	14	0.0155	0.0014	14
0.18	0.0205	0.0020	14	0.0191	0.0018	14	0.0169	0.0016	14
0.21	0.0222	0.0023	14	0.0209	0.0021	14	0.0182	0.0018	14
0.24	0.0240	0.0026	14	0.0226	0.0024	14	0.0195	0.0020	14
0.27	0.0255	0.0028	14	0.0242	0.0026	14	0.0206	0.0022	14
0.3	0.0272	0.0031	14	0.0258	0.0029	14	0.0218	0.0024	14
0.33	0.0287	0.0034	14	0.0272	0.0031	14	0.0228	0.0026	14
0.36	0.0303	0.0036	14	0.0288	0.0033	14	0.0241	0.0028	14
0.39	0.0317	0.0039	14	0.0301	0.0036	14	0.0252	0.0030	14
0.42	0.0333	0.0042	14	0.0315	0.0038	14	0.0262	0.0032	14
0.45	0.0349	0.0044	14	0.0329	0.0040	14	0.0274	0.0034	14
0.48	0.0362	0.0047	14	0.0342	0.0042	14	0.0285	0.0036	14
0.51	0.0376	0.0049	14	0.0357	0.0044	14	0.0296	0.0037	14
0.54	0.0390	0.0051	14	0.0371	0.0046	14	0.0306	0.0039	14
0.57	0.0403	0.0054	14	0.0382	0.0049	14	0.0315	0.0040	14
0.6	0.0418	0.0057	14	0.0395	0.0052	14	0.0324	0.0041	14
0.63	0.0433	0.0059	14	0.0407	0.0054	14	0.0332	0.0042	14
0.66	0.0447	0.0063	14	0.0417	0.0056	14	0.0339	0.0044	14
0.69	0.0460	0.0066	14	0.0429	0.0058	14	0.0348	0.0045	14
0.72	0.0472	0.0069	14	0.0440	0.0060	14	0.0357	0.0046	14
0.75	0.0482	0.0072	14	0.0451	0.0061	14	0.0366	0.0048	14
0.78	0.0494	0.0076	14	0.0461	0.0063	14	0.0375	0.0048	14
0.81	0.0506	0.0080	14	0.0472	0.0065	14	0.0384	0.0050	14
0.84	0.0520	0.0084	14	0.0485	0.0067	14	0.0393	0.0051	14
0.87	0.0534	0.0087	14	0.0496	0.0069	14	0.0403	0.0052	14
0.9	0.0545	0.0090	14	0.0507	0.0071	14	0.0412	0.0054	14
0.93	0.0561	0.0093	14	0.0519	0.0073	14	0.0423	0.0056	14
0.96	0.0574	0.0096	14	0.0529	0.0075	14	0.0435	0.0057	14
0.99	0.0591	0.0101	14	0.0540	0.0077	14	0.0442	0.0059	14
1.02	0.0608	0.0105	14	0.0554	0.0079	14	0.0448	0.0060	14

Table 6.3: related to Figure 18

$GABA_AR$ mean sqaure displacement (MSD)									
	Nogo-A Ab (synaptic)								
Time (min)	**0 min**			**5 min**			**10 min**		
Time (s)	Mean MSD	SEM	N	Mean MSD	SEM	N	Mean MSD	SEM	N
0.03	0.0089	0.0005	14	0.0092	0.0003	14	0.0099	0.0003	14
0.06	0.0112	0.0007	14	0.0125	0.0006	14	0.0135	0.0007	14
0.09	0.0130	0.0009	14	0.0153	0.0009	14	0.0162	0.0011	14
0.12	0.0148	0.0010	14	0.0182	0.0012	14	0.0192	0.0015	14
0.15	0.0158	0.0012	14	0.0203	0.0015	14	0.0211	0.0018	14
0.18	0.0168	0.0013	14	0.0226	0.0018	14	0.0232	0.0022	14
0.21	0.0183	0.0014	14	0.0249	0.0021	14	0.0256	0.0025	14
0.24	0.0190	0.0016	14	0.0266	0.0024	14	0.0275	0.0030	14
0.27	0.0201	0.0017	14	0.0287	0.0026	14	0.0294	0.0034	14
0.3	0.0214	0.0018	14	0.0307	0.0029	14	0.0315	0.0037	14
0.33	0.0217	0.0020	14	0.0322	0.0032	14	0.0329	0.0042	14
0.36	0.0230	0.0021	14	0.0341	0.0035	14	0.0352	0.0045	14
0.39	0.0239	0.0023	14	0.0358	0.0038	14	0.0371	0.0048	14
0.42	0.0245	0.0025	14	0.0374	0.0041	14	0.0387	0.0053	14
0.45	0.0259	0.0027	14	0.0392	0.0044	14	0.0408	0.0057	14
0.48	0.0264	0.0028	14	0.0403	0.0047	14	0.0425	0.0063	14
0.51	0.0272	0.0030	14	0.0421	0.0051	14	0.0442	0.0068	14
0.54	0.0280	0.0031	14	0.0440	0.0054	14	0.0464	0.0074	14
0.57	0.0283	0.0032	14	0.0451	0.0057	14	0.0478	0.0080	14
0.6	0.0289	0.0033	14	0.0468	0.0061	14	0.0499	0.0085	14
0.63	0.0299	0.0034	14	0.0487	0.0064	14	0.0519	0.0090	14
0.66	0.0303	0.0037	14	0.0501	0.0067	14	0.0535	0.0097	14
0.69	0.0317	0.0039	14	0.0520	0.0070	14	0.0553	0.0101	14
0.72	0.0325	0.0042	14	0.0535	0.0072	14	0.0571	0.0106	14
0.75	0.0333	0.0044	14	0.0553	0.0075	14	0.0590	0.0112	14
0.78	0.0346	0.0045	14	0.0572	0.0077	14	0.0617	0.0118	14
0.81	0.0350	0.0046	14	0.0586	0.0078	14	0.0634	0.0124	14
0.84	0.0358	0.0047	14	0.0601	0.0080	14	0.0653	0.0130	14
0.87	0.0366	0.0049	14	0.0621	0.0083	14	0.0674	0.0135	14
0.9	0.0369	0.0051	14	0.0638	0.0086	14	0.0695	0.0139	14
0.93	0.0378	0.0052	14	0.0658	0.0089	14	0.0712	0.0140	14
0.96	0.0393	0.0056	14	0.0681	0.0092	14	0.0734	0.0145	14
0.99	0.0408	0.0059	14	0.0694	0.0095	14	0.0755	0.0151	14
1.02	0.0431	0.0059	14	0.0721	0.0098	14	0.0782	0.0156	14

Table 6.4: related to Figure 18

$GABA_AR$ mean sqaure displacement (MSD)									
	Nogo-A Ab (extrasynaptic)								
Time (min)	**0 min**			**5 min**			**10 min**		
Time (s)	Mean MSD	SEM	N	Mean MSD	SEM	N	Mean MSD	SEM	N
0.03	0.0087	0.0004	14	0.0099	0.0004	14	0.0097	0.0005	14
0.06	0.0113	0.0006	14	0.0137	0.0006	14	0.0134	0.0008	14
0.09	0.0134	0.0008	14	0.0169	0.0010	14	0.0165	0.0011	14
0.12	0.0157	0.0011	14	0.0201	0.0013	14	0.0196	0.0015	14
0.15	0.0173	0.0014	14	0.0226	0.0016	14	0.0221	0.0018	14
0.18	0.0191	0.0017	14	0.0254	0.0019	14	0.0245	0.0021	14
0.21	0.0211	0.0019	14	0.0281	0.0022	14	0.0271	0.0024	14
0.24	0.0224	0.0022	14	0.0303	0.0026	14	0.0293	0.0027	14
0.27	0.0240	0.0024	14	0.0327	0.0029	14	0.0317	0.0030	14
0.3	0.0256	0.0026	14	0.0351	0.0031	14	0.0343	0.0033	14
0.33	0.0267	0.0029	14	0.0370	0.0034	14	0.0363	0.0036	14
0.36	0.0283	0.0031	14	0.0395	0.0037	14	0.0388	0.0039	14
0.39	0.0295	0.0034	14	0.0415	0.0039	14	0.0410	0.0042	14
0.42	0.0307	0.0036	14	0.0433	0.0042	14	0.0428	0.0044	14
0.45	0.0323	0.0038	14	0.0457	0.0045	14	0.0450	0.0048	14
0.48	0.0332	0.0040	14	0.0472	0.0048	14	0.0468	0.0050	14
0.51	0.0346	0.0042	14	0.0489	0.0051	14	0.0489	0.0052	14
0.54	0.0360	0.0044	14	0.0509	0.0053	14	0.0510	0.0055	14
0.57	0.0367	0.0046	14	0.0522	0.0055	14	0.0526	0.0057	14
0.6	0.0380	0.0048	14	0.0543	0.0057	14	0.0546	0.0059	14
0.63	0.0391	0.0050	14	0.0562	0.0059	14	0.0563	0.0061	14
0.66	0.0398	0.0052	14	0.0575	0.0062	14	0.0578	0.0063	14
0.69	0.0410	0.0054	14	0.0596	0.0063	14	0.0596	0.0064	14
0.72	0.0418	0.0056	14	0.0611	0.0066	14	0.0612	0.0066	14
0.75	0.0427	0.0059	14	0.0623	0.0067	14	0.0628	0.0067	14
0.78	0.0440	0.0061	14	0.0642	0.0069	14	0.0648	0.0069	14
0.81	0.0448	0.0063	14	0.0657	0.0071	14	0.0664	0.0070	14
0.84	0.0458	0.0065	14	0.0677	0.0073	14	0.0682	0.0072	14
0.87	0.0470	0.0066	14	0.0699	0.0076	14	0.0702	0.0075	14
0.9	0.0478	0.0069	14	0.0712	0.0079	14	0.0718	0.0078	14
0.93	0.0493	0.0072	14	0.0731	0.0080	14	0.0739	0.0081	14
0.96	0.0507	0.0075	14	0.0748	0.0082	14	0.0758	0.0083	14
0.99	0.0517	0.0078	14	0.0765	0.0083	14	0.0772	0.0084	14
1.02	0.0531	0.0081	14	0.0793	0.0084	14	0.0797	0.0086	14

Table 7: related to Figure 18

$GABA_AR$ confinement						
	Ctrl Ab			**Nogo-A Ab**		
Time (min)	Mean (µm)	SEM	N	Mean (µm)	SEM	N
0	0.393	0.042	11	0.292	0.030	13
5	0.319	0.045	11	0.456	0.051	13
10	0.403	0.049	11	0.480	0.080	13
15	0.378	0.071	11	0.364	0.048	13
20	0.280	0.038	11	0.381	0.055	13

Table 8: related to Figure 19

$GABA_AR$ diffusion coefficient					
		Time [min]	0	5	10
Ctrl Ab	**Synaptic**	N (QDs)	3352	2452	2360
		N (FOV)	13	13	13
		25% Percentile	0.004	0.004	0.005
		Median	0.008	0.007	0.009
		75% Percentile	0.016	0.016	0.012
		Mean	0.014	0.011	0.014
		Std. Error	0.004	0.003	0.005
	Extrasynaptic	N (QDs)	8081	6986	6006
		N (FOV)	13	13	13
		25% Percentile	0.007	0.007	0.007
		Median	0.015	0.011	0.009
		75% Percentile	0.025	0.028	0.033
		Mean	0.017	0.018	0.017
		Std. Error	0.003	0.005	0.004
Nogo-A Ab	**Synaptic**	N (QDs)	4309	3539	2873
		N (Exp)	13	13	13
		25% Percentile	0.005	0.006	0.01
		Median	0.01	0.013	0.019
		75% Percentile	0.014	0.048	0.032
		Mean	0.013	0.025	0.022
		Std. Error	0.004	0.006	0.004
	Extrasynapti	N (QDs)	7704	6482	5127
		N (Exp)	13	13	13
		25% Percentile	0.006	0.009	0.01
		Median	0.01	0.021	0.37
		75% Percentile	0.025	0.033	0.045

		Mean	0.017	0.023	0.032
		Std. Error	0.005	0.004	0.005

Table 9: related to Figure 20

MWM latency				
	Day	**Time (s)**	**SEM**	**N**
WT	**1**	56.445	2.346	6
	2	41.442	6.385	6
	3	29.647	5.729	3
	4	22.400	2.899	3
	5	19.395	3.820	3
	6	18.092	5.271	3
	7	7.438	0.453	3
	8	4.846	1.069	3
	9	9.027	1.737	3
	10	7.726	0.738	3
Nogo-A KO	**1**	55.181	1.971	6
	2	51.145	4.453	6
	3	44.311	3.102	3
	4	28.045	3.343	3
	5	20.880	3.226	3
	6	12.376	2.146	3
	7	11.967	3.240	3
	8	6.637	2.659	3
	9	7.867	3.144	3
	10	4.738	1.108	3

Table 10: related to Figure 22

PV intensity (cumulative frequency distribution)					
			Swim Ctrl	**MWM 2 days**	**MWM 10 days**
WT	**dorsal**	N	138	126	103
		25% Percentile	35.488	18.005	18.047
		Median	61.601	40.471	56.138
		75% Percentile	84.548	71.159	91.990
		Mean	59.328	46.256	55.924
		Std. Error	2.536	2.862	3.534
	mid	N	45	75	109
		25% Percentile	16.090	20.875	31.531
		Median	45.808	39.069	62.495
		75% Percentile	88.560	62.384	86.796
		Mean	51.544	44.522	58.616
		Std. Error	4.972	3.365	2.995
	ventral	N	272	262	240
		25% Percentile	31.401	16.359	31.333
		Median	54.513	33.895	56.532
		75% Percentile	81.263	53.088	83.463
		Mean	54.542	38.952	55.884
		Std. Error	1.765	1.693	1.906
Nogo-A KO	**dorsal**	N	109	161	122
		25% Percentile	30.206	18.818	17.016
		Median	56.398	42.344	52.758
		75% Percentile	88.370	68.537	89.846
		Mean	56.530	46.712	52.911
		Std. Error	2.961	2.398	3.219
	mid	N	60	79	48
		25% Percentile	22.250	17.054	32.374
		Median	45.477	40.841	59.644
		75% Percentile	86.246	67.586	86.865
		Mean	52.179	42.985	57.927
		Std. Error	4.303	3.530	4.839
	ventral	N	247	299	252
		25% Percentile	26.480	19.705	26.129
		Median	46.152	39.478	55.006
		75% Percentile	75.029	60.943	81.465
		Mean	50.944	42.175	53.395
		Std. Error	1.840	1.600	1.954

Table 11: related to Figure 24

Nogo-A intensity (cumulative frequency distribution)					
			Swim Ctrl	**MWM 2 days**	**MWM 10 days**
WT	**dorsal**	N	138	126	103
		25% Percentile	33.796	28.491	22.819
		Median	54.409	53.346	50.754
		75% Percentile	83.708	82.199	80.053
		Mean	56.490	55.195	52.819
		Std. Error	2.376	2.658	3.121
	mid	N	45	75	109
		25% Percentile	41.586	38.188	29.697
		Median	61.215	52.644	49.177
		75% Percentile	87.117	73.299	69.800
		Mean	61.106	55.403	52.499
		Std. Error	3.943	2.791	2.506
	ventral	N	272	271	239
		25% Percentile	38.051	25.272	29.973
		Median	58.107	44.890	47.124
		75% Percentile	77.440	69.019	71.650
		Mean	57.619	48.712	50.837
		Std. Error	1.512	1.663	1.744

Table 12: related to Figures 25-28

PV and Nogo-A intensity fractions upon MWM training													
			Low (0-25 %)			Int. low (25-50 %)			Int. high (50-75 %)			High (75-100 %)		
			Mean	SEM	N	Mean	SEM	N	Mean	SEM	N	Mean	SEM	N
WT (PV intensity)	Swim Ctrl	dorsal	19.765	2.970	18	15.948	3.237	18	27.375	3.783	18	36.913	3.828	18
		mid	28.075	6.470	6	24.206	4.062	6	15.873	7.451	6	31.845	7.036	6
		ventral	22.963	2.512	18	20.607	2.716	18	26.563	2.611	18	29.867	2.669	18
	MWM 2 d	dorsal	34.241	3.674	17	21.471	2.835	17	23.380	4.082	17	20.908	1.997	17
		mid	29.732	4.708	6	31.373	7.795	6	20.028	7.420	6	18.867	7.423	6
		ventral	39.840	3.325	18	31.020	4.612	18	16.041	2.689	18	13.098	1.957	18
	MWM 10 d	dorsal	33.320	4.943	18	12.903	3.417	18	10.946	3.335	18	42.831	2.977	18
		mid	18.532	4.090	10	20.144	2.699	10	17.565	3.966	10	43.759	4.991	10
		ventral	17.881	2.592	18	25.436	2.441	18	25.163	2.798	18	31.521	1.851	18
Nogo-A KO (PV intensity)	Swim Ctrl	dorsal	17.817	2.832	16	25.845	3.511	16	24.680	3.284	16	31.659	3.891	16
		mid	29.339	5.646	6	22.596	4.612	6	14.709	1.299	6	33.356	4.207	6
		ventral	24.162	2.800	18	30.028	1.837	18	18.694	2.874	18	27.116	2.581	18
	MWM 2 d	dorsal	29.640	2.687	18	28.444	2.877	18	21.860	3.197	18	20.056	2.274	18
		mid	38.601	3.129	8	22.113	3.616	8	21.622	4.485	8	17.664	3.169	8
		ventral	32.250	2.373	18	32.063	3.066	18	19.854	3.025	18	15.832	2.106	18
	MWM 10 d	dorsal	31.136	4.623	18	17.650	3.817	18	13.752	3.217	18	37.461	3.914	18
		mid	20.918	5.904	6	12.145	3.975	6	25.782	8.651	6	41.156	9.621	6
		ventral	21.428	2.663	18	22.358	2.014	18	25.107	2.194	18	31.107	1.905	18
WT (Nogo-A intensity)	Swim Ctrl	dorsal	9.742	4.230	18	31.148	4.014	18	30.610	4.344	18	28.501	3.361	18
		mid	14.881	3.335	6	17.262	5.895	6	38.492	7.285	6	29.365	3.710	6
		ventral	11.438	2.154	18	30.024	4.004	18	29.525	2.850	18	29.013	3.288	18
	MWM 2 d	dorsal	17.647	4.077	17	27.435	4.856	17	24.330	3.427	17	30.588	3.584	17
		mid	10.305	3.141	6	36.730	2.364	6	29.064	3.453	6	23.900	4.307	6
		ventral	24.938	4.351	18	30.544	3.823	18	21.915	4.066	18	22.603	3.004	18
	MWM 10 d	dorsal	27.083	4.086	18	18.955	4.090	18	22.560	3.442	18	31.402	3.921	18
		mid	15.484	3.414	9	32.194	3.634	9	25.688	4.445	9	26.635	4.451	9
		ventral	20.627	4.212	18	30.782	3.818	18	25.236	3.146	18	23.356	2.844	18

Table 13: related to Figure 32

MWM latency				
	Day	**Time (s)**	**SEM**	**N**
Nogo-A$^{flox/flox}$ (Ctrl for PV-cre)	**1**	31.531	6.773	4
	2	29.788	7.068	4
	3	20.869	4.186	4
	4	16.906	3.212	4
	5	11.300	3.440	4
	6	13.563	4.207	4
	7	10.394	2.788	4
	8	9.438	0.479	4
PV-cre/ Nogo-A$^{flox/flox}$	**1**	35.861	4.742	7
	2	31.400	4.926	7
	3	24.425	5.217	7
	4	20.621	5.243	7
	5	17.618	6.859	7
	6	13.721	2.899	7
	7	12.464	2.242	7
	8	11.629	1.770	7
Nogo-A$^{flox/flox}$ (Ctrl for CaMKII-cre)	**1**	30.094	4.051	8
	2	20.441	2.191	8
	3	22.309	2.478	8
	4	20.538	5.051	8
	5	12.003	2.543	8
	6	10.209	1.666	8
	7	9.472	2.377	8
	8	9.841	1.957	8
CaMKII-cre/ Nogo-A$^{flox/flox}$	**1**	29.905	5.619	5
	2	22.680	4.664	5
	3	18.250	4.792	5
	4	11.205	1.391	5
	5	10.350	2.038	5
	6	7.095	2.385	5
	7	9.105	1.856	5
	8	7.250	1.870	5

Table 14: related to Figure 32

MWM Probe trials at days 3 and 9					
			Mean	**SEM**	**N**
Nogo-A$^{flox/flox}$ (Ctrl for PV-cre)	**PT day 3**	NT quadrant	23.093	1.554	4
		T quadrant	30.667	4.643	
	PT day 9	NT quadrant	18.815	2.403	
		T quadrant	43.511	7.238	
	Platform crossings	Day 3	2.250	0.629	
		Day 9	3.500	0.866	
PV-cre/ Nogo-A$^{flox/flox}$	**PT day 3**	NT quadrant	22.861	1.552	8
		T quadrant	31.389	4.619	
	PT day 9	NT quadrant	16.037	2.020	
		T quadrant	51.861	6.023	
	Platform crossings	Day 3	1.857	0.508	
		Day 9	3.857	0.857	
Nogo-A$^{flox/flox}$ (Ctrl for CaMKII-cre)	**PT day 3**	NT quadrant	21.277	1.575	8
		T quadrant	38.805	5.763	
	PT day 9	NT quadrant	14.666	1.969	
		T quadrant	54.945	5.371	
	Platform crossings	Day 3	2.000	0.423	
		Day 9	3.000	0.378	
CaMKII-cre/ Nogo-A$^{flox/flox}$	**PT day 3**	NT quadrant	19.466	2.480	5
		T quadrant	37.380	5.423	
	PT day 9	NT quadrant	13.526	2.345	
		T quadrant	61.154	7.822	
	Platform crossings	Day 3	2.200	0.970	
		Day 9	4.000	0.775	

Acknowledgements

At last, I would like to thank everyone involved for the invaluable help and support I received during my time as a PhD student. I learned early on that in science you rely on the guidance of the people around you. And, fortunately, I had the opportunity to work with all of you:

First off, I want to thank my supervisor of now 6.5 years, Dr. **Marta Zagrebelsky**. Thank you for all your help, support, advice, patience and light pushes when needed (not necessarily in that order) throughout all my time as bachelor, master and PhD student. I don't think that in science one could have a better supervisor who is herself so fascinated by and enthusiastic for science.

I would like to thank Prof. Dr. **Martin Korte** who has supported me from the very first talk we had in 2013 before the start of my bachelor thesis in his lab. Thank you for all the advice and patience and most of all, for giving me the opportunity to begin my scientific voyage in your lab.

I would also like to thank Prof. Dr. **Jochen Meier** and Prof. Dr. **Robert Hänsch** for reviewing my thesis and being part of my thesis committee.

Of course I want to thank all the people in and around the Korte lab and the Zoological Institute who paved my way. Thank you: **Jonas** and **Niklas** for everything and, most importantly, for always being around. We've had quite a journey, haven't we. **Kristin** for all the fun and science we had. You always made me laugh and enjoy my time in our little office. **Max**, for positivity and singing! **Charlotte**, for gin & tonic and always staying calm. **Shirin**, for brightening every day and being the politest person I know. **Abi**, for being ironic and hilarious. **Jan**, for our weekend meetings. **Susann**, for taking care of what feels like everything and always helping me. **Hendrik**, for making our little office more fun! **Diane**, for all the culture preparations and being amazing. **Caroline**, for all the discussion and fun in our little time since you joined our lab. **Akila**, for being super nice and always smiling. **Yves**, for your excellent supervision during my first years in science. **Florian** and **Vanessa**, for helping me with patch clamp and teaching me new methods. **Melanie**, **Stefan** and **Eike**, for being fun and polite students. You made being a supervisor for the first times amazingly easy for me. **Tania**, for knowing what to do in every situation and all of the help and support with everything in and around lab 184! **Andreas**, for sliding soccer into conversations and always being happy to answer questions. **Kristin** MP, for laughing out loud and making science fun. **Carmen**

and **Heike**, for taking care of so many things and always helping me. **Martin R**., for knowing almost everything about biochemistry and helping me so much, science- and computer-related.

Thanks to the Magdeburg- and, by now, Mainz-crew! Thank you: Prof. Dr. **Martin Heine** for giving me the opportunity to learn and perform single particle tracking in your lab! I always felt welcomed and I could ask you for help at any time. **Anita**, for preparing all the cultures and being so nice and welcoming. **Jenni**, for helping me so much in the lab and at the microscope. You made Magdeburg fancy. **Oli**, for your support in the lab and being an outstanding neighbor in our dorm!

Thanks also to the Utrecht gang! Thank you: Dr. **Corette Wierenga** and Prof. Dr. **Casper Hoogenraad** for letting me perform experiments and write my master thesis in your lab. **Hai Yin**, for teaching me how to patch and being so calm. **Cátia**, for being less calm and making me laugh. **Mirte** and **Tom** for all the discussion and everyday advice for living in Utrecht.

Thank you: **Kristina**, **Sylvia** and **Wilfried**, for being family. **Viola** and **René**, for becoming family. And **Robert**, for being Robert.

Franzi. Thank you so, SO much for everything… You are awesome.

Curriculum Vitae

PERSONAL INFORMATION

Born	05th October 1990 in Braunschweig
Current Address	Wabestraße 2 38106 Braunschweig Germany
Mobile Phone	+49 (0)1578/2 33 55 16
E-mail	steffen.fricke@tu-bs.de

EDUCATION AND WORK EXPERIENCE

10/2015-today TU Braunschweig – PhD position

Division of cellular neurobiology,
laboratory of Martin Korte

- Topic: 'Role of Nogo-A in regulating synaptic transmission in the hippocampus – the involvement of inhibition'
- Teaching: supervision of Bachelor and Master theses
- Presentation of research results at national and international conferences
- Organization of public events as the 2nd and 3rd Brainswick Symposiums 2017/18 or the annual 'TU Night' representing the research group

10/2013- 09/2015 TU Braunschweig

Master of Science in Biology

- Topic: 'The role of Nogo-A in regulating excitatory postsynaptic transmission in CA3 pyramidal neurons in the hippocampus: Is inhibition involved?', laboratory of Martin Korte
- Specialization: Cellbiology, Biochemistry & Neurobiology

10/2010 - 09/2013	TU Braunschweig • Bachelor of Science in Biology Topic: 'Role of Nogo-A in regulating activity-dependent structural plasticity at dendritic spines of CA3 hippocampal neurons', laboratory of Martin Korte
08/2003 – 05/2010	Gymnasium Martino-Katharineum, Braunschweig, Germany Abitur

INTERNSHIPS & RESEARCH STAYS

02/2015-05/2015	Universiteit Utrecht, Netherlands, laboratory of Casper Hoogenraad • Purpose: Examining the role of Nogo-A in excitatory synaptic transmission in the hippocampus with the help of patch clamp electrophysiology
04/2018 & 08/2018	Leibnitz Institute for Neurobiology, Magdeburg, Germany, laboratory of Martin Heine • Purpose: Examining the role of Nogo-A in $GABA_AR$ diffusion dynamics via single particle tracking and calcium imaging
06/2019	Johannes Gutenberg Universität Mainz, Germany, laboratory of Martin Heine • Purpose: Data analysis

COMPETENCES

Languages	German (native) English (fluent) French (basic)

IT skills	MS Office
	Adobe Photoshop & Illustrator
	Image J
	GraphPad Prism
Scholarships	ERASMUS Placement
	Mobility scholarship
	(Faculty of Life Sciences, Biology, TU Braunschweig)
Miscellaneous	Utrecht Summer School 2014 – Neuronal Circuit Development and Plasticity, Utrecht – Netherlands 2014
	FELASA B

REFERENCES

Prof. Dr. Martin Korte

TU Braunschweig

Zoological Institute

Cellular Neurobiology

Spielmannstr. 7

38106 Braunschweig, Germany

Tel.: +49 (0)531 391 3220

E-Mail: m.korte@tu-bs.de

Dr. Marta Zagrebelsky

TU Braunschweig

Zoological Institute

Cellular Neurobiology

Spielmannstr. 7

38106 Braunschweig, Germany

Tel.: +49 (0)531 391 3225

E-Mail: m.zagrebelsky@tu-bs.de

PUBLICATION LIST

Kellner, Y., **Fricke, S.**, Kramer, S., Iobbi, C., Wierenga, C. J., Schwab, M. E., Korte, M. & Zagrebelsky, M. (2016). Nogo-A controls structural plasticity at dendritic spines by rapidly modulating actin dynamics. Hippocampus, 26(6), 816-831.

Zagrebelsky, M., Lonnemann, N., **Fricke, S.**, Kellner, Y., Preuß, E., Michaelsen-Preusse, K., & Korte, M. (2017). Nogo-A regulates spatial learning as well as memory formation and modulates structural plasticity in the adult mouse hippocampus. Neurobiology of learning and memory, 138, 154-163.

Fricke, S., Metzdorf, K., Ohm, M., Haak, S., Heine, M., Korte, M., Zagrebelsky, M. Fast regulation of $GABA_AR$ diffusion dynamics by Nogo-A signaling (in press).

Poster presentations on national & international conferences

Fricke, S., Lonnemann, N., Kellner, Y., Metzdorf, K., Korte, M. & Zagrebelsky, M. Role of Nogo-A signaling in regulating spatial learning and memory formation by modulating hippocampal parvalbumin (PV)-interneuron networks. 12th Meeting of the German Neuroscience Society, Göttingen (2017).

Fricke, S., Metzdorf, K., Korte, M., Zagrebelsky, M. Fast effects of Nogo-A neutralization on the excitation/inhibition (E/I) balance in the hippocampus. 11th FENS Forum of Neuroscience, Berlin (2018).

Metzdorf, K., **Fricke, S.**, Haak, S., Ohm, M., Korte, M. & Zagrebelsky, M. Nogo-A signaling modulates synaptic transmission on a fast time scale. 13th Meeting of the German Neuroscience Society, Göttingen (2019).